EMI RISK ASSESSMENT IN A HOSPITAL WARD WITH ROAMING WIRELESS TRANSMITTERS

Mehdi Ardavan

A thesis
in
The Department
of
Electrical and Computer Engineering

Presented in Partial Fulfillment of the Requirements
For the Degree of Doctor of Philosophy
Concordia University
Montréal, Québec, Canada

May 2014

CONCORDIA UNIVERSITY
SCHOOL OF GRADUATE STUDIES

This is to certify that the thesis prepared

By: Mehdi Ardavan

Entitled: EMI Risk Assessment in a Hospital Ward with Roaming Wireless Transmitters

and submitted in partial fulfillment of the requirements for the degree of

Doctor of Philosophy (Electrical & Computer Engineering)

complies with the regulations of the University and meets the accepted standards with respect to originality and quality.

Signed by the final examining committee:

Chair
Dr. M. Chen

External Examiner
Dr. Y. Antar

External to Program
Dr. G.J. Gouw

Examiner
Dr. R. Paknys

Examiner
Dr. D. Qiu

Thesis Supervisor
Dr. C.W. Trueman

Thesis Supervisor
Dr. K. Schmitt

Approved by: Dr. A. R. Sebak , Graduate Program Director

May 15, 2014 Dr. C. Trueman, Interim Dean
Faculty of Engineering and Computer Science

Abstract

EMI Risk Assessment in a Hospital Ward with Roaming Wireless Transmitters

Mehdi Ardavan, Ph.D.

Concordia University, 2014

Between 44,000 and 98,000 patients die each year in US hospitals due to medical errors which may be prevented by providing the medical staff with instant access to patient records using wireless technology. If the electric field intensity of a wireless transmitter is greater than the *immunity level* of an electronic medical device (EMD), the device may malfunction. The consequences of this electromagnetic interference (EMI) can be as serious as harm to the patient. This thesis presents a quantitative assessment of the *risk of exceeding immunity* (REI) and an analysis of some EMI control policies by developing methods for fast estimation of the probability distribution of the electromagnetic field strength in indoor environments accounting for the mobility of transmitters.

To determine the REI, ray-tracing, the Sabine method from acoustics, and the Ricean probability density function (pdf) are used. A commercial software is used to show that the presence of some furniture has negligible effect on the pdf of the field strength.

An approximation of the power in higher order reflections in ray-tracing is used to present the *modified ray-tracing-Rice* method, immensely increasing the computational speed with no loss of accuracy compared to the Ray-tracing-Rice method.

The Ricean and Nakagami pdfs are compared. It is shown that determining the Nakagami parameters requires more computation with no improvement in accuracy

hence the Nakagami distribution is not recommended in indoor propagation.

The *two-wave with diffuse power* theory is shown to be unreliable in estimating the pdf of the sum field of two fixed transmitters and reliable in the case of roaming transmitters. The Ricean function is then shown to approximate the pdf of the sum field of two roaming transmitters.

The *presence-weighted risk of exceeding immunity* (PWREI) is introduced accounting for the mobility of one and two transmitters which can be present at distances close to and far from the EMD. The PWREI is useful for large-scale decision-making processes where both low- and high-risk scenarios are considered, contrary to worst-case analyses where the transmitters are fixed at close distances. The PWREI accounts for a policy where the staff members carrying the transmitters are required to maintain a *minimum separation distance* (MSD) from the EMD, and a non-compliance possibility. The PWREI is applied to a hospital ward using transmitters radiating 100 mW at 2.45 GHz.

With full compliance, any low level of PWREI can be reached by increasing the MSD. Assuming some non-compliance, there exists an *optimal MSD* at which the PWREI reaches the *risk floor* and remains constant for greater MSDs, suggesting that larger MSDs are not necessarily safer. The MSD suggested by the International Electrotechnical Committee is too conservative compared to the optimal MSD. A vertical separation between the transmitter and the EMD is useful and recommended for increasing the efficacy of the MSD policy.

Acknowledgments

I would like to express my sincere gratitude to my supervisors, Dr. Christopher Trueman and Dr. Ketra Schmitt. This work would not have been finished without their guidance, patience and invaluable comments. I feel fortunate to have worked with them.

Thanks are also due to Dr. Robert Paknys, Dr. Yahia Antar, Dr. Gerard Gouw and Dr. Dongyu Qiu for their priceless comments and serving in my examining committee.

Many thanks to my friend, Dr. Amir Moradifam, for helping me keep a clear mind and critical perception in the most uncertain times.

I would also like to thank my father, mother and sister for their everlasting support and love.

Contents

List of Figures

List of Tables

List of Acronyms

cdf	Cumulative Distribution Function
CW	Continuous Waveform
ECG	Electrocardiography
EMD	Electronic Medical Device
EMI	Eletromagnetic Interference
FEM	Finite Element Method
FDTD	Finite-Difference Time-Domain
GO	Geometrical Optics
GPRS	Global Packet Radio Service
GSM	Global System for Mobile Communications
GTD	Geometrical Theory of Diffraction
IEC	International Electrotechnical Committee
MIMO	Multiple-Input Multiple-Output
MMV	Multipath Mean Value
MRTR	Modified Ray-tracing-Rice
MSD	Minimum Separation Distance
pdf	Probability Density Function
PHS	Personal Handy Phone System
PTD	Physical Theory of Diffraction
PWREI	Presence-Weighted Risk of Exceeding Immunity
REI	Risk of Exceeding Immunity

RFID	Radio-Frequency Identification
RMS	Root Mean Square
RTMV	Ray-tracing Mean Value
RTR	Ray-tracing-Rice
SBR	Shooting and Bouncing Rays
SR	Sabine-Rice
TWDP	Two-Wave with Diffuse Power
UMTS	Universal Mobile Telecommunications System
UTD	Uniform Theory of Diffraction

Chapter 1

Literature Review and Background Theory

1.1 Introduction

Between 44,000 and 98,000 patients die each year in US hospitals due to medical errors [2]. Some of these medical errors are caused by poorly designed systems of care and might be prevented by providing the medical staff with wireless devices and instant access to patient records [3]. Wireless technology is used for remotely monitoring the patient, providing reliable communication channels between staff members and providing access to medication history and lab results. Hence a universal and pervasive use of the wireless technology in hospitals, as a part of the health-care system, seems inevitable. However, wireless transmitters can cause electromagnetic interference (EMI) with the electronic medical devices (EMDs). The EMI consequences can range from a simple noise on the screen of the EMD to its serious malfunction resulting in harm to the patient. In some cases, the noise appearing on the display screen of the device disappears by moving the transmitter away. In more serious cases, the effect of the EMI on a medical device may be to a degree where the attention of the

medical staff is required to reset the equipment.

The likelihood of occurrence of an EMI incident is related to the strength of the electromagnetic field which is composed of two intertwined components: electric and magnetic fields. The electromagnetic field strength can be expressed by stating the intensity of any of these components. It is customary to use the electric field intensity for this purpose. Increasing the electric field intensity at the location of an EMD increases the EMI risk. Manufacturers of electronic medical devices provide a figure for each device, called the *immunity level*. If the electric field intensity at the location of the EMD remains below the immunity level, the device will experience no EMI-based malfunction.

In free space, the field intensity at the location of the EMD decreases as the distance from the transmitter increases. Thus, it is easy to determine the separation distance at which the electric field intensity, caused by the radiating antenna of a wireless device, equals the immunity level of the EMD. In an indoor environment such as a hospital ward, the field intensity fluctuates rapidly as the observer approaches or moves away from the transmitter. The computational cost of providing a full-wave solution of the field in indoor environment is extremely large. Instead of full-wave solutions, probabilistic methods are sought. These methods give the *probability density function* (pdf) for the field strength within a local area occupied by an EMD or a part it. The pdf is a function of the electric field intensity. The value of this function at a given field strength represents the likelihood of observing that field strength.

Using the probability density functions, the *risk of exceeding immunity* (REI) is defined. The REI gives the likelihood that within a local area, the field intensity is greater than the immunity level. The objective of this thesis is to provide a quantitative assessment of the REI in a hospital ward with roaming wireless transmitters and to analyze some policies to control the risk.

Any idealistic attempt in achieving an REI value of zero requires elimination of the use of wireless technology for always there exists a scenario where the radiation from multiple transmitters poses a threat on the functionality of the EMD. A realistic approach will attempt to *control* the EMI-related risk so that using wireless devices can be deemed *safe* for a real-life scenario.

To ensure safety, some policies have been suggested to control the electromagnetic interference. Some of these policies are based on reducing the power of the transmitter or smart design of the wireless system to reduce the amount of radiation. There are also policies which suggest a *minimum separation distance* (MSD) between the transmitter and the EMD [7–9]. The proposed separation distances do not account for the nature of indoor propagation nor do they consider the mobility of the wireless transmitters. No quantitative risk assessment has been given in the literature for the EMI control policies in hospital wards especially in the presence of roaming transmitters. This may be partly due to the large computational cost of determining the field distribution in indoor environments.

This thesis uses the existing techniques and develops new methods for fast estimation of the probability distribution of the electromagnetic field strength and presents a quantitative analysis of the risk of exceeding immunity. The results presented in this thesis enable the medical staff to safely use wireless transmitters in hospitals and thus reduce the risk of medical errors.

In this chapter, reported occurrences of EMI and different immunity levels in the literature are reviewed. Existing methods – deterministic and probabilistic – for obtaining the field distribution are reviewed. Next, the problem considered in this thesis is introduced. Then a brief description of the methods and contributions is given.

1.2 EMI Should Be Controlled

The electromagnetic field of wireless devices can interfere with the functionality of electronic medical devices. In a recent study [6], three of the 45 tested EMDs experienced electromagnetic interference. Malfunction of the electronic medical device observed in two of these cases could have caused clinical consequences for the patient. GPRS and UMTS signals were used to test 61 EMDs in [4] where 26 of the devices experienced interference. An EMI incident with a ventilator due to a GPRS-1 signal radiated from a transmitter at about three meters away was reported as hazardous. In study [12], 123 EMI tests were performed on 41 EMDs using RFID signals. Thirty four incidents of electromagnetic interference were reported. Twenty two of the incidents were considered hazardous. Two of the incidents were classified as significant and 10 as light. Different EMDs could also interfere with each other. Electromagnetic radiation from electrosurgical units can interfere with other critical-care EMDs in operating rooms leading to a medical system failure [16].

In an older study [5], cellular phones, transmitting either 600 or 800 mW at 800 MHz or 1.5 GHz, caused EMI on 66% of the 108 tested electronic medical devices. In this study PHS (personal handy-phone) terminals transmitting 80 mW at 1.9 GHz caused interference on 8% of the tested EMDs such that wrong values were shown on anesthetic equipment, an external cardiac pacemaker could not produce the required pulse and an alarm stopped syringe pumps. The first two incidents were reversible by moving away the phone. However the last incident required the attention of the medical staff to reset the equipment.

In study [17], cell-phone signals induced considerable changes in the values read from an electroencephalography (EEG) brain monitor and an incubator. It was suggested in this study that the cell-phones should be switched off near near electronic medical devices.

To ensure safety, it has been suggested that an *EMI control policy* be adopted [7,

8, 18]. Study [19] suggests that a new branch in science and industry dealing with the risk management of electromagnetic compatibility problems is emerging. A *total ban* on the use of wireless transmitters in hospitals can be considered as an EMI control policy. Also the EMI control policy can be as complex as a smart design of the wireless system where the amounts of electromagnetic radiation can be increased or decreased when appropriate [18, 20]. Also a minimum separation distance between the wireless device and the EMD [7, 8] may be used as an EMI control policy.

The MSD policy is widely suggested and is a focus of this thesis. A typical 1-meter separation between the EMD and the wireless transmitter is suggested in [7, 8]. However this number is not based on a quantitative risk assessment. Comparison of the efficacy of different MSDs or even different control policies require knowledge of the EMI risk. A qualitative assessment of the risk of patient injury due to EMI is given in [21]. To the author's knowledge, there are no strong quantitative assessments of the risk of EMI specially with roaming wireless sources nearby.

1.3 Immunity Level

No EMI control policy can be developed without knowledge of the immunity level of the EMD. Some older EMDs have been tested in study [22]. An LP6 Plus ventilator and a Lifepak-6S defibrillator with (electrocardiography) ECG monitor failed at 5.8 V/m and 3 V/m respectively. In [22], a 50% 1-kHz amplitude modulation at a frequency range of 1-2000 MHz was used. However in a more recent study [13], a Pulse Oximeter had an immunity level of more than 30 V/m when exposed to an 80% AM 1-kHz modulation signal. Two defibrillators experienced no electromagnetic interference in the presence of a 2 W dipole antenna at a 1-cm distance causing an electric field intensity larger than 30 V/m. The spread-spectrum GSM900/PCS1800/3G signals were used in [15] to test the immunity of the medical devices. An ECG monitor

and an ultrasonic fetal heart detector experienced interference when the electric field strength was less than 1 V/m. An Audio Evoked Potential System was reported to have an immunity level of 10 V/m. In study [23] where 16 devices were tested, six EMDs experienced malfunction. A vital sign monitor was reported to experience interference caused by cellular phone radiating 0.6 W at a 43-cm distance. A half-wavelength dipole antenna would generate a 13-V/m electric field at this distance. Also some noise was observed on the display screen of an EEG desktop system at a distance at which the have-wavelength dipole antenna generates a field strength of 16 V/m.

It is seen that the measured immunity levels and also the methods with which the immunity of medical devices are tested vary from a study to another. It is not a focus of this work to investigate immunity levels. Standards have been developed to ensure the electromagnetic compatibility of EMDs. Two different immunity levels of 3 and 10 V/m, for non-life-support and for life-support equipment respectively, as suggested by the International Electrotechnical Commission (IEC) 60601-1-2 standard [9], are used in this thesis.

This standard assumes a plane wave with an AM modulation of index $m = 80\%$ and an information frequency of either 2 Hz or 2 kHz signals. Regardless of the information frequency, the total power is $P_t = P_c(1 + m^2/2)$ where P_c is the carrier power. Now the equivalent root mean square (RMS) value of the total signal (voltage) across a resistor R is related to the integral of the instantaneous power in the total signal over the larger period (or the product of the two time periods). Since this integral is already denoted by P_t, the equivalent RMS value of the total voltage is given by $\sqrt{P_t R}$ regardless of the modulation. Therefore one can ignore the AM modulation in the above mentioned standard and assume that the antenna is transmitting a CW non-modulated signal with power P_t.

1.4 Electromagnetic Field Distribution

The field strength of a mobile transmitter depends on the power radiated, the directional properties of the mobile device as transmitting antenna, the distance from the EMD and the surrounding structure or environment. The method of Moments (MoM), Finite Element Method (FEM) or Finite Difference Time Domain (FDTD) can be used to determine the electromagnetic field [24,25]. A two dimensional FDTD method was used in [26] to determine the field distribution in a multi-floor environment. Isotropic spreading in the third dimension extended their method to 2.5 dimensions. The simulation time for their method was more than 30 days at 4.5 GHz using a 1.8 GHz Intel Xeon CPU. At the electromagnetic wave frequency of 1 GHz, the CPU time is reduced to 80 hours. A 3D full-wave solution would require more computational power. In indoor environments, as the dimensions of the structures increase, the full-wave methods become impractical due to the large computational cost [1].

At high frequencies, instead of the full-wave solution of the Maxwell equations, geometrical optics (GO) is used. GO, or ray optics, has been used in light propagation and may be used in electromagnetic problems where the wavelength is very small compared to the structures considered. GO is much faster than the full-wave methods. The GO method does not account for the diffracted rays and has a discontinuity in transition to the shadow region where this method cannot provide a nonzero field. The geometrical theory of diffraction (GTD) accounts for the wedge diffraction and gives a nonzero field at the shadow region [29]. However it fails at the shadow boundary and at areas very near the diffracting edge. The uniform theory of diffraction (UTD) improves the solution at the transition region but due to its geometrical nature fails at caustics as do GO and GTD solutions [30]. The physical theory of diffraction (PTD) does not require tracing a ray from the transmitter to the receiver but it does need a current integration over the reflecting surfaces [31].

In an observation area which is completely out of the shadow region and is far from the diffracting edges, the accuracy of the GO method is not much improved by the diffraction corrections offered by the GTD, UTD and PTD methods. Ray-tracing, as a GO technique, can be used to account for multiple reflections between the surfaces. If all the walls and reflecting surfaces are assumed to be flat, then the caustics are moved to the infinity and this type of problem is not encountered. The spatial factor needs not be accounted for as it equals unity.

1.4.1 Ray-tracing

Ray-tracing, as a GO technique, is widely used in indoor propagation [32–34]. There are a number of paths for the rays to reach the receiver. Ray-tracing can be implemented using an image tree algorithm or using the method of shooting and bouncing rays (SBR). In the SBR method many rays are emitted from the source [35]. Each ray represents a ray tube. The ray paths are tracked until they are reflected from a surface. At the reflection point the perpendicular and parallel reflection coefficients are applied. Tracing the rays continues until the field intensity associated with a ray falls below a threshold. At an observation point, all the center rays of the ray tubes encompassing the point of interest contribute to the field. The SBR method is particularly useful for calculating the radar cross section of an object where the incident field is plane wave.

In large indoor environments and for a specified level of accuracy, the number of the rays required by the SBR method grows with the dimensions of the room. In large and simple indoor environments, with flat walls, floors and ceilings, it is easier to implement the *image tree* algorithm of ray-tracing. This algorithm is described in [32]. Fig. 1.1 shows parts of a long corridor. One ray is directly received at the receiver whose associated field is equivalent to the field of the transmitter in free space. This is called the direct field. Some rays are reflected once from a either

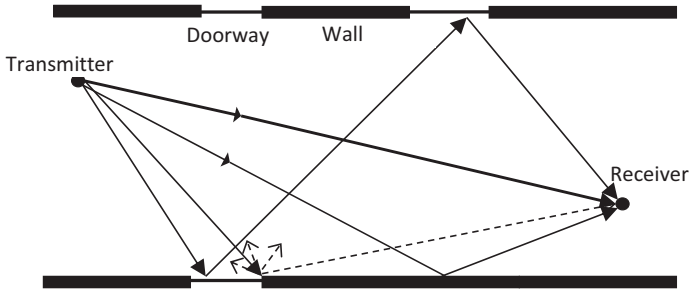

Figure 1.1: Raytracing diagram. (Inspired by [1])

a wall, floor, ceiling or a door. Some are reflected twice, thrice and so forth. The electric field associated with each ray is represented by a vector phasor. The vector sum of the these phasors gives the total electric field intensity at the receiver located at (x, y) and is given by

$$\mathbf{E_t}(x, y, z) = \mathbf{E_d}(x, y, z) + \sum_{k=1}^{R} \sum_{i=1}^{N_k} \mathbf{E_r}^{(k)}(i, x, y, z) \tag{1.1}$$

where $\mathbf{E_r}^{(k)}(i, x, y, z)$ is the i'th ray among those reflected k times, and N_k is the number of rays which have been reflected k times. The highest value of k is infinity in theory. However the series is truncated when the reflections with orders higher than R do not have a discernible contribution to the field. Hence R is the highest order of reflection which is considered. $\mathbf{E_d}$ is the direct field that is the field of the antenna as in free space. Its description follows the definition of the multipath field, ray-tracing mean value and multipath mean value.

Equation (1.1) accounts for the phase of the field vectors of the rays arriving at an observation point. These phases can significantly change from a point to an adjacent one. The field components in one point may add up and in an adjacent point may cancel out. This results in a rapidly varying field and this phenomenon is referred to as the *fast fading*.

For simplicity, the notation for dependence on the location (x, y, z) may be removed. Nevertheless it is always accounted for in the calculations unless stated otherwise.

In free space, only the direct field component exists. In an indoor environment, the multipath field is defined as

$$\mathbf{E_{multi}} = \sum_{k=1}^{R} \sum_{i=1}^{N_k} \mathbf{E_r}^{(k)}(i) \tag{1.2}$$

The power-based sum of the field intensities of the rays arriving at one point is called the *ray-tracing mean value* (RTMV) [36]. The RTMV, denoted by E_{RM}, is defined by

$$E_{RM} = \sqrt{|\mathbf{E_d}|^2 + \sum_{k=1}^{R} \sum_{i=1}^{N_k} \left|\mathbf{E_r}^{(k)}(i)\right|^2}. \tag{1.3}$$

If the direct field is not accounted for, the *multipath mean value* (MMV) is obtained. The MMV is denoted by E_m and is defined by

$$E_m = \sqrt{\sum_{k=1}^{R} \sum_{i=1}^{N_k} \left|\mathbf{E_r}^{(k)}(i)\right|^2}. \tag{1.4}$$

The direct field, $\mathbf{E_d}$, is obtained using the free space model of a transmitter held by a person. If the transmitter itself is assumed to be a half-wavelength dipole antenna held vertically, oriented in the z-direction, the body of the person holding it will change its radiation pattern especially in the H-plane that is in the horizontal plane. The person holding the transmitter might face any direction. Averaging over all possible directions a person can face (e.g. 36 directions separated by 10 degrees accounting for a full circle), the averaged radiation pattern in the H-plane is similar to the uniform pattern of the dipole antenna. An averaged radiation pattern is suitable for analyses of probabilistic nature. Hence the radiation pattern of a half-wavelength

dipole antenna is used and the direct field is given by

$$\mathbf{E_d} = \sqrt{\frac{\eta D P_t}{4\pi}} \frac{e^{-j\beta r}}{r} \hat{\boldsymbol{\theta}}_{tx} \tag{1.5}$$

where r is the distance to the observation point, D is the directivity of the transmitter at the direction of the observation point, P_t is the transmitted power, β is the free space wave number and η is the intrinsic impedance of free space. Also $\hat{\boldsymbol{\theta}}_{tx}$ is a unit vector in the spherical coordinate system where the transmitter is at the center.

The field intensity vector associated with each ray is determined as follows.

Ray-tracing Algorithm (Image Tree)

A three-dimensional ray-tracing algorithm was developed in [32]. The images of the transmitter are generated regarding the position of the reflecting surfaces that is the walls, floor and ceiling. The images of the image sources are generated. This process is repeated for a total of R times and thus the image tree is generated. All possible ray paths are determined by tracing a ray from the observation point back to the transmitter using the image sources. If the reflection point associated with an image source does not lie on the corresponding reflecting surface, the ray under test is discarded.

The field intensity of a valid ray at the first reflection point from the transmitter is determined using the directional properties of the transmitting antenna. The reflected field is determined by decomposing the incident field into two components: parallel and perpendicular to the plane of incidence. The reflection field is determined after applying the corresponding reflection coefficients. Repeating this process for all reflection points and accounting for the total length of the ray the total electric field vector phasor at the observation point, $\mathbf{E_r}^{(k)}(i)$, is obtained.

The parallel and perpendicular reflection coefficients of a multilayer wall are determined as follows.

Reflection Coefficients of a Multilayer Wall

Reflection coefficients for a flat dielectric slab is given in [28]. To determine the coefficients, plane-wave incidence is assumed. The field of a point source such as a dipole antenna far enough from the reflecting surface can be assumed as plane wave. Walls can be multi-layered. The reflection coefficients of the multilayer walls, for perpendicular and parallel incidents, are given in [28] assuming the layers are flat and homogeneous. The reflection coefficients derived for the flat and multilayer walls with homogeneous layers can sometimes estimate the reflection coefficients of the walls that have a certain level of non-homogeneity and roughness.

The reflection coefficients of rough-surfaced walls made of limestone blocks, glass and brick were obtained through measurement in [37] for a frequency range of 1.9 GHz to 4 GHz. The measured reflection coefficients were compared to the theoretical solution, for a dielectric slab, given by the Fresnel reflection coefficients corrected by a scattering loss factor accounting for surface roughness. The measurement and theoretical results showed no agreement for the limestone wall, little for the glass and acceptable agreement for the brick wall.

In the same frequency range, it was shown in [38] that the Fresnel reflection formula for smooth surfaces provides an acceptable prediction of the measurement results for glass and brick walls. The Gaussian roughness of the surface of the limestone wall had to be accounted for in order to describe the reflective properties of the wall.

Interior walls are usually different from simple and flat walls. There is some inhomogeneity in the walls. The reflection coefficient of some typical interior walls were measured in [39] and compared to the theoretical solution obtained assuming flat surfaces. In the theoretical model for the gypsum board wall, metal studs are ignored.

In the concrete model, a periodic structure accounts for the air gaps. Comparison with the measurement results confirmed that the effect of the metal studs can be ignored if the spacing between them is large enough.

Dielectric properties of brick and concrete were measured in [40]. The relative permittivity, ϵ_r, and conductivity, σ, of brick at 2.6 GHz were found to be 4.26 and 19.7 mS/m respectively. Those of concrete were 5.10 and 146 mS/m. Reference [37] used 4.44 and 10 mS/m as the relative permittivity and conductivity of brick at 4 GHz. As listed in a table in [28], the permittivity and conductivity of glass varies largely due to the availability of different types. The relative permittivity of the glass wall used in [37] is 5 and its conductivity varies between 10^{-12} and 5 S/m.

The relative permittivity of wood at 2.45 GHz was reported to be 1.59 in [41] and 2.2 in [42]. The electrical conductivity of wood varies significantly by moisture [43]. It can be considered as a good insulator when absolutely dry and as conductive as water when saturated with moisture. The conductivity of water varies between 10 and 4000 mS/m [28].

The computational cost of ray-tracing grows exponentially with the highest reflection order accounted for. If the location of the transmitter changes, the image tree needs to be regenerated. If the fast fading behavior of the field needs not be demonstrated, E_m and E_{RM} can be estimated using the Sabine method.

1.4.2 Sabine Method

If a source (such as live voice, musical instrument or a loudspeaker) in a room is maintained steadily, "the rapid accumulation of reflected waves quickly set up a level of sound energy which is essentially uniform throughout the room and remains constant until the source is cut off" [44]. The reverberation energy density of the reflected field in a room caused by an electromagnetic field is given in [45]. This method is used in [36] to approximate the multipath mean value (MMV), a power-based sum of the

multipath components.

The MMV determined by the Sabine method is uniform throughout an enclosed room. In an enclosed room, variations in the location of the transmitter or the receiver do not affect the Sabine estimation of the MMV. Hence it is much faster but less accurate than ray-tracing.

The surfaces of the room consist of M patches of material, each of area S_j. The room absorption is defined by

$$A = \sum_{j=1}^{M} S_j \tilde{\alpha}_j \tag{1.6}$$

in which the angle-averaged power absorption coefficient $\tilde{\alpha}_j$ is given by

$$\tilde{\alpha}_j = 2 \int_0^{\frac{\pi}{2}} \left(1 - \frac{1}{2} \left(\left| \Gamma_{\parallel} \right|^2 + \left| \Gamma_{\perp} \right|^2 \right) \right) \sin\theta \cos\theta \, \mathrm{d}\theta$$

where $\Gamma_{\perp}$ and $\Gamma_{\parallel}$ are respectively the perpendicular and parallel reflection coefficients for the surface j. The reflection coefficients are frequency-dependent. The incident angle is denoted by θ for which the $(0, \pi/2)$ interval of integration indicates averaging for all possible incident angles. If S_T is the sum of all S_j's then the multipath absorption is given by

$$A_m = \frac{A S_T}{S_T - A}. \tag{1.7}$$

Then the average MMV over a local area, estimated by the Sabine method, is denoted by E_{ms} and is given by

$$E_{ms} = \sqrt{\frac{4\eta P}{A_m}}. \tag{1.8}$$

The power-based value of the total field strength, i.e. the ray-tracing mean value, is estimated by considering the direct field and is given by

$$E_{sab} = \sqrt{\frac{\eta D P}{4\pi r^2} + \frac{4\eta P}{A_m}} \tag{1.9}$$

where r is the distance from the source to the observation point. E_{sab} is an estimation of E_{RM}.

The Sabine method does not predict the fast fading behavior but the ray-tracing method does. The ray-tracing computational times increase directly with the number of observation points. To obtain the statistics of the rapidly varying field strength in indoor environments, probability distributions may be used in order to reduce the computational time.

1.4.3 Probabilistic Estimation of the Field

Ricean, Rayleigh and Nakagami distribution functions have been used for characterizing indoor propagation [46]. In a line-of-sight channel, the parameters of the Ricean function is extracted from numerous measurement data in [47]. A Rayleigh distribution was used in [48] to determine an optimal power allocation scheme in the links over relayed transmissions. The Nakagami distribution was compared to Rayleigh and Ricean distributions in [49] to characterize a multiple-input multiple-output (MIMO) channel. The Nakagami and Ricean distributions matched the measurement data whereas the Rayleigh distribution failed in providing a valid estimation of the measured signal.

The parameters of these functions are determined using techniques based on the moment method [50] or the maximum-likelihood method [51, 52]. Of course it is always possible to estimate the parameters using curve-fitting techniques. However all of these methods require a large number of data points (field values) to estimate the parameters. This is contrary to the intention of reducing the time of the computation. The ray-tracing computational time directly increases with the number of observation points; and the full-wave solutions are impractical to be applied. The Sabine method is much faster but does not give the fast-fading behavior. Fortunately, the parameters of two of the aforementioned three pdfs have physical meanings which makes their

determination easy.

The Rayleigh and Ricean distributions are different from the Nakagami function. The parameters of the Rayleigh and Ricean functions have interpretations in terms of the signal power. Rayleigh in 1880 introduced his function which gives the probability distribution for "*the resultant of a large number of vibrations of the same pitch* [*magnitude*] *and of arbitrary phase*" [53]. Existence of a dominant component is accounted for by S. O. Rice in 1944 [54], leading to the Ricean pdf. The Ricean function gives the probability distribution for an event ideally consisting of a large number of outcomes, N, which add up to

$$Ee^{j\phi} = A_0 e^{j\phi_0} + \sum_{k=1}^{N} Ae^{j\phi_k} \tag{1.10}$$

in which A_0 and A are positive real numbers. A_0 is usually large thus called the dominant component. All ϕ_k for $k \geq 0$ are real random numbers uniformly distributed between 0 and 2π. Let ${E_m}^2 = NA^2$ and $E_d = A_0$. The pdf of the Ricean event is given by

$$p(E) = \frac{2E}{{E_m}^2} e^{-\frac{E^2+{E_d}^2}{{E_m}^2}} I_0\left(\frac{2E \cdot E_d}{{E_m}^2}\right), \quad E \geq 0 \tag{1.11}$$

where I_0 is the modified Bessel function of the first kind and order zero. The Ricean pdf has an alternative representation given by

$$p(E) = \frac{2(K+1)E}{\Omega} e^{-K-\frac{(K+1)E^2}{\Omega}} I_0\left(2E\sqrt{\frac{K\,(K+1)}{\Omega}}\right), \quad E \geq 0 \tag{1.12}$$

where $\Omega = {E_d}^2 + {E_m}^2$ and $K = {E_d}^2/({E_m}^2)$. In fact Ω is comparable to ${E_{RM}}^2$.

If A_0 in (1.10) becomes equal to zero, the Ricean pdf reduces to the Rayleigh probability density function which is given by

$$p(E) = \frac{2E}{{E_g}^2} e^{-\frac{E^2}{{E_g}^2}} \tag{1.13}$$

where E_g is equal to E_m assuming $A_0 = 0$.

Beside the Ricean and Rayleigh distribution, the Nakagami probability density function is also used and is given as below.

$$p(E) = \frac{2m^m}{\Gamma(m)w^m} E^{2m-1} e^{-\frac{m}{w}E^2}, \quad E \geq 0 \tag{1.14}$$

where Γ is the gamma function and m and w are the parameters of the Nakagami distribution function.

The Rayleigh, Ricean and Nakagami pdfs all are used in the case of a single transmitter. In the presence of more transmitters the probability distribution changes.

1.4.4 Field Distribution in the Presence of Two Transmitters

There might be more than one transmitter in a hospital ward. The probability distribution function for the sum of random numbers from more than one independent event was analyzed in [55] where there are two independent events and both have Ricean distribution individually. A simplified and numerically more convenient model is given in [56].

The pdf of sum of two Ricean events is given in [55, 56]. The event obtained from the sum of two events is usually referred to as the two-wave with diffuse power (TWDP). A random event with two dominant components is represented by

$$Ee^{j\phi} = A_0 e^{j\phi_0} + A_1 e^{j\phi_1} + \sum_{k=2}^{N} A e^{j\phi_k}. \tag{1.15}$$

The components A_0 and A_1 are arbitrary but usually large thus called dominant. The probability distribution of the two-wave with diffuse power signal is given by

$$p(E) = E \int_0^\infty \exp\left(-\frac{x^2 {E_{dp}}^2}{4}\right) J_0(xE) J_0(A_0 x) J_0(A_1 x) x \, \mathrm{d}x \tag{1.16}$$

where J_0 is the Bessel function of the first kind and order zero and the *diffuse power* is given by ${E_{dp}}^2 = (N-1)A^2$.

This theory has been used in digital communications to determine the bit error rate and characterize channels for different modulation schemes [57–61]. In none of these studies the field distribution obtained from an electromagnetic solution or measurement has been compared to the theoretical formula. Study [62], to the best of author's knowledge, is the only work which compares the TWDP theory with the electromagnetic field. In [62], the pdf of the measured field did not match its TWDP prediction.

Whether there is one or two transmitters, the probability density function is used to determine the risk of exceeding immunity. The REI is defined as the integral of the pdf from the immunity level to the infinity. The REI concept is extended in the present report to account for roaming transmitters.

1.5 Problem Statement

Electromagnetic interference can be studied from different points of view. It is suggested in [63] that the EMI consists of two events: 1) the electromagnetic field exceeds the immunity of the EMD and 2) an adverse clinical event takes place due to malfunctioning of the EMD.

In this thesis, the focus is on the risk of exceeding immunity for a medical device in a hospital ward with a roaming wireless transmitter whose exact location in not known. The effect of adding a second roaming transmitter is analyzed. Medical staff members carrying wireless devices may be required to keep a minimum separation distance from the EMD. The effect of the MSD policy on the risk is investigated. Also the effect of non-compliance with the MSD policy on its efficacy is studied.

The risk assessment is performed in a four-bed hospital ward which is shown in

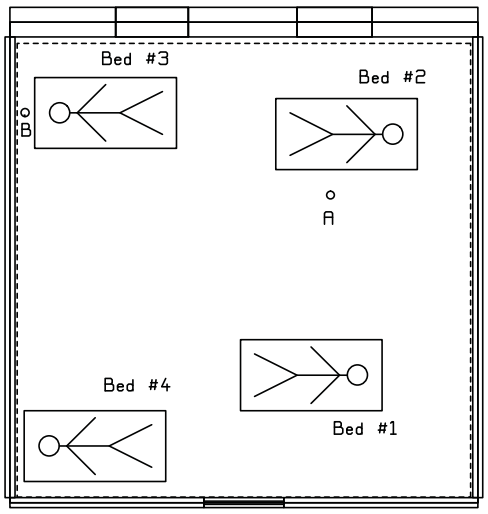

Figure 1.2: The floor plan of a four-bed ward. Beds are located in different positions and numbered as 1, 2, 3 and 4.

Fig. 1.2. This ward measures 6.4 m by 6.5 m and the transmitters are assumed to be a half-wavelength dipole antenna transmitting 100 mW at 2.45 GHz. However different floor plans will be used throughout this thesis to develop new tools for field estimation in indoor propagation.

1.6 Methods and Contributions

In this thesis, the image tree algorithm of ray-tracing – as a GO technique – is used to obtain the field distribution. The results are verified using a commercial software called the Computer Simulation Technology (CST).

In modelling the room for the ray-tracing and Sabine methods, $\epsilon_r = 4.38$ and $\sigma = 18.5$ mS/m are used as the relative permittivity and conductivity of the brick. Concrete is modeled using $\epsilon_r = 5.37$ and $\sigma = 149.5$ mS/m. For the glass wall, $\epsilon_r = 5.9$ and $\sigma = 500$ mS/m are used. For wood, a relative permittivity of 1.8 and electric conductivity of 11 mS/m are used. Different values of the constitutive parameters are used if the effect of different reflective properties is analyzed.

In this thesis, it is shown that the statistics of the electromagnetic field strength

with a volume of size a by a by a is very well approximated by the field data over the area a by a at the center of the volume, given that the value of a does exceed a certain limit. Obtaining the field data over an area by ray-tracing is much more time efficient than obtaining the data within a volume. The data along a line in the volume is shown to be an inaccurate representation of the volumetric data.

The effect of the furniture on the field distribution is analyzed. It is shown in this thesis that despite some effect on the point values of the electric field, the probability distribution of the field within a local area does not change considerably if some furniture is added to the room.

Ray-tracing is used to obtain the direct field and the multipath mean value. These values, calculated only at a single point at the center of a local area, may be used as the parameters of the Ricean function to give the pdf of the field strength for thousands of closely spaced points within the local area [64]. This method is called the ray-tracing-Rice (RTR) method. The Ricean distribution, the RTR method, loses its accuracy when the observation region is too close to the transmitter. The accuracy is shown to be regained if the size of the local area is reduced.

If the multipath mean value is estimated by the Sabine method, the Sabine-Rice (SR) approximation is obtained.

The performance of the Ricean and Nakagami distributions are compared to each other. It is shown that the Nakagami distribution does not offer a better accuracy but requires more computations hence is not recommended.

It is shown in this thesis that the third and higher order reflection components in the multipath mean value do not much vary by the location of the observer. This fact is then used to present the *modified ray-tracing-Rice* (MRTR) method which can be several orders of magnitude faster than the RTR method with no loss of accuracy in predicting the field of one transmitter.

The two-wave with diffuse power theory is shown to be unreliable in predicting

the probability distribution of the sum field of two fixed transmitters and reliable in the case of roaming transmitters. The Ricean pdf is then shown to predict the sum field of two roaming transmitters.

The probability distribution of the field is affected if the transmitter(s) have large movements and roam in the ward. In this thesis a presence probability function is defined to account for the roaming nature of the transmitters. The *presence-weighted risk of exceeding immunity* (PWREI) is introduced to determine the REI while accounting for all possible locations of the transmitter(s). Using the presence probability function, the effect of the MSD policy on the PWREI is analyzed. Also the effect of non-compliance with the MSD policy is studied. Using the PWREI method, the vulnerability of EMDs with different immunity levels are studied as well.

The ray-tracing, Sabine, RTR, SR and MRTR methods have been simulated using source codes written by the author in Fortran for the purpose of this thesis.

1.7 Thesis Outline

Chapter 2 compares the CST and ray-tracing results and investigates the effects of the furniture on the field distribution. Also the maximum size for local area is determined such that its field distribution matches the pdf of the volumetric data. This chapter uses the ray-tracing-Rice and Sabine-Rice methods. The Nakagami distribution is analyzed in this chapter.

The modified ray-tracing-Rice method is devised and presented in Chapter 3.

Chapter 4 shows that the TWDP fails to predict the pdf of the field due to two transmitters. It then shows that, if the transmitters are allowed to move around, the TWDP theory regains its validity. In this chapter it is shown that the Ricean formula can be used to estimate the field of two and more transmitters.

Chapter 5 introduces the presence probability function and the presence-weighted

risk of exceeding immunity. The MSD policy and the non-compliance considerations are accounted for. Chapter 6 summarizes the thesis and discusses some possibilities for future work.

Chapter 2

Probabilistic Estimation of the Electromagnetic Field and the Furniture Effect

2.1 Introduction

The objective of this chapter is to provide fast and reliable methods for estimating the electromagnetic field distribution. This chapter compares the Rayleigh, Ricean and Nakagami distributions and suggests the Ricean distribution for indoor applications. It shows that the Ricean parameters can be obtained using the Sabine method in an empty room and can be used in the Ricean function to estimate the pdf of the electromagnetic field strength in the room with some furniture. The Sabine-Rice approximation is used in Chapter 5 to estimate the risk of exceeding immunity in the presence of one and two roaming transmitters.

In this chapter, the time-domain solver of the Computer Simulation Technology Microwave Studio software is used to show that the probability distribution of the field strength over an area provides a reliable estimation of the volumetric data if the

size of the area does not exceed a certain level. This is useful when the ray-tracing method is used to obtain the field values as the computational time of ray-tracing is directly related to the number of observation points and this number is much smaller in the case of a local area than a volume.

The CST software is used to show that the presence of furniture does not have a considerable effect on the probability distribution of the field strength within a local area. In a room without furniture, the pdf of the field strength over a local area is once obtained using using ray-tracing and then using the CST results; the two pdfs are shown to be in agreement. To obtain both pdfs, many point values of the field strength over the local area are required. This emphasizes the need for a very large mesh with closely-spaced observation points even for ray-tracing.

In this chapter, the ray-tracing-Rice method is used [64] which does not require closely-spaced observation points. It is accurate in regions near and far from the transmitter. If the Ricean function is replaced by the Rayleigh function, the accuracy decreases in regions near the transmitter. If the local observation area further approaches the transmitter, the ray-tracing-Rice method loses its accuracy. The accuracy of the RTR method is regained if the size of the local area is reduced.

The Nakagami distribution is compared to the Ricean distribution. It is shown that determining the parameters of the Nakagami pdf requires more computation without offering a better accuracy. Hence The use of the Nakagami distribution is not recommended.

Also the Sabine-Rice approximation [65] is used and compared to the field statistics obtained from the ray-tracing method. The SR method is much faster than the RTR method.

2.2 Effect of Furniture on Field Distribution

The presence of furniture affects the electromagnetic field distribution. In this section it is shown that despite some differences in the point values of the field strength, the field distribution within a local area is not considerably affected by the presence of furniture. First, the electromagnetic field in a small room is determined using the CST software with and without furniture. Before comparing the cumulative distributions (with and without the furniture) of the field strength at some local areas, it is necessary to determine how large a local area should be. After determining the local area size, the furniture effect on the cdf of the field strength is investigated.

2.2.1 Furniture Effect on the Point Values of the Field

A small hospital ward, 3 m by 4 m by 3 m, with a bed and a medical device on a trolley is shown in Fig. 2.1. The floor and ceiling are made of 30 cm concrete blocks. The walls, too, are concrete blocks but with a thickness of 10 cm. The door is a 5 cm wooden block. The bed has four metallic (PEC) legs with a polyester-cotton mattress. The medical device is modeled as a plastic box inside which there are 11 metallic cubes. Each of these PEC cubes have a side of 10 cm. Nine of the 11 cubes are put right next to the surface of the plastic box facing the bed. The half-wave dipole antenna is located vertically at ($x = 1.7$ m, $y = 3.5$) between the medical device and the patient bed, at the height of 1.6 m. The transmitter is radiating 427 mW at 2.45 GHz ($\lambda = 12.2$ cm) which is one of the frequencies of the IEEE 802.11 standards. In the next chapter, it is seen that for the risk calculations, even this rather high power is barely sufficient to have a risk graph which is well expanded over the y-axis. The expansion of the risk graph is desired for demonstrating the results. The step size between observation points in the ray-tracing simulation is 1 cm. The CST results are obtained using a mesh slightly finer than when $\Delta x = \Delta y = \Delta z = \frac{\lambda}{10} = 1.22$ cm.

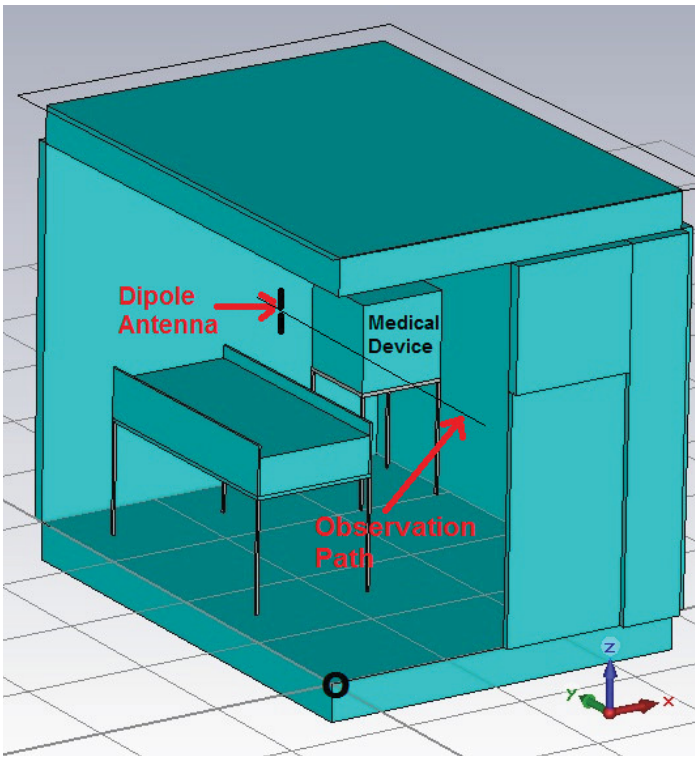

Figure 2.1: A hospital ward with a patient bed and a medical device on a trolley. The center of the coordinates is shown with a black 'o'.

The cell size is much smaller where the transmitting dipole is modeled. The CST model of the dipole is a PEC wire of radius 0.7 mm. Its length is 0.475λ. This model is tested in free space where the CST yields a total electric field vector with a magnitude of 12.35 V/m at a 35.6 cm radial distance from the vertically oriented antenna. The x- and y-components of the field vector were at the 10^{-7} V/m range. At the 35.6 cm distance, the far field formula for an ideal dipole predicts an electric field of 12.86 V/m. At a much closer distance of 8.5 cm, where the far field conditions are not much satisfied, the CST yields 52.38 V/m whose x- and y-components are in the 10^{-6} V/m range. The dipole formula predicts 54.02 V/m. At the distance of 6.1 cm, the CST yields 74.23 V/m whose x- and y-components are in the 10^{-6} V/m range while the dipole formula predicts an electric field of 74.91 V/m. At a distance of slightly less than 2 cm, the two electric field values are off by a factor of almost 2. So the half-wavelength dipole formula gives a correct value of the direct field of

antenna in free space for distances larger than 6 cm, that is almost everywhere in the room.

The electric field intensity in the ward without the patient bed and without the medical device and its trolley is determined using the CST software. The simulation is repeated in the presence of the furniture. The electric field intensity, in both cases, is plotted in Fig. 2.2 along the line $x = 1.7$ m, $z = 1.6$ m which is parallel to the y axis. This observation path is shown in Fig. 2.1. The ray-tracing result shown in Fig. 2.2 will be discussed later in this chapter.

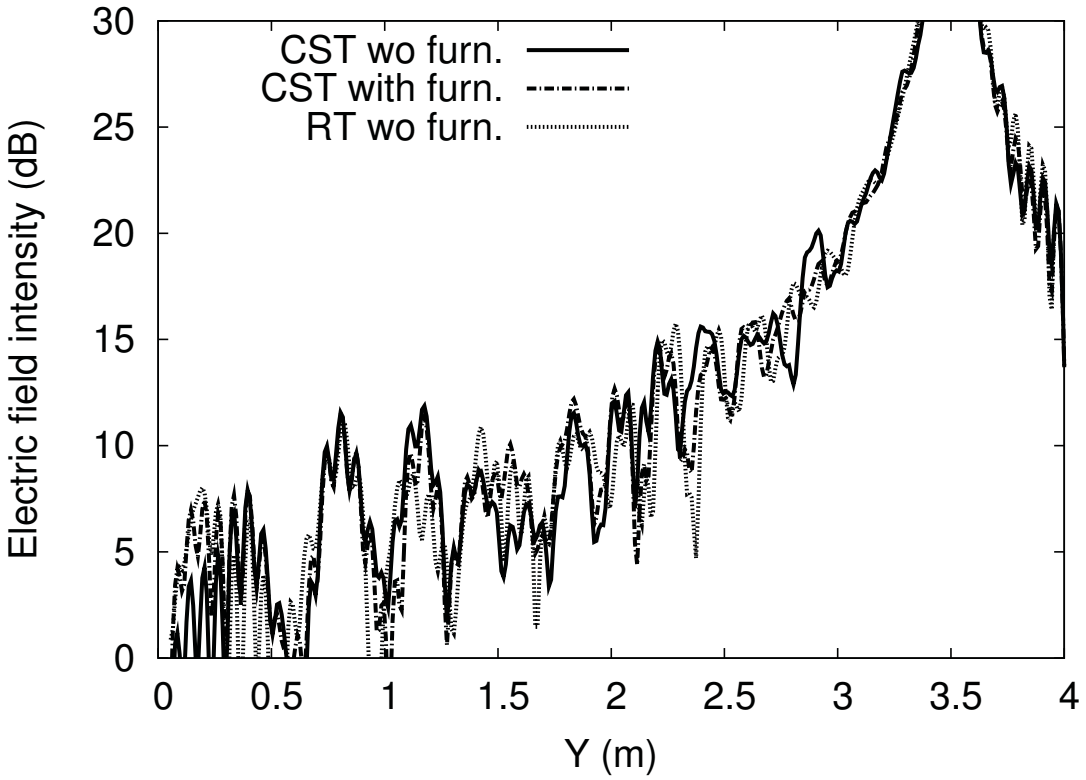

Figure 2.2: Electric field intensity along a line parallel to the y-axis and passing through the antenna. The CST with furniture versus the CST without the furniture versus the ray-tracing without the furniture.

Comparison of the CST results of the with- and without-the-furniture cases, presented in Fig. 2.2, shows that the effect of the furniture on the point values of the field strength is not negligible. However it is evident that at some small sections along

the line of observation, the two curves provide very close values. However at most sections of the graph the two curves are not in good agreement.

It is seen in Fig. 2.2 that there are some points at which the CST curve accounting for some furniture has higher values than the CST curve accounting for no furniture. Also it is seen that at an adjacent or a nearby point, the field accounting for some furniture has lower value than the field accounting for no furniture. This can make one anticipate that if the probability distribution of the field strength around some point is obtained, the with- and without-furniture cases may not show a big difference. This implies that the calculation of the risk of exceeding immunity, which is a major objective of this thesis, may be immune to the presence of furniture.

But should the distribution function be obtained for a set of points along a small line segment or over a local area or within a volume? And how large should the line segment/local area/local volume be? These questions are answered in the following. Afterwards the effect of furniture on the probability distribution of the field strength over a local area is investigated.

2.2.2 Volume, Area and Line Distributions

An object, a medical device for example, occupies a volume. Hence the probability distribution should be given for a volumetric region. In an indoor environment such as a large emergency room, full-wave solutions of the Maxwell equations cannot be used. Ray-tracing is much more time-efficient and is widely used for these purposes. In ray-tracing, the burden of determining the field value at one point is independent from another. After determining the image tree, obtaining the field values for N points takes N-fold more computational time than for one point. Thus using the statistics of many points within a local volume to obtain the probability distribution can be too expensive. Using the local area and line statistics can reduce the computational time.

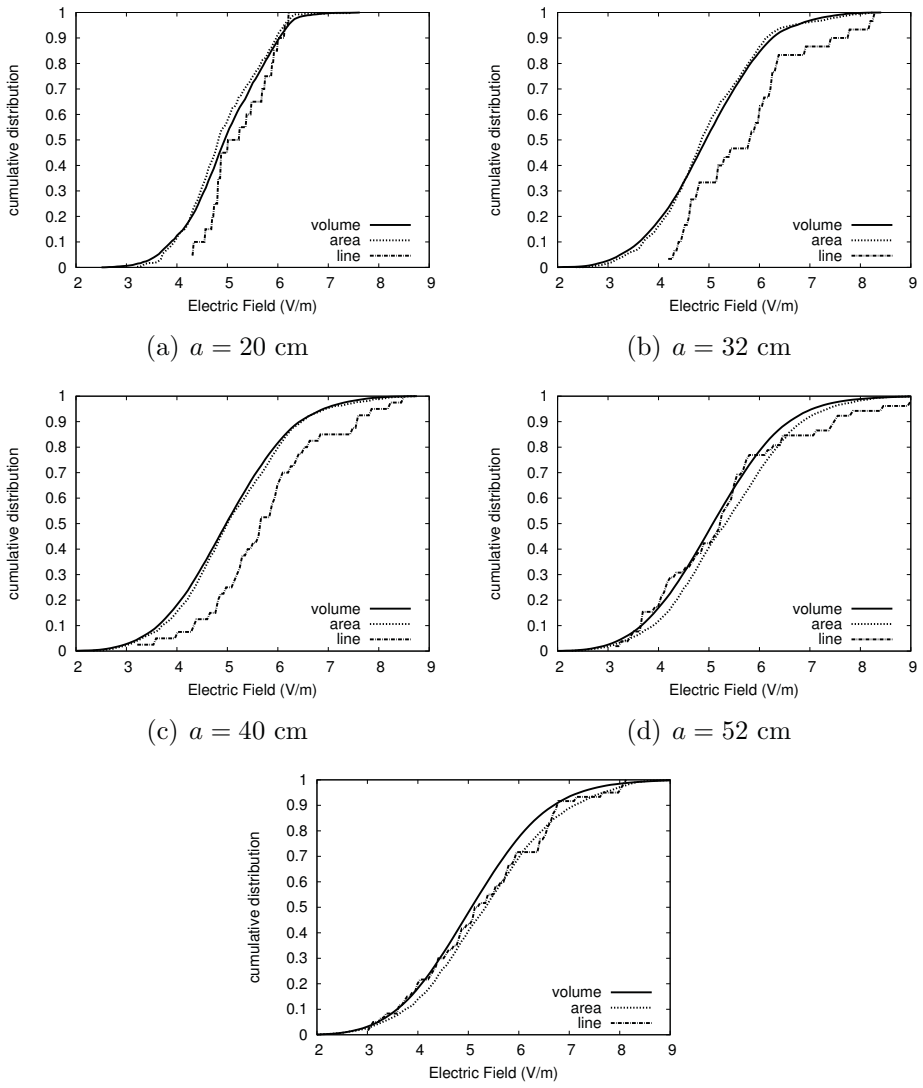

(a) $a = 20$ cm

(b) $a = 32$ cm

(c) $a = 40$ cm

(d) $a = 52$ cm

(e) $a = 60$ cm

Figure 2.3: Comparison of the cdf of the electric field intensities within a volume, area and line around a point P located at ($x = 1.8$ m , $y = 2.3$ m, $z = 1.6$ m). In all cases the furniture is included in the simulation.

The values of the electric field intensity obtained by the CST in the presence of the furniture at many points around point P at ($x = 1.8$ m , $y = 2.3$ m, $z = 1.6$ m) with the aforementioned spacing are used to get three sample universes: one along a line segment of size a and parallel to the y axis, one over an area a by a in the xy plane and one within a volume a by a by a. The line segment and the local area are horizontal and located at the center of the volume. For each of the three sample universes, the cdf is obtained and presented in Fig. 2.3. All cdfs are obtained for five different sizes of a.

Figure 2.3 shows that if a is smaller than 40 cm, which is almost 3.3λ, the area cdf can very well approximate the volume cdf. However the line cdf never gives a good approximation of the volume cdf. Hence the local area estimate of the field strength statistics is used instead of the volumetric statistics. By the term *local area*, is meant a horizontal area of size equal to or smaller than 3.3λ by 3.3λ.

Having defined the local area and chosen it over the line and volume statistics of the field strength and having determined the size of the local area, the problem of the effect of furniture on the probability distribution of the field strength can now be addressed.

2.2.3 Furniture Effect on the Probability Distribution of the Field

The cdfs of the CST results (with and without furniture) over an area of $3.3\lambda \times 3.3\lambda$ are compared to each other. The cdf is obtained for the field distribution over a horizontal area (normal to z-axis) of 40 cm by 40 cm around point Q located at ($x = 1.7$ m , $y = 2.6$ m , $z = 1.6$ m) once with and then without the furniture. The two cdfs, compared in Fig. 2.4(a), are seen to be in close agreement. Hence the presence of some furniture does not considerably affect the field distribution.

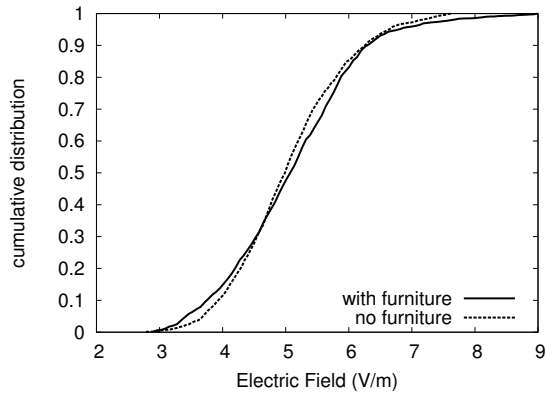

(a) Cdfs are obtained for a local area around point Q at (1.7 , 2.6 , 1.6).

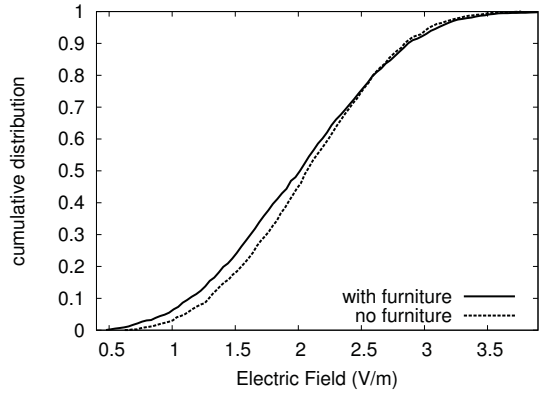

(b) Cdfs are obtained for a local area around point Q' at (1.7 , 1.1 , 1.6)

Figure 2.4: Cdf comparison (with furniture vs without furniture) at two different local areas of the same size: $3.3\lambda \times 3.3\lambda$.

This conclusion should not be generalized to all types of furniture. The furniture considered here includes 11 PEC cubes as part of the medical device located near point Q. The bed has metallic legs. The furniture considered here scatters the electromagnetic field. However the reflection from large metallic objects near the observation points may have stronger effects than small PEC cubes.

The comparison of the cdfs is repeated for a similar area around another point Q' located at (1.7 m , 1.1 m , 1.6 m) at a farther distance from the antenna. As seen in Fig. 2.4(b), the cdf of the field strength obtained without considering the furniture is a good approximation of the field distribution when the furniture is accounted for.

The results presented in Fig. 2.4(a) and 2.4(b) are obtained using the full-wave solution of the Maxwell equations. Some approximative methods are used in the following to reduce the computational time.

2.3 Approximative Methods for Determining Field Distribution

The local area cdf obtained by the ray-tracing method is shown to approximate the cdf obtained using the full-wave solver of the CST. Although the Sabine method cannot demonstrate the fast fading behavior of the field, it estimates the ray-tracing mean value and the multipath mean value. The Sabine method is not much used in the electromagnetic literature. Hence an application of this method in estimating E_{RM} and E_m is shown. The ray-tracing and Sabine methods are used later in this chapter to determine the risk of exceeding immunity.

2.3.1 Ray-tracing

The ray-tracing method is used to obtain the electromagnetic field in the hospital ward, shown in Fig. 2.1, accounting for no furniture. The electric field along a line parallel to the y-axis and passing through the antenna is seen in Fig. 2.2 where it is compared to the CST results. It is seen that there are small sections of the graph where the ray-tracing results match those of the CST (with no furniture). However in most parts of the graph, the results are slightly different. The purpose of using the ray-tracing method in this thesis is to determine the probability distribution of the field strength. Hence here the point values of the field strength, determined by ray-tracing, at many points within a local area are used to obtain the cdf. This cdf is compared to the cdf obtained using the CST results.

The cdfs are obtained for the field distribution over the same horizontal area

(normal to z-axis) of $3.3\lambda \times 3.3\lambda$ (40 cm by 40 cm) around the same point Q located at ($x = 1.7$ m, $y = 2.6$ m, $z = 1.6$ m). The two cdfs, compared in Fig. 2.5(a), show some agreement. The difference between the two curves are mostly below 0.05. The maximum difference is 0.12. The comparison is repeated at the point Q' which is even farther from the antenna. This comparison, given in Fig. 2.5(b), shows that the agreement between the ray-tracing and CST results is improved.

It is then concluded that the ray-tracing method is a reliable replacement of the full-wave methods in determining the probability distribution of the field strength over a local area. The results of Section 2.2.3 showed that the effect of some furniture on the cdf over a local area can be disregarded. Hence the ray-tracing results within an empty room can be used to estimate the probability distribution of the field strength in the presence of some furniture.

The probability distribution of the field strength cannot be directly obtained using the Sabine method. However the Sabine method gives the multipath mean value. Later in this chapter, it is shown that the Sabine estimate of the multipath mean value can be used together with a probability density function to give the field distribution.

2.3.2 Sabine Method

In the microwave lab (room H853) at Concordia University, which measures 7 m by 9 m and is shown in Fig. 2.6, a half-wave dipole is located at $x = 1.67$ m and $y = 5.1$ m and at the height of 1 m above the floor and is transmitting a 100 mW of CW signal at 2.45 GHz. There are some metal lockers at one end of the room.

It is seen in Fig. 2.7 that the Sabine estimate of the ray-tracing multipath mean value, E_m, along the path shown in Fig. 2.6, is within 0.9 dB of the ray-tracing result. With this similarity between the ray-tracing MMV and its Sabine estimate and considering the dominance of the direct field, the total ray-tracing mean value, E_{RM}, is expected to be well approximated by the Sabine method. This expectation

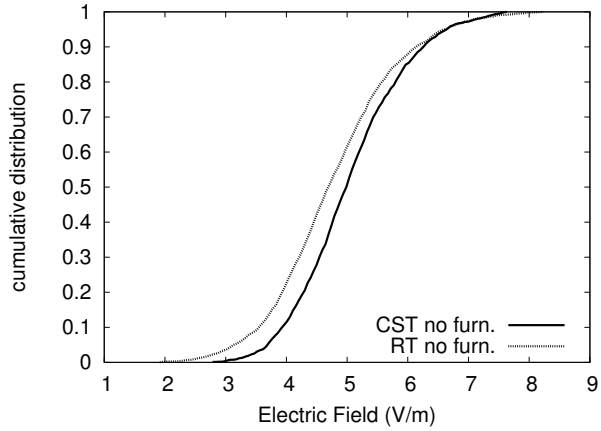

(a) Cdfs are obtained for a local area around point Q at (1.7 , 2.6 , 1.6).

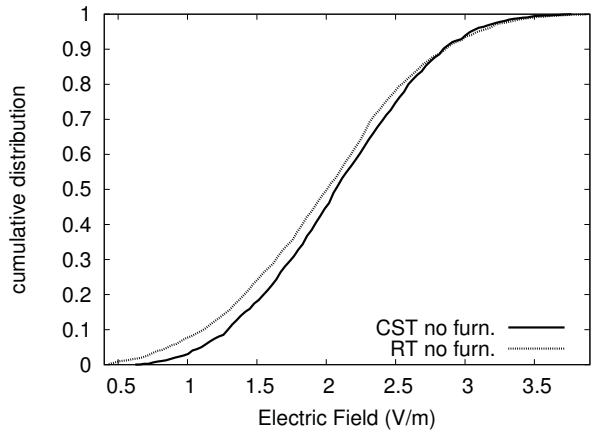

(b) Cdfs are obtained for a local area around point Q' at (1.7 , 1.1 , 1.6).

Figure 2.5: Cdf comparison. CST vs ray-tracing. No furniture is accounted for.

is proven correct in Fig. 2.8.

The multipath mean value, determined by ray-tracing or estimated by the Sabine method, and the direct field can be used together with a probability density function to provide the field distribution.

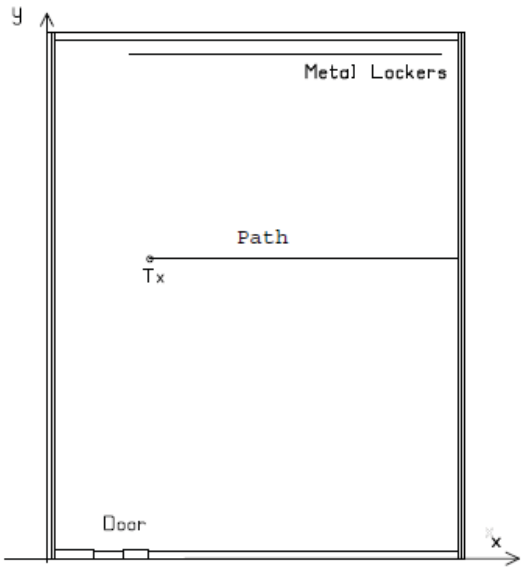

Figure 2.6: Microwave Lab Floor Plan

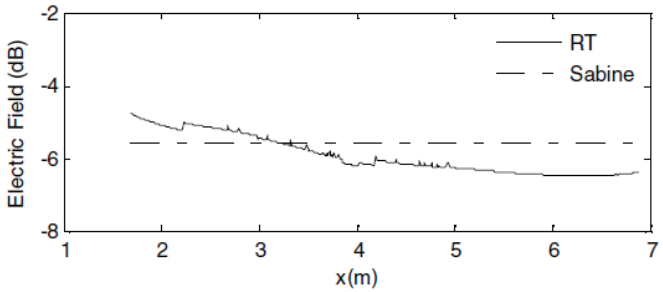

Figure 2.7: Multipath mean value; ray-tracing vs its Sabine approximation

2.4 Probability Density Functions Estimate the Electromagnetic Field

The Ricean, Rayleigh and Nakagami probability density functions are widely used to estimate the field distribution. These functions have parameters which are determined using large amounts of measurement or simulation data. The objective of this section is to emphasize that it is possible to use the direct field and multipath mean value at one single point to give the probability distribution of thousands of points within a local area around that point. The probability distribution is provided by a probability

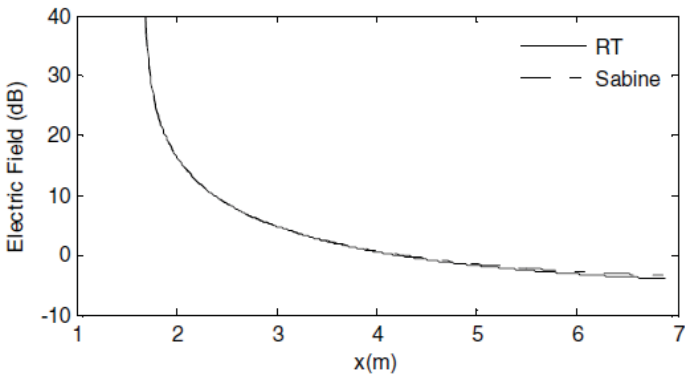

Figure 2.8: Ray-tracing mean value vs. its Sabine approximation.

density function whose parameters are obtained using the two mentioned quantities.

The Ricean and Rayleigh functions are compared in the following and the ray-tracing-Rice method is shown to be reliable even in close distances to the transmitter. Then the Ricean and Nakagami functions are compared. Finally in this chapter the Sabine-Rice approximation is used to obtain the risk of exceeding immunity.

2.4.1 The Ray-tracing-Rice Method

The Ricean and Rayleigh distributions are compared using a large and long room shown in Fig. 2.9. The direct field and the MMV are calculated at the center of each region (A, B, C, D and E) using ray-tracing. E_d and E_m are directly used as the Ricean parameters whereas $\sqrt{{E_d}^2 + {E_m}^2}$ is used as the Rayleigh parameter, E_g. Regions A, B, C and D measure $10\lambda \times 10\lambda$. Region E measures $6\lambda \times 6\lambda$. The transmitter is a half-wavelength dipole transmitting a 500 mW CW signal at the frequency of 2.45 GHz and located at (x = 2 m, y = 1.5 m), at the same height as the five regions i.e. 1.6 m. The Ricean and Rayleigh equations are then used to estimate the field at each region. These estimations are compared to the ray-tracing results which are statistically obtained from the field values of for 10,000 points spaced closely at distances of $\lambda/10$ within each region. The comparison is shown in Fig. 2.10.

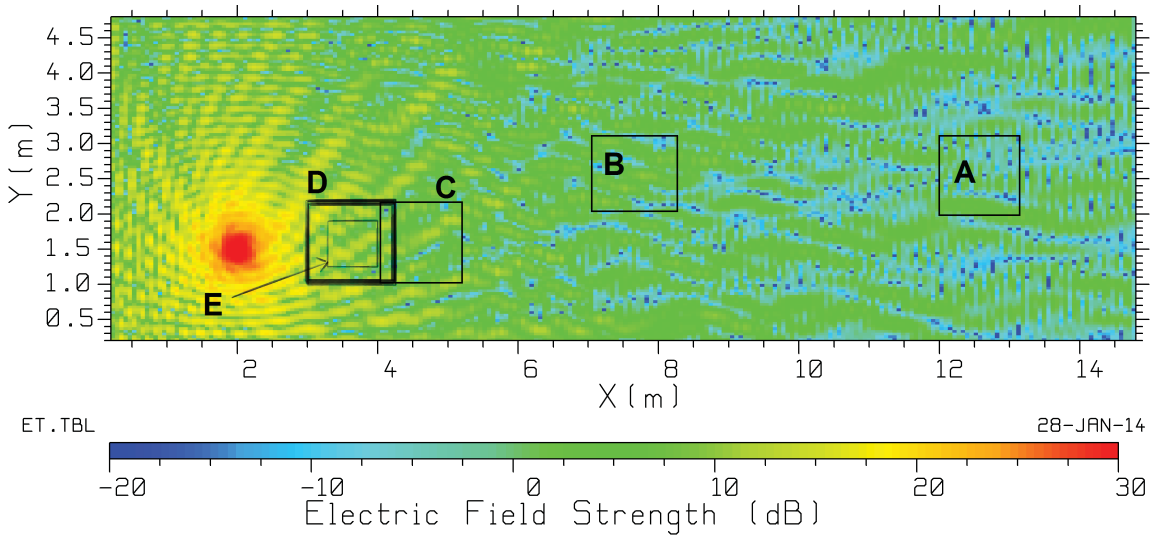

Figure 2.9: The floor plan and the field distribution in a long room.

It is shown in Fig. 2.10(a) that in the far zone, region A, the Rayleigh distribution is as accurate as the Ricean distribution. As the observation region is moved closer to the antenna, region B, it is shown in Fig. 2.10(b) that the Rayleigh distribution starts deviating slightly from the ray-tracing results. In the near region (C), it is seen in Fig. 2.10(c) that the difference between the Rayleigh distribution and the ray-tracing results is conspicuous while the Ricean distribution provides a much better estimate. In region D which is even closer to the transmitter, it is seen in Fig. 2.10(d) that even the Ricean estimation of the ray-tracing results is not accurate. This is due to the variations of the direct field in the region. As the observation area approaches the transmitter the direct field variations become more important. In a smaller region, E, it is seen in Fig. 2.10(e) that the Ricean distribution becomes reliable again. This is because of the smaller size of this region which prevents large variations of the direct field. The transmitter location might be close to the antenna therefore the Ricean function is preferred over the Rayleigh function. Using the direct field and multipath mean value as the parameters of the Ricean pdf is called the ray-tracing-Rice method.

So the Ricean distribution is a powerful tool in estimating the field distribution. In the following it is shown that this function is preferred to the Nakagami distribution.

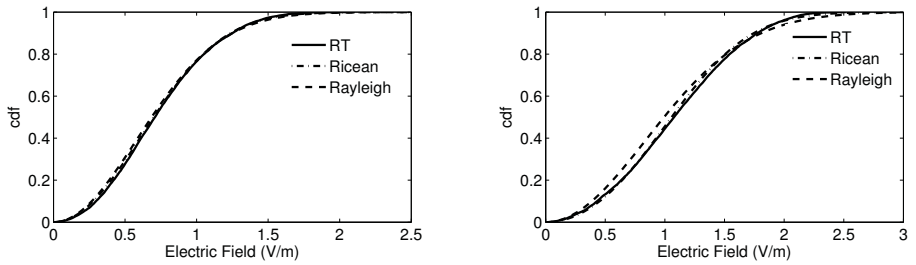

(a) The far region, A

(b) The medium distance region, B

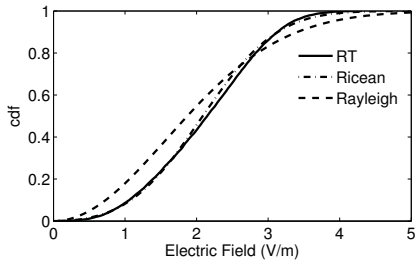

(c) The near region, C

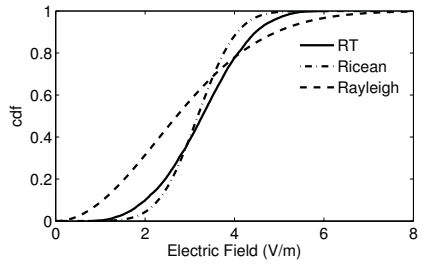

(d) The nearest region, D

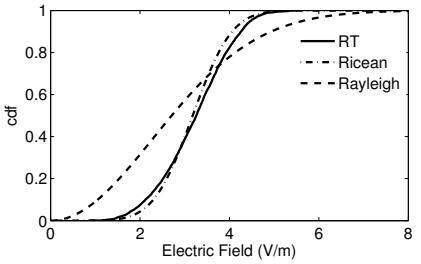

(e) The near and small region, E

Figure 2.10: The Ricean and Rayleigh distributions estimate the ray-tracing results in far, medium distance and near regions.

2.4.2 Ricean Distribution Preferred over Nakagami

Assume function F_1 of x with parameters a_0 and a_1 and function F_2 of x with parameters b_0 and b_1, both defined for $x > 0$. If for all pairs of a_0 and a_1, there exists a pair of b_0 and b_1 such that $F_1(x) = F_2(x)$ for $x > 0$, and if for all pairs of b_0 and b_1, there exists a pair of a_0 and a_1 such that $F_2 = F_1$ then F_1 and F_2 are different representations of each other. This means that in practical usage, there is no benefit in choosing one over the other unless for simplicity and computational reasons.

In the following, it is shown that there is a pair of Nakagami parameters such that the Nakagami function can closely approximate the Ricean function for any pair of Ricean parameters. Then it is shown that for the electromagnetically meaningful range of Nakagami parameters, there is a pair of Ricean parameters such that the Ricean function closely estimates the Nakagami distribution.

Nakagami Function Represents Ricean Function

It is shown here that for all Ricean parameters, i.e. E_d and E_m, the Nakagami parameters, m and w, can be found such that the two functions are equal. This means that the Ricean distribution can be represented by the Nakagami distribution. In the following, different values of the Ricean parameters are chosen.

Eight pairs of Ricean parameters, (E_d, E_m), are assumed. The parameters of the Nakagami distribution are found, using the *least squares* as a curve-fitting technique, such that the Nakagami function (1.14) gives the best possible approximation of the Ricean function (1.11). This is repeated for the following cases: A) $E_d = 10$ and $E_m = 0.7071$ B) $E_d = 5$ and $E_m = 0.7071$ C) $E_d = 2$ and $E_m = 0.7071$ D) $E_d = 1$ and $E_m = 0.7071$ E) $E_d = 0.5$ and $E_m = 0.7071$ F) $E_d = 0.1$ and $E_m = 0.7071$ G) $E_d = 0$ and $E_m = 0.7071$ H) $E_d = 0$ and $E_m = 7.0711$. In terms of the Ricean K-factor these cases cover a wide range of K, from high to zero.[1] The assumed Ricean parameters and the calculated Nakagami parameters for each of the eight cases are given in Table 2.1. In each case, the assumed Ricean function and the obtained Nakagami function are compared in Fig. 2.11 where all the eight cases are presented. This figure contains eight cases or comparisons thus 16 curves.

In the plot of case A, shown in Fig. 2.11, there are two curves; one for the Ricean function with the assumed parameters and one for the Nakagami function with the parameters obtained such that it matches the Ricean function. The two curves are

[1] A Ricean K-factor is considered small if it is smaller than 1, large if greater than 100, and medium if between the two.

Table 2.1: Ricean and Nakagami Parameters

	Ricean parameters (assumed)		Nakagami parameters (calculated)	
cases	E_d	E_m	m	w
A	10.00	0.7071	100.6564	100.6248
B	5.000	0.7071	25.6572	25.6243
C	2.000	0.7071	4.6618	4.6197
D	1.000	0.7071	1.6662	1.5914
E	0.500	0.7071	1.0607	0.7710
F	0.100	0.7071	1.0001	0.5101
G	0.000	0.7071	1.0000	0.5000
H	0.000	7.0711	1.0000	5.000

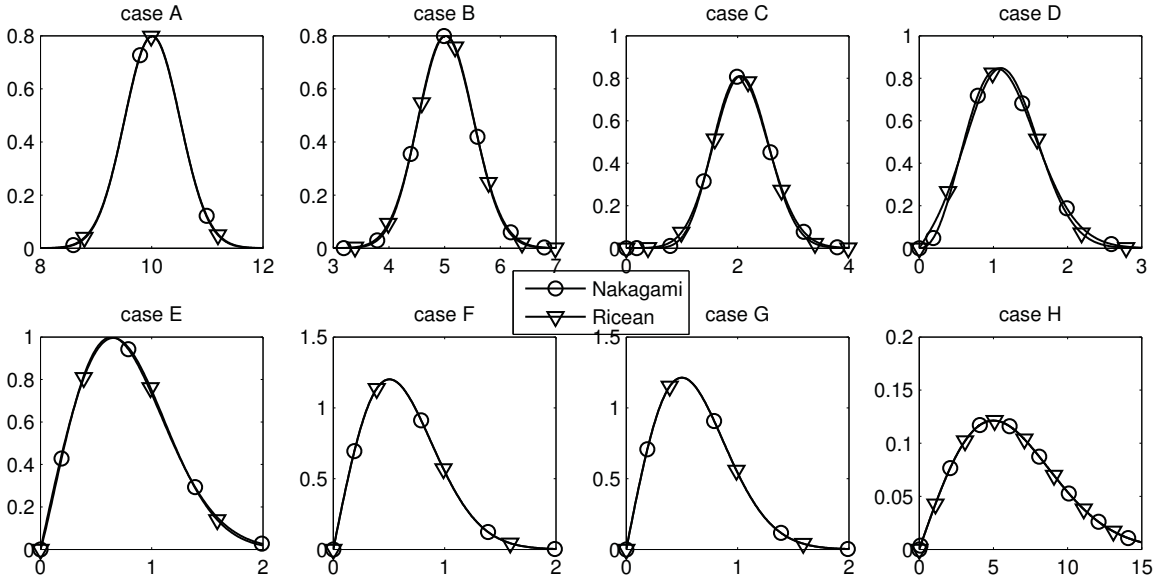

Figure 2.11: Ricean distribution with predefined E_d and E_m, vs Nakagami function with parameters determined to estimate the Ricean function as closely as possible. The comparison is repeated for eight different value-pairs of E_d and E_m, grouped as A through H. For the Ricean and Nakagami parameters see Table 2.1. In all plots, the horizontal axes show E and the vertical axes show the pdf.

on top of each other thus are identical. A similar observation is made in Case B. In both A and B cases, the direct field is much higher than the MMV. Also in cases E, F, G and H where the direct field is either much smaller than the multipath mean value or zero, the Nakagami distribution is the same as the Ricean. Hence the Nakagami distribution cannot offer any improvement over the Ricean, in these cases.

It is in cases C and D that some slight changes between the Nakagami and Ricean distributions are observed. These cases, in which the direct field is neither much greater than the multipath mean value nor much smaller, are comparable to the medium range distance of Fig. 2.9. For this range, it is shown in Fig. 2.10(b) that the Ricean distribution is already an accurate estimation of the field strength. Any modification the Nakagami distribution could offer would either damage the accuracy or be trivial and negligible.

Ricean Function Partly Represents Nakagami Function

To show that the Ricean function can represent the Nakagami function, start with assuming a pair of Nakagami parameters, (m, w), and determine the Ricean parameters such that the two functions equal or are as close as possible. Use the calculated Nakagami parameters in the foregoing as the assumed parameters here. Now there is no need to calculate the Ricean parameters. The assumed Ricean parameters in the foregoing can be used now as the calculated Ricean parameters. Repeat this for all eight cases. Hence the values given in Table 2.1 can be used here again except the titles "calculated" and "assumed" must be exchanged. Does this mean that there exists a Ricean function such that it can represent the Nakagami function for any pair of its parameters?

A closer look at Table 2.1 reveals that all of the values of the m parameter of the Nakagami distribution are above 1. Further computations show that no pair of Ricean parameters can be found such that m is calculated to be below 1.

In the following it is shown that the Nakagami distribution with $m < 1$ does not represent a likely electromagnetic field. In Table 2.1 it is shown that as the direct field tends to zero, m tend to 1. For a fixed value of $w = 0.5$, the Nakagami pdf is plotted for different value of m less than or equal to 1. Fig. 2.12 shows that as m

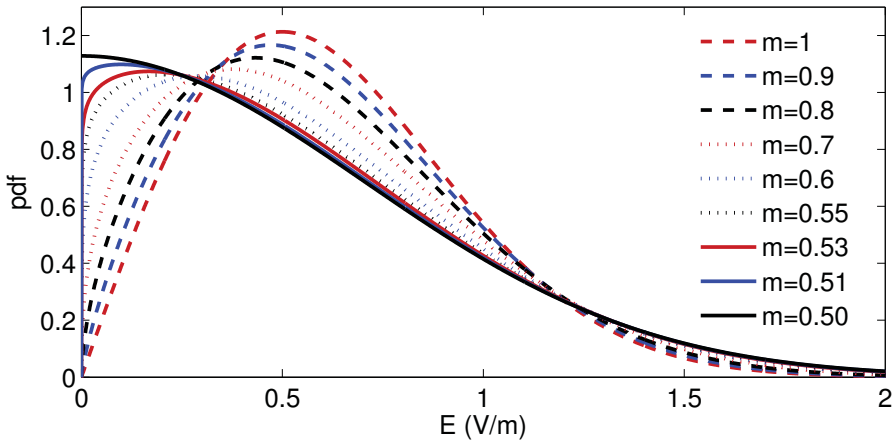

Figure 2.12: Nakagami pdf for different values of m. The parameter w is fixed at 0.5

decreases the peak of the pdf curve occur at smaller values of E.

Let E_{pR} be the value at which the Ricean pdf has a maximum and let E_{pN} be the value at which the Nakagami distribution has a maximum. We know that for a given E_m, E_{pR} gets smaller and tends to a nonzero value as E_d tends to zero. This nonzero limit of E_{pR} is in fact where the Rayleigh distribution with $E_g = E_m$ has a maximum.

When $E_d = 0$, there is only the multipath field with no direct field. If with $E_d = 0$ and a given E_m, the peak of the pdf of certain electromagnetic field distribution occurs at a value less than where the Rayleigh distribution has a maximum, this means that the phases of the field components are not perfectly random and they are mostly out of phase. This behavior is not simulated by a Rayleigh or a Ricean event by their definitions. However it seems that the Nakagami distribution can account for this behavior.

The curves in Fig. 2.12 demonstrate this behavior. When $m = 0.5$, the peak of

the Nakagami curve occurs at 0. Lower values of the m parameter are not shown here. In the extreme case when m tends to zero, the Nakagami pdf resembles the Dirac delta function concentrated at zero. In terms of the multipath field this could mean that the set of the rays arriving at all observation points can be divided into two subsets. In one subset the phases may be distributed over very small fraction of the interval $(0, 2\pi)$ and in the other subset the phases are distributed over the same interval but with a π phase difference. To examine this hypothesis, the following analysis is conducted.

The pdf of a universe of random samples, with two related phase distributions, is shown to be well approximated by the Nakagami function. The Ricean function is shown to fail in providing any estimate. To generate one Nakagami random outcome, 1000 random numbers are generated. 500 of these random numbers are distributed uniformly over the open interval $(-\pi/10, \pi/10)$ and 500 over $(\pi - \pi/10, \pi + \pi/10)$. Each of these distributions are called D_1 and D_2 respectively. The following number is evaluated.

$$Ee^{j\phi} = \sum_{i=1}^{500} ae^{j\phi_i^{(1)}} + \sum_{i=501}^{1000} ae^{j\phi_i^{(2)}} \tag{2.1}$$

where $\phi_i^{(1)}$'s have D_1 type distribution and $\phi_i^{(2)}$'s have D_2 type distribution. The MMV is 1 V/m hence a is $\sqrt{1^2/1000}$ V/m.

Generating random numbers using (2.1) is repeated 10,000 times and the probability distribution of this random event, $p_D(E)$, is statistically obtained. The Ricean function is expected not to be capable of estimating $p_D(E)$, for the phases are far from being uniformly distributed over the entire range of $(0, 2\pi)$. The performance of Nakagami and Ricean functions in estimating this distribution is compared in Fig. 2.13. To obtain the Ricean and Nakagami curves, the parameters of both functions are found to give the closest possible estimate of this distribution. There is no dominant component so for the Ricean distribution it is assumed that the direct field is zero,

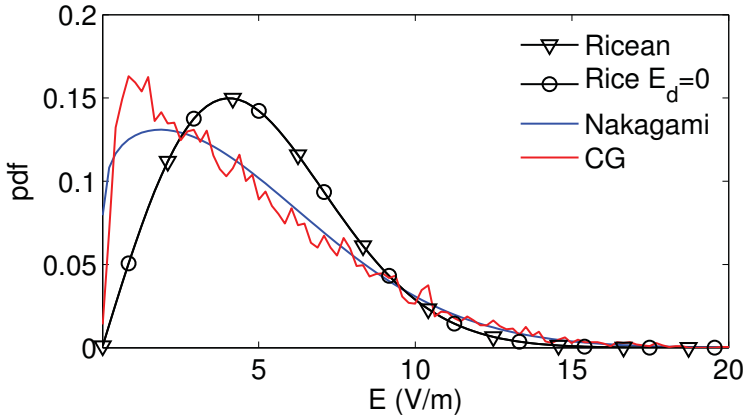

(a) pdf

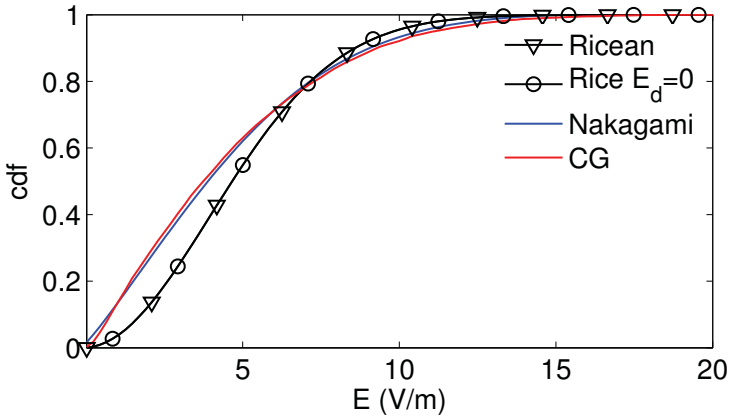

(b) cdf

Figure 2.13: Nakagami function can but Ricean cannot estimate the probability distribution of the computer generated (CG) random numbers whose phases are distributed uniformly over these intervals: $(-\pi/10, \pi/10)$ and $(\pi - \pi/10, \pi + \pi/10)$

$E_d = 0$, making it in fact a Rayleigh distribution. Hence in Ricean estimation, only the parameter E_m is determined which is found to be 5.7205 V/m. For this Ricean function, see the curve marked "Rice $E_d = 0$" in Fig. 2.13. The Nakagami parameters are found to be $m = 0.5721$ and $w = 32.72$. Note that m is smaller than 1.

It is shown in Fig. 2.13 that, as expected, the Ricean function is not capable of providing a valid estimate of the distribution of the computer-generated (CG) random numbers. However the Nakagami distribution provides a close estimate of p_D.

It is worthwhile to estimate the computer-generated randoms numbers using a

Ricean function where both E_d and E_m can take any values. This estimation is performed and E_d is found to be 0.22 V/m and E_m is found to be 5.7169 V/m.[2] The curve of this Ricean function with two degrees of freedom is shown in Fig. 2.13 which is the curve marked "Ricean". It is seen that this curve is almost identical to the curve of the Ricean function with $E_d = 0$.

This concludes the proof that the Ricean function cannot estimate the pdf of the random numbers described by (2.1) while the Nakagami function provides a close estimate.

The distribution defined by (2.1) is not very likely to happen in a real electromagnetic scenario. It is then deduced that for all the electromagnetically meaningful range of the parameters of the Nakagami distribution and for the entire range of the Ricean parameters, the two functions are simply different representations of each other. Hence the two functions are almost equally valid in estimating the field distribution. However the parameters of the Ricean function was shown to be directly obtained using ray-tracing. The Nakagami parameters are found with further computations, e.g. using some curve-fitting techniques. Hence the use of the Nakagami distribution is not recommended for characterizing indoor propagation.

So it is confirmed that the RTR method is the best solution for providing the probability distribution within an area. However there are situations in which the transmitter location changes. Determining the multipath mean value at the centers of all the local areas and then repeating it for thousands of different locations of the transmitter might be computationally expensive. In this situation the Sabine-Rice approximation can provide a faster estimate of the field distribution.

[2] E_d was expected to be 0. According to the initial value of E_d and the error tolerance in the curve-fitting process, it is possible to obtain a lower value of E_d however it is insightful to see that increasing E_d from 0 to 0.22 V/m does not considerably affect the Ricean function when $E_m = 5.72$ V/m.

2.4.3 The Sabine-Rice Approximation

The risk of exceeding immunity is obtained using the Sabine-Rice approximation and is compared to the ray-tracing results. It is shown that the SR approximation is a reliable estimate of the ray-tracing results.

Part of a hospital emergency room is shown in Fig. 2.14. The large observation area over which the field will be determined is enclosed by dashed lines and extends from $x = 44$ m to $x = 53$ m and from $y = 11$ m to $y = 15$ m. The transmitter is located at ($x = 45$ m, $y = 13$ m, $z = 1.4$ m), radiating 800 mW of power at 2450 MHz. The Sabine method is used to obtain the multipath mean value over the large observation area which is at the same height as the antenna. The Sabine-estimated MMV and the direct field intensity at the center of small local areas are used in the Ricean formula to give the probability distribution of the field strength within the area. This is called the Sabine-Rice approximation. Instead of showing the cdf curves for several local areas, the Ricean pdf (evaluated using the Sabine-approximated parameters) is used to obtain the risk of exceeding immunity over the large observation area.

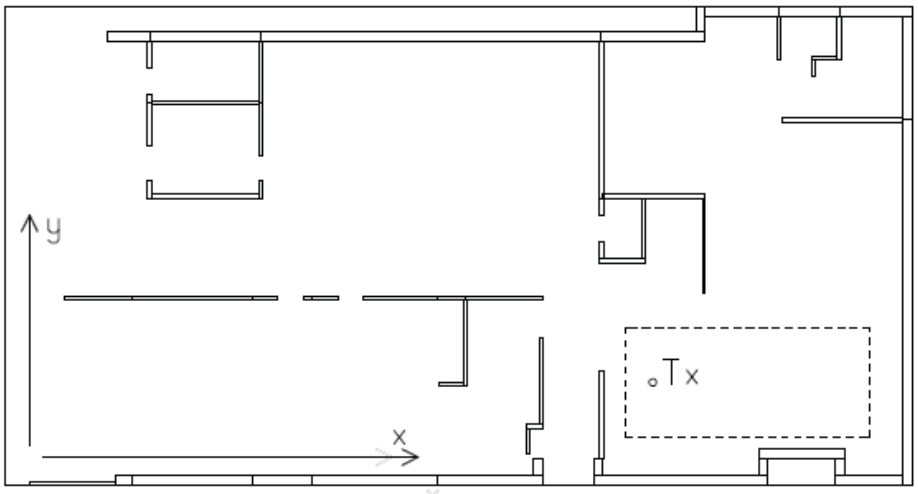

Figure 2.14: The floor plan of an emergency room.

Risk of Exceeding Immunity

The risk of exceeding immunity is defined as the likelihood of having an electric field intensity greater than the immunity level of a medical device within a local area occupied by the EMD. With this definition, the REI becomes equal to $1 - \mathrm{cdf}(\mathrm{E_I})$.

Suppose that the transmitter at (x', y') and the receiver at (x, y) are separated by distance r. If the immunity level is $\mathrm{E_I}$, then the risk of exceeding immunity for this distance is

$$P_c\left(E \geq \mathrm{E_I}, x, y, x', y'\right) = \int_{\mathrm{E_I}}^{\infty} p_c(E)\,\mathrm{d}E \tag{2.2}$$

where $p_c(E)$ is given by (1.11).

Over the large observation area, the REI is obtained using both the SR approximation and the ray-tracing results. The observation area is divided into 3.3λ by 3.3λ areas. The ray-tracing results at many points within a local area is used statistically to determine the REI within that local area. The REI is a function of location and the calculated value of the REI is associated with the center point, Q, of the local area, LA. So the REI at an adjacent point, Q', is associated with a local area, LA', of the same size but centered at Q'. LA and LA' may or may not overlap depending on the distance between Q and Q'.

At the center point of a local area, the direct field and the MMV obtained by the Sabine method are used in the Ricean pdf to determine the SR estimate of the risk of exceeding immunity. Using both methods, the risk maps are obtained for $\mathrm{E_I} = 3$ V/m and presented in Fig. 2.15. Also the risk of exceeding immunity is given over the line $y = 13$ which passes through the antenna. This comparison of the SR and ray-tracing methods, given for two different immunity levels (3 and 10 V/m), is shown in Fig. 2.16. It is seen that the SR approximation provides a sound estimate of the REI obtained by ray-tracing.

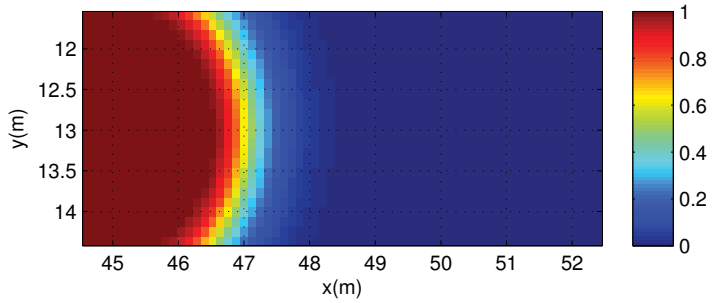

(a) REI by Sabine-Rice

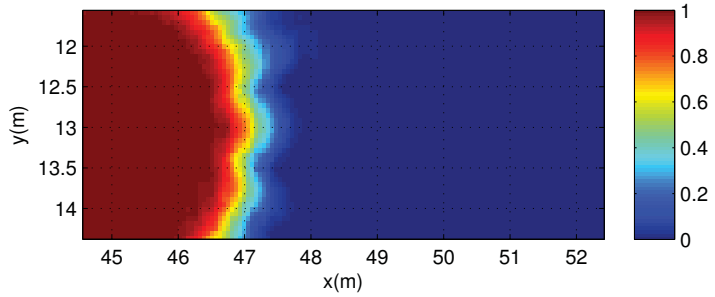

(b) REI by GO

Figure 2.15: The risk of exceeding the immunity of 3 V/m over the large observation area shown by the dashed line in Fig. 2.14.

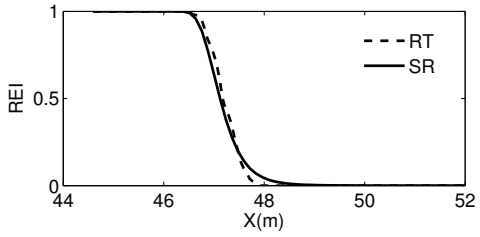

(a) $E_I = 3$ V/m

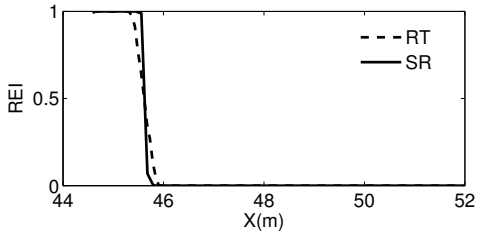

(b) $E_I = 10$ V/m

Figure 2.16: The REI along the line $y = 13$ passing through the Tx and within the dashed line shown in Fig. 2.14. Ray-tracing vs Sabine-Rice

The REI is one of the most important parameters considered. The REI is approximated using the SR method in Chapter 5. Hence it is worthwhile to give a quantitative gauge for measuring the agreement between the REI obtained using the ray-tracing method and its Sabine-Rice approximation.

Error Calculation Assume the REI is defined over an interval $a \leq x \leq b$. Let P_1 be a partition of this interval given by the finite sequence of $x_0^{(1)}, x_1^{(1)}, \ldots, x_n^{(1)}$. Assume that the REI obtained using the ray-tracing method, REI(RT), is defined over P_1. Let P_2 be a partition of the aforementioned interval given by the finite sequence of $x_0^{(2)}, x_1^{(2)}, \ldots, x_m^{(2)}$. Assume that the REI obtained using the SR approximation, REI(SR), is defined over P_2. The error, REI(SR)−REI(RT), is determinable only when the two partitions P_1 and P_2 are the same which is not the case here. Different meshes were used to to apply the ray-tracing and Sabine methods. Hence a common refinement of the two partitions is determined: P_3. Linear interpolation is used to obtain the REI(RT) and REI(SR) over P_3. Thus the error is calculated at each point of P_3.

The *mean value*, arithmetic mean, and the *standard deviation* of error in the case of the 3 V/m immunity level are -0.0022 and 0.0281 respectively. The maximum REI is 1 according to which the percentage of the mean and standard deviation are -0.22% and 2.81% respectively. In the case of 10 V/m immunity level, the mean value and the standard deviation are 1.1% and 4.75%.

2.5 Summary

In this chapter, the probability distribution of the electromagnetic field in the presence of one transmitter with fixed location was investigated. The effect of furniture on the field distribution was investigated. A local area of a certain size was shown to be a good approximation of the volumetric data. The ray-tracing-Rice and Sabine-Rice

methods were used and shown to be reliable in field estimation.

The time-domain solver of the CST software was used to obtain the electromagnetic field in a small room with a half-wave dipole antenna operating at 2.45 GHz. Fig. 2.3 showed that the probability distribution of the volumetric data of the field strength can be approximated by the area distribution if each side of the considered area and volume is chosen to be no more than around 3.3 wavelengths. The cdf along a line does not provide a good approximation of the volume statistics of the field.

It was shown that the presence of furniture affects the point values of the electric field. Figs. 2.4(a) and 2.4(b) showed that the effect of some furniture on the probability distribution of the field strength within a local area is negligible.

Figs. 2.5(a) and 2.5(b) show that the ray-tracing method gives a good estimate of the field distribution obtained by the CST full-wave solution. Hence the room with some light furniture can be simulated with ray-tracing disregarding the furniture.

The ray-tracing solution at the center of an area was used to defined the *multipath mean value*. The MMV is used to obtain the parameters of the The Ricean and Rayleigh distributions. These pdfs were used to estimate the probability distribution of thousands of field values obtained using ray-tracing at the points within the local area. It is seen in Fig. 2.10 that the Rayleigh distribution is not suitable for near regions. It was shown that if the size of the local area is small enough, the Ricean distribution is accurate even in the regions near the antenna. Using the MMV at a single point with the Ricean function to estimate the field within a local area is called the ray-tracing-Rice method.

It was shown in Fig. 2.11 that for almost any pair of Ricean parameters, a pair of Nakagami parameters can be found such that the two functions are almost identical. Also if the Nakagami parameter m is greater than 1 then for any pair of Nakagami parameters, a pair of Ricean parameters were found such that both functions were

almost identical. The inequality $m > 1$ appears to represent the fact that, in ray-tracing, the phases of the field of all reflected rays arriving at a given location are uniformly distributed between 0 and 2π. Hence, if the phase distribution is almost uniform, which is the case in most indoor environments, the Nakagami and Ricean functions can be considered as different representations of each other. Determining the Ricean parameters is straightforward; they are equal to the direct field and the MMV at the center of the local area of interest. Nakagami parameters are not directly associated with electromagnetic concepts and their determination requires more computation. Hence the use of the Nakagami function in determining the probability distribution of the field strength in indoor environments is not recommended if no strong evidence exists suggesting any considerable degree of non-uniformity in the above-mentioned phase distribution.

Using the ray-tracing-Rice method provides significant improvement over the ray-tracing method where the tracing the rays are repeated for thousands of points within a local area. However this improvement in the computational time may not be sufficient if the transmitter moves and takes thousands of different locations for each of which the MMV calculation must be repeated. The Sabine method approximates the MMV much faster than ray-tracing. The Sabine-Rice approximation was shown, in Figs. 2.16(a) and 2.16(b), to provide a reliable estimate of the risk of exceeding immunity compared to the ray-tracing results. Hence The Sabine-Rice approximation is used in Chapter 5 to estimate the risk of exceeding immunity.

So the probability distribution of the electromagnetic field in a room equipped with some furniture can be given using the ray-tracing method ignoring the furniture. Also the RTR and the SR methods provide a close estimate of the probability distribution of the ray-tracing results. Hence a major conclusion is that the RTR and the SR methods, accounting for no furniture, can be used to give the probability distribution of the field strength in a room with some furniture. To maintain a reliable accuracy,

the size of the observation area must be reduced in regions close to the transmitter to compensate for the effect of the rapidly varying direct field.

In the next chapter, the RTR method is modified (the MRTR) to obtain a much higher computational speed while keeping the same accuracy. However, the MRTR is slower the SR method which is used in Chapter 5.

Chapter 3

The Modified Ray-Tracing-Rice Method

3.1 Introduction

The multipath mean value, used in the ray-tracing-Rice method, was obtained in the previous chapter considering reflections of up to order R. It is shown in the present chapter that the MMV associated with reflections of only third and higher orders is almost constant throughout the room and hence it does not need to be computed over the entire room. This fact is then used to develop and present the modified ray-tracing-Rice method. The MRTR is as accurate as but up to many orders of magnitude faster than the RTR method.

The MRTR method may still lack the required speed for a risk assessment problem where the transmitter takes thousands of different locations in the room. The Sabine-Rice method is much faster and is used in Chapter 5 where roaming transmitters are considered. The MRTR method is suitable for determining the risk of exceeding immunity in a worst-case scenario where several staff members carrying wireless devices have known locations in the room near a medical device. The MRTR is also useful in

a scenario where each of a few staff members can take a limited number of locations near an EMD.

In this chapter, the The MRTR is used to determine the REI in a small room. The result is compared to the REI obtained from the full-wave solution of the CST software, the ray-tracing and the RTR methods. The REI results obtained using the CST, ray-tracing and the RTR method are discussed first.

3.2 The REI in a Small Ward

The risk of exceeding immunity is calculated in the room shown in Fig. 2.1 along the observation path. This line passes through the antenna located at (1.7 m, 3.5 m, 1.6 m) and is along the $y-$axis. The dipole antenna is transmitting 427 mW at 2.45 GHz. For a point Q_y on the observation path, which is located at $(1.7, y, 1.6)$, the REI is determined statistically using the field intensity values of many points within the local area around this point. The field intensity values are once obtained using the CST software and then using ray-tracing. The furniture is not accounted for. Then for the point Q_y, the multipath mean value is determined using the ray-tracing method. The MMV and the direct field values at the single point Q_y are used in the Ricean function to estimate the probability distribution of the field over the local area around Q_y. This is the ray-tracing-Rice method. The REI given by (2.2), is

$$P_c\left(E \geq \mathrm{E_I}, x, y, x', y'\right) = \int_{\mathrm{E_I}}^{\infty} p_c(E)\,\mathrm{d}E.$$

where p_c is probability density function of the field that is the Ricean function.

The two statistical evaluations (using CST and ray-tracing results) of the risk of exceeding immunity and its RTR estimation are shown in Figs. 3.1 and 3.2 for the two immunity levels of 3 and 10 V/m. It is seen in Fig. 3.1 that the risk of exceeding the immunity of 3 V/m, determined by the statistical use of the field values obtained

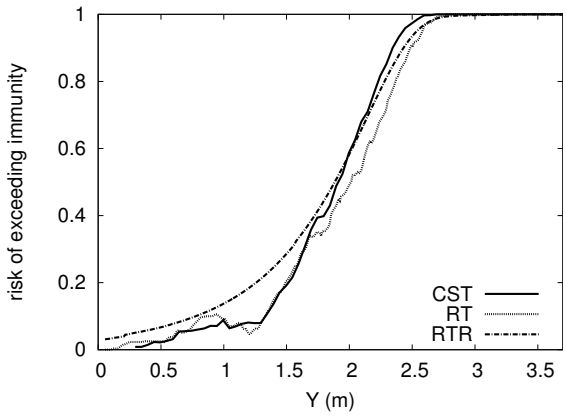

Figure 3.1: Risk of exceeding immunity. CST vs ray-tracing vs ray-tracing-Rice. $E_I = 03$ V/m.

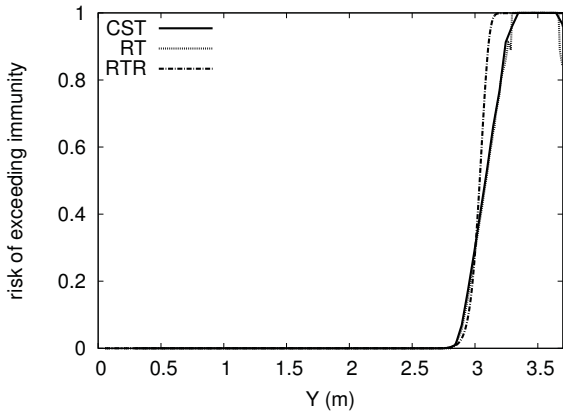

Figure 3.2: Risk of exceeding immunity. CST vs ray-tracing vs ray-tracing-Rice. $E_I = 10$ V/m.

by the CST software, is well matched by the RTR method's approximation at close distances to the antenna located at $y = 3.5$ m. At farther distances the RTR method provides a conservative, i.e. slightly larger, estimate of the CST results.

For a larger value of the immunity, that is for $E_I = 10$ V/m and at far distances from the antenna, it is seen in Fig. 3.2 that the risk given by the RTR method is in good agreement with the risk obtained using the CST results. For closer distances, the RTR approximation is rather conservative compared to the risk obtained using the full-wave solution.

Error Calculation The mean value, arithmetic mean, and the standard deviation of the error between the CST and RTR results, REI(CST)−REI(RTR), is determined according to the procedure explained in the previous chapter. For $E_I = 3$ V/m, the mean value of the error is -2.25% and its standard deviation is 4.52%. When $E_I = 10$ V/m, the error mean value is -1.56% and the standard deviation is 6.46%.

Therefore the RTR estimation of the risk, at both low and high immunity levels, is a safe approximation of the risk of exceeding immunity obtained using the full-wave solutions. This method is much faster than the full-wave solution. It is also faster than the ray-tracing solution where the risk is obtained using many field intensity values within a local area. It is shown in the following that the RTR method can be modified to further reduce the computational time.

3.3 The Modified Ray-tracing-Rice Method

Evaluation of the multipath field is computationally expensive; especially when higher orders of reflection are accounted for. In this section, it is shown that as the order of reflection increases, the power in the corresponding reflected rays becomes less dependent on the location of the receiver. This is then used to devise the modified ray-tracing-Rice method.

The power-based sum of the electric field in different levels of reflections are obtained and compared to each other in Fig. 3.3. Each curve is associated with a certain order of reflection. Evaluation is made along the line $x = 1.7$ m, $z = 1.6$. For example the value of the curve indicating the k'th order of reflection, at a given location is the square root of $\sum_{i=1}^{N_k} \left|\mathbf{E_r}^{(k)}(i)\right|^2$ where $\mathbf{E_r}^{(k)}(i)$ is the electric field vector phasor of the i'th ray, among a total of N_k which have been reflected exactly k times and have arrived at the given location. The square root of $\sum_{i=1}^{N_k} \left|\mathbf{E_r}^{(k)}(i)\right|^2$ is called the k'th order rays mean value.

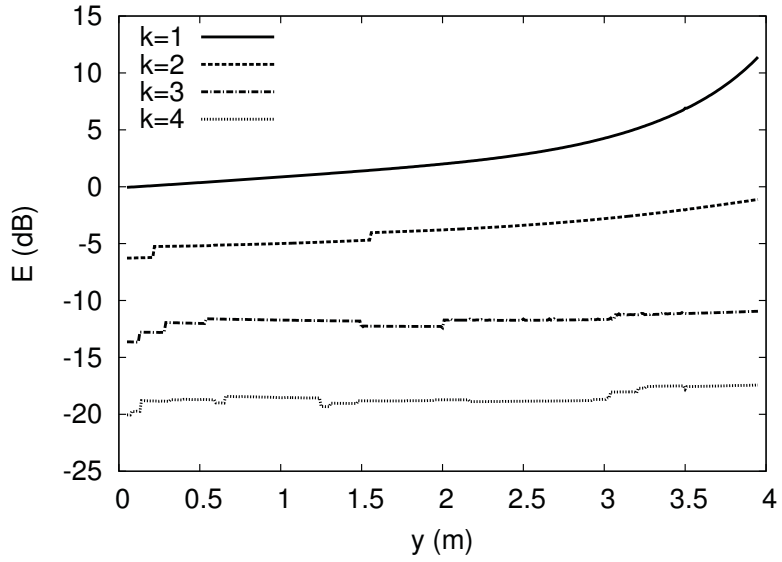

Figure 3.3: The k'th order rays mean value as a function of location.

It is seen in Fig. 3.3 that the field strength associated with the first order reflections, i.e. the first order rays mean value, varies significantly by location. Over the observation path, from near $y = 0$ to near $y = 4$ m more than 10 dB change is seen in the first order rays mean value. The second order rays mean value does not vary as much but shows a 5 dB change along the line. However the third and fourth order rays mean values are seen to be almost constant. They vary by almost 1 dB along the line of observation for $y > 0.5$ m. Higher order rays mean value are expected to vary less or equally.

This property is used here to modify the ray-tracing-Rice method. The direct field remains to be the same as in the RTR method. The multipath mean value, at a location (x, y, z), was previously defined by (1.4) which is repeated in the following.

$$E_m(x, y, z) = \sqrt{\sum_{k=1}^{R} \sum_{i=1}^{N_k} \left| \mathbf{E_r}^{(k)}(i, x, y, z) \right|^2}.$$

The multipath mean value, in the new MRTR method, is defined by

$$E_m(x,y,z) = \sqrt{\sum_{i=1}^{N_1} \left|\mathbf{E_r}^{(1)}(i,x,y,z)\right|^2 + \sum_{i=1}^{N_2} \left|\mathbf{E_r}^{(2)}(i,x,y,z)\right|^2 + {E_{res}}^2}. \tag{3.1}$$

where E_{res} is called *the residual field* and is a constant number which is given by

$${E_{res}}^2 = \sum_{i=1}^{N_3} \left|\mathbf{E_r}^{(3)}(i,x_0,y_0,z_0)\right|^2 + \sum_{i=1}^{N_4} \left|\mathbf{E_r}^{(4)}(i,x_0,y_0,z_0)\right|^2 + \ldots + \sum_{i=1}^{N_R} \left|\mathbf{E_r}^{(R)}(i,x_0,y_0,z_0)\right|^2 \tag{3.2}$$

in which (x_0, y_0, z_0) indicates the position of the center of the room at the height of $z_0 = 1.6$ m. The residual field, E_{res}, which is computationally the most expensive part of the MMV, is calculated for one single point. But it can be used elsewhere to evaluate (3.1).

The multipath mean value given in (3.1) and the direct field are used in the Ricean equation to give the probability distribution of the field. Then the Ricean equation is integrated from $\mathrm{E_I}$ to ∞ to obtain the REI. Fig. 3.4 shows that for the immunity level of 3 V/m, the REI obtained by the modified ray-tracing-Rice method is almost identical to the ray-tracing-Rice results. In Fig. 3.5, it is that the REI ($\mathrm{E_I} = 10$ V/m) obtained by the MRTR method is almost identical to the MRTR method.

The accuracy of the MRTR method is accompanied by an immense reduction in the computational time which is what makes it intriguing.

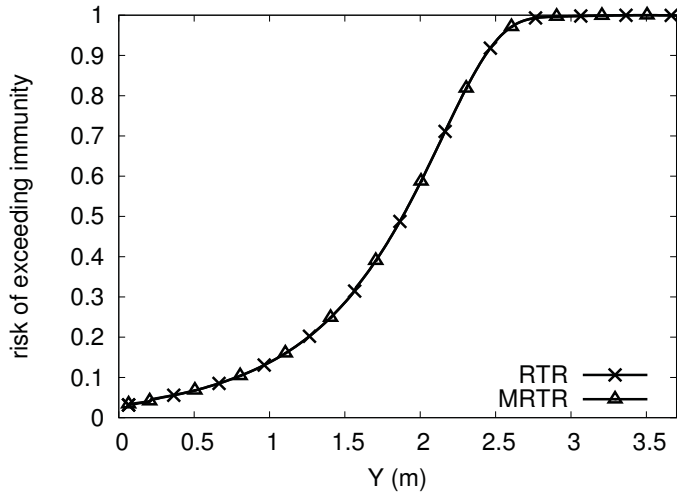

Figure 3.4: Risk of exceeding immunity. ray-tracing-Rice vs the new modified ray-tracing-Rice $E_I = 03$ V/m.

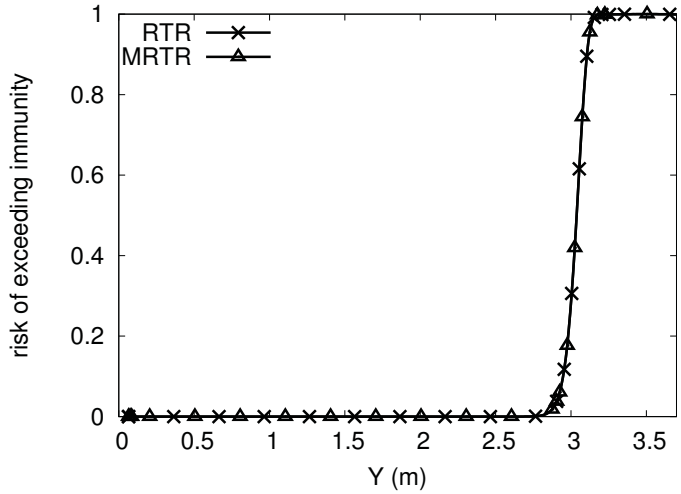

Figure 3.5: Risk of exceeding immunity. ray-tracing-Rice vs the new modified ray-tacing-Rice. $E_I = 10$ V/m.

3.3.1 Reduction in the Computational Time

If the total number of reflecting surfaces is W then the computational time for evaluating the first order rays mean value is proportional to W. In fact W is the number of first order images. Each image source has its own W images. Hence the number of second order images is W^2. Therefore the computational time for evaluating the second order rays mean value is proportional to W^2 and so forth. Hence the computational time for evaluating the multipath mean value, given by (1.4), is proportional to

$$W + W^2 + \ldots + W^R.$$

If there are N_{rx} receiver (observation) points, the total computational time in the RTR method is denoted by t_{RTR} for which the following holds.

$$t_{RTR} \propto N_{rx}(W + W^2 + \ldots + W^R). \tag{3.3}$$

In the MRTR method, the time required for one-time calculation of E_{res} is proportional to

$$W^3 + W^4 + \ldots + W^R.$$

Thus the time for evaluating (3.1) at N_{rx} points is denoted by t_{MRTR} for which the following holds.

$$t_{MRTR} \propto N_{rx}(W + W^2) + (W^3 + W^4 + \ldots + W^R) \tag{3.4}$$

The factor by which the computational time is reduced by the MRTR method is given by

$$q_t = \frac{t_{RTR}}{t_{MRTR}} = \frac{N_{rx}(W + W^2 + \ldots + W^R)}{N_{rx}(W + W^2) + (W^3 + W^4 + \ldots + W^R)}. \tag{3.5}$$

Since the Ricean equation is to be used to give the pdf of the field within a local

area, N_{rx} is in fact the number of the local areas. The direct field and the MMV are computed at the center of each local area measuring for example $3.3\lambda \times 3.3\lambda$. For this size of local area, the number of the local areas and the number of the observation points, N_{rx}, is 28. In the room shown in Fig. 2.1 the number of reflecting surfaces is 9 and reflections are accounted for up to the sixth level, meaning $R = 6$. Computing q_t, one can see that the MRTR is more than 27 times faster than the RTR method. Of course no accuracy is lost.

To get a smoother curve of REI, a larger N_{rx} is required. In general, if W is large and N_{rx} is much greater than W^{R-2}, then q_t tends to W^{R-2}. On the other hand, if W^{R-2} becomes much greater than N_{rx}, then q_t tends to N_{rx}.

3.4 Summary

In this chapter, the ray-tracing-Rice method was tested in a small room for two immunity levels. Then a concept called the residual field was defined and used in order to present the modified ray-tracing-Rice method which is much faster than but as accurate as the ray-tracing-Rice method.

For a local area, the RTR method uses the multipath mean value and the direct field at a single point in the center of the area as the Ricean parameters in order to give the probability distribution of the field strength within the area. In was shown in Section 3.2, that the RTR method is a reliable and conservative estimate of the risk of exceeding immunity for both immunity levels of 3 and 10 V/m.

The multipath mean value used in the RTR method is the power-based sum of the field strengths of all of the rays reflected once, twice, thrice and more. The power-based sum of the field values of the rays reflected exactly k times and arriving at a location, k'th order *rays mean values*, was determined separately for $k = 1, 2, 3$ and 4. It was shown in Fig. 3.3 that the first and the second order rays mean value can

considerably vary over the room. The third and higher order rays mean value did not show large variations. Hence they were considered to be constant and were used to define the residual field.

The residual field was defined for a single point in the room. It was obtained using (3.2). It is the power-based sum of all the field values of the rays arriving at a given location which have been reflected three times or more. Then (3.1) was used to obtain the MMV at the center points of all local areas of interest. The field distribution was determined using the Ricean function. This is called the modified ray-tracing-Rice method.

It was shown in both Fig. 3.4 and Fig. 3.5 that the result of the MRTR method is almost identical to that of the RTR method. The modified ray-tracing-Rice method is one or more orders of magnitude faster than the RTR method.

Using the residual field significantly reduces the computational time of determining the multipath mean value. The ray-tracing computational time grows linearly by the number of observation points but exponentially by the order of reflections accounted for. Since the reflections of orders three and higher are accounted for only at a single point in the room, the computational time of the modified ray-tracing-Rice method may be up to orders of magnitude lower than that of the ray-tracing-Rice method.

In the MRTR method, for each transmitter location, the first and second order reflections has to be calculated. Therefore this method may not be suitable when the transmitter takes thousands of different locations. In Chapter 5, where higher computational speed is required, the Sabine-Rice method is used. The accuracy of the Sabine-Rice approximation was found to be acceptable in the previous chapter.

The methods presented so far assume the presence of only one transmitter. The field distribution may be different in the presence of two transmitters which is the subject of the following chapter.

Chapter 4

On the Use of Ricean pdf for Characterizing Indoor Propagation in the Presence of Two and More Transmitters

4.1 Introduction

The Ricean probability density function was used in the previous two chapters to estimate the field distribution due to one transmitter. This chapter investigates whether the probability distribution of the sum field of two and more transmitters can be estimated using the Ricean function. The sum of two or more Ricean events does not match the criteria assumed for a Ricean random outcome. The Ricean random outcome was defined in (1.10) which is

$$Ee^{j\phi} = A_0 e^{j\phi_0} + \sum_{k=1}^{N} Ae^{j\phi_k}$$

where A_0 and A are arbitrary positive real numbers. A_0 is usually larger hence it is called the *dominant component*. The phase values, $\phi_k, k \geq 0$, are random numbers distributed uniformly between 0 and 2π.

A sum event is composed of two or more dominant components whereas in (1.10) there is one dominant component and the rest are small. Hence the probability distribution of the sum event is expected to be non-Ricean. The objective of this chapter is to show that the Ricean formula can be used to estimate the distribution of sum of the fields of two and more transmitters.

This chapter consists of two major parts: Section 4.2 and Section 4.3. The two sections and their conclusions are connected together since both of them use computer-generated random numbers as part of their simulations. In Section 4.2, the probability distributions of sum events consisting of two, three and four ideal Ricean events are given using computer-generated random numbers. Each Ricean event is generated using its parameters, E_{di} and E_{mi}. These parameters are then used to find E_{dt} and E_{mt} such that, when used as the parameters of the Ricean function, can give the pdf of the sum event.

In Section 4.3, a more in-depth analysis is given for the two-transmitter case. If there are two dominant components in (1.10), this event is represented by (1.15) which is

$$Ee^{j\phi} = A_0 e^{j\phi_0} + A_1 e^{j\phi_1} + \sum_{k=2}^{N} A_k e^{j\phi_k}$$

where A_0, A_1 and A are arbitrary positive real numbers. A_0 and A_1 are usually large thus called dominant. The phase values, $\phi_k, k \geq 0$, are random numbers distributed uniformly between 0 and 2π. The probability density function of an event whose many outcomes are defined by (1.15) is given by (1.16) which is

$$p(E) = E \int_0^\infty \exp\left(-\frac{x^2 {E_{dp}}^2}{4}\right) J_0(xE) J_0(A_0 x) J_0(A_1 x) x \, \mathrm{d}x$$

where J_0 is the Bessel function of the first kind and order zero.

The *diffuse power*, given by ${E_{dp}}^2 = (N-1)A^2$, is finite and nonzero. Equation (1.15) describes the phenomenon which is usually referred to as the two wave with diffuse power.

The TWDP has never been investigated using electromagnetic simulation. In [62], the pdf of the measured field did not match its TWDP prediction.

This chapter, for the first time, presents an electromagnetic verification of the TWDP formula. Ray-tracing is used for this purpose. In the TWDP theory the phases of all the components are assumed to be random. In indoor environment, the randomness of the phases of the field intensity vectors associated with the multipath or the reflected rays is almost guaranteed by the fact that these rays are reflected many times and a small change in the location of the observation point results in the increase of the phases of some components and decrease in some others. However the phases of the two direct fields, ϕ_0 and ϕ_1, might be correlated.

Assume the two transmitters in a room are in a position such that the phases of their direct fields over a local area, ϕ_0 and ϕ_1, behave as if they have little or no correlation. Without the TWDP formula, *only* the following can be surmised about the field distribution. At some points within the local area, the two dominant components are in-phase thus add up. So the field is determined by $A_0 + A_1$ plus (or minus) the multipath field. At some other points where the two phases have a difference of around π, the field is determined by $|A_0 - A_1|$ plus (or minus) the multipath field. There will also be some points with the total field intensity between $|A_0 - A_1|$ and $A_0 + A_1$. No further information can be given about the probability density function of the field over the local area from an electromagnetic point of view. It is shown in this chapter that, in case of non-correlated direct field phases, the pdf of the electric field is given by the TWDP formula (1.16) which is rather unknown in the electromagnetics community.

If the two transmitters are in a configuration where the phases of their direct fields in the local area are *correlated*, the TWDP theory is expected to fail. An example of such a configuration is when the two transmitting antennas are in line with the center of the local area. This situation resembles the end-fire direction of a two-antenna array in free space. When ϕ_0 and ϕ_1 are *related*, the TWDP must fail. The TWDP is used in the communications field where these cases are not investigated. Hence this very expected failure may be interesting in the communications society. The pdf obtained from the field values of many points over the local area is expected to be concentrated around A_0+A_1, if the distance between the transmitters (approximately) equals to an integer multiple of λ. The pdf obtained from the field values of many points over the local area is expected to be concentrated around $|A_0-A_1|$ if the distance between the transmitters is (approximately) equal to an odd multiple of $\lambda/2$. Assume that all of the field values over the local area for different distances between the two transmitters are collected together. Will the probability density of this collection be concentrated around $|A_0 - A_1|$ or $A_0 + A_1$ or somewhere between them? What will the exact pdf be?

The answer to this question is unknown. In this chapter, in Section 4.3.2, it is shown that the TWDP theory gives the pdf of the collection of the field intensities over the local area for many different distances between the two transmitters.

Later in this chapter for a specific and fixed location of the two transmitters in line with the center of the local area, it is shown that if the phases of the two direct fields are replaced by computer-generated random numbers, the pdf of the sum field follows the TWDP formula with no need for the movement of the transmitters. This concludes the proof that, for the fixed-location transmitters, in order for the TWDP to be always valid, ϕ_0 and ϕ_1 must be uncorrelated. This may initiate another research in the communications field to analyze the phase of the radiated signal of a transmitter in communication with an access point antenna.

To summarize, this chapter shows that the Ricean function gives the pdf of the sum of two Ricean events. This is shown in Section 4.2. The sum of two Ricean events is described by the TWDP theory which is shown to give the pdf of the field of two moving transmitters in Section 4.3.2. Hence it can be concluded that the pdf of the field of two moving transmitters can be approximated by a Ricean function. The Ricean approximation of the field due to two transmitters is used in Chapter 5 in order to determine the risk of exceeding immunity.

4.2 Two, Three and Four Ricean Events

The field distribution due to more than one transmitter is analyzed using computer-generated random numbers. The field of each transmitter is simulated as a Ricean event with a direct field and a multipath mean value. Assume that the set $ED = \{E_{d1}, E_{d2}, \ldots, E_{dN}\}$ contains all the values of the direct fields of the transmitters (independent events). N is the number of independent events. Similarly, EM, the set of multipath mean values, is $\{E_{m1}, E_{m2}, \ldots, E_{mN}\}$. Each event is created using many computer-generated random numbers following (1.10).

The Ricean function, given in (1.11), is used to estimate the probability distribution of the sum of the N events. The parameters of this Ricean function are denoted by E_{dt} and E_{mt} representing the largest direct field and the total multipath mean value. These parameters are defined by

$$E_{dt} = \max ED, \tag{4.1}$$

$$E_{mt} = \sqrt{\sum_{i=1}^{N}({E_{di}}^2 + {E_{mi}}^2) - {E_{dt}}^2}. \tag{4.2}$$

Equations (4.1) and (4.2) are used in (1.11) to approximate the distribution of sum of two, three and four distributions. The results are presented for three cases of

$N = 2$, 3 and 4.

4.2.1 Two Ricean Events, $N = 2$

To generate two Ricean events, some practical field values are used. These values are obtained in Chapter 5 where a 6.4 m by 6.5 m, four-bed hospital ward is considered. Two transmitters are in the room, each radiating 100 mW at 2.45 GHz. The multipath mean value for each transmitter is approximated by the Sabine method and is slightly more than 0.5 V/m thus here E_{m1} and E_{m2} are both assumed to be 0.5 V/m. The direct field intensity of an antenna in free space, E_{d1} or E_{d2}, is 10 V/m at 22 cm, 3 V/m at 74 cm and 1 V/m at 2.2 m. For these direct field values, respectively, the Ricean K-factors are 400, 36 and 4.

Four different cases are analyzed: (i) $E_{d1} = 10$ and $E_{d2} = 1$, (ii) $E_{d1} = 10$ and $E_{d2} = 3$, (iii) $E_{d1} = 3$ and $E_{d2} = 3$ and (iv) $E_{d1} = 10$ and $E_{d2} = 10$. For each event, 10,000 computer-generated Ricean random numbers are considered. This large set of outcomes is equivalent to considering 10,000 observation points for monitoring the field due to a transmitter in indoor environment. For generating each Ricean random number, 1000 values are used to represent the uniform phase distribution of the components in (1.10). This is equivalent to the arrival of 1000 rays at one observation point in ray-tracing. Two corresponding outcomes from the two Ricean events are added together to form one outcome of the sum event. Then the probability distribution of the sum event is determined statistically.

The probability and cumulative distribution functions of the sum events are compared to the estimation provided by the Ricean formula (1.11) in Figs. 4.1, 4.2, 4.3 and 4.4. It is seen in Fig. 4.1 that when one of the direct fields is much larger than the other (10 V/m and 1 V/m), the Ricean formula provides an estimation almost identical to the cdf of the sum of two Ricean events. When the smaller direct field is raised to 3 V/m, the probability distribution curves presented in Fig. 4.2 indicate

that the Ricean formula has slightly lost its perfect accuracy in estimating the cdf of the sum event.

If the dominant components, are both equal to 3 V/m, the accuracy in estimating the cdf is further decreased as shown in Fig. 4.3.

The worst case is when the direct fields are the same (10 V/m and 10 V/m) and both are much larger than the multipath mean values. The probability distribution curves are shown in Fig. 4.4. However even in this case, the difference in the risk of exceeding an immunity level, $1 - \mathrm{cdf}(\mathrm{E_I})$, would remain below 0.05 for most of the range of the electric field and would not exceed 0.15 at its worst situation.

It is shown in the following that adding a third transmitter improves the accuracy of the Ricean estimation of the sum events.

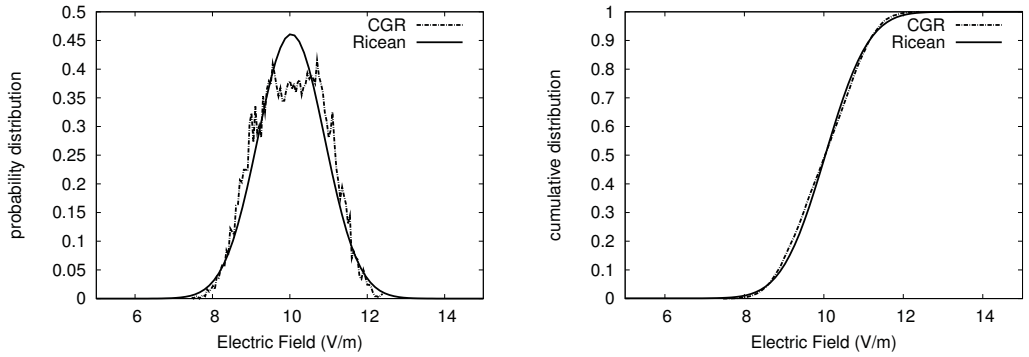

(a) pdf (b) cdf

Figure 4.1: Ricean approximation for the sum of two independent Ricean events simulated using computer-generated random numbers (CGR): $E_{d1} = 10$ and $E_{d2} = 1$.

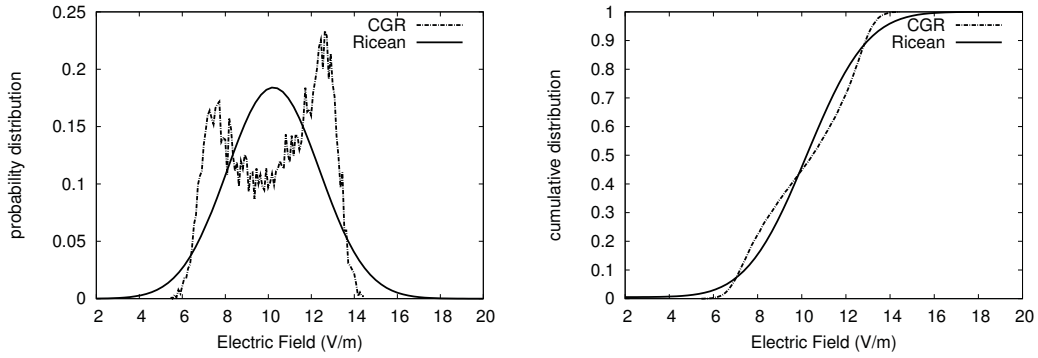

(a) pdf (b) cdf

Figure 4.2: Ricean approximation for the sum of two independent Ricean events simulated using computer-generated random numbers (CGR): $E_{d1} = 10$ and $E_{d2} = 3$.

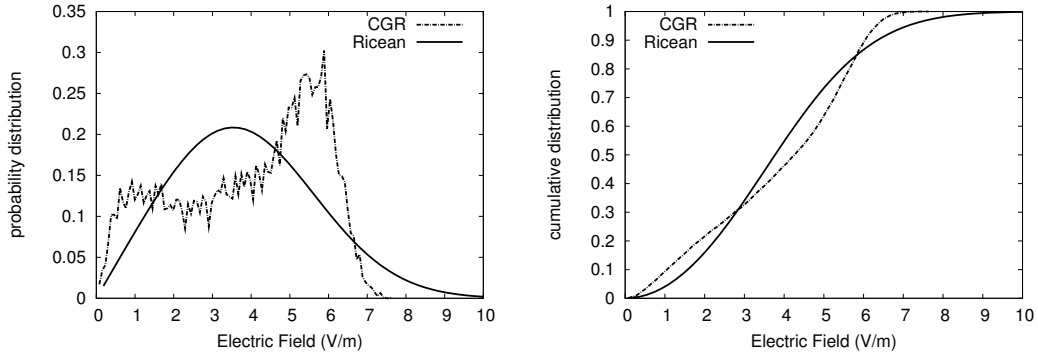

(a) pdf (b) cdf

Figure 4.3: Ricean approximation for the sum of two independent Ricean events simulated using computer-generated random numbers (CGR): $E_{d1} = 3$ and $E_{d2} = 3$.

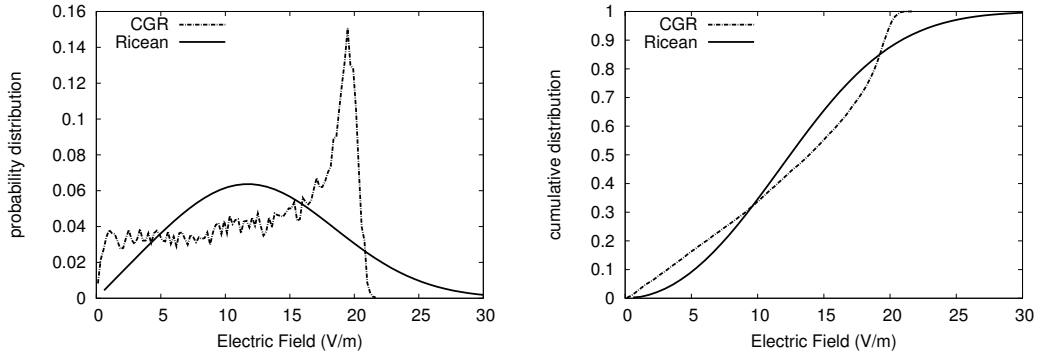

(a) pdf (b) cdf

Figure 4.4: Ricean approximation for the sum of two independent Ricean events simulated using computer-generated random numbers (CGR): $E_{d1} = 10$ and $E_{d2} = 10$.

4.2.2 Three Ricean Events, $N = 3$

Three Ricean events are generated. To obtain the sum event, the corresponding outcomes from the three events are added. The probability distribution of the sum event is compared to its estimation given by the Ricean formula with parameters as given in (4.1) and (4.2).

The multipath mean value for each three transmitter is 0.5 V/m. The direct field intensities are 12, 5 and 2 V/m. Thus all three K-factors are rather large: 576, 100 and 16. It is seen in Fig. 4.5(a) that the pdf curves have some disagreement. However, as seen in Fig. 4.5(b), the maximum difference between the cdf curves is around 0.05 which is the same as the maximum difference in the risk or probability of exceeding immunity.

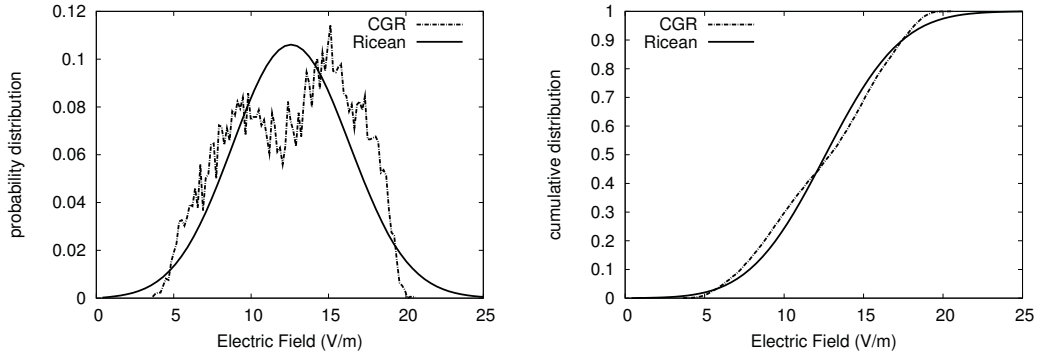

(a) pdf (b) cdf

Figure 4.5: Ricean approximation of the sum field of three transmitters which is simulated by computer-generated random numbers (CGR) when the direct field values are 12, 5 and 2 V/m.

If the direct field values are all equal to 10 V/m, the accuracy is further increased. The multipath mean values are kept intact that is 0.5 V/m. The distribution curves are given in Fig. 4.6. It is seen in Fig. 4.6(b) that the agreement between the Ricean estimate and the distribution of the sum of the independent events has been improved compared to Fig. 4.5(b) where the dominant components were different.

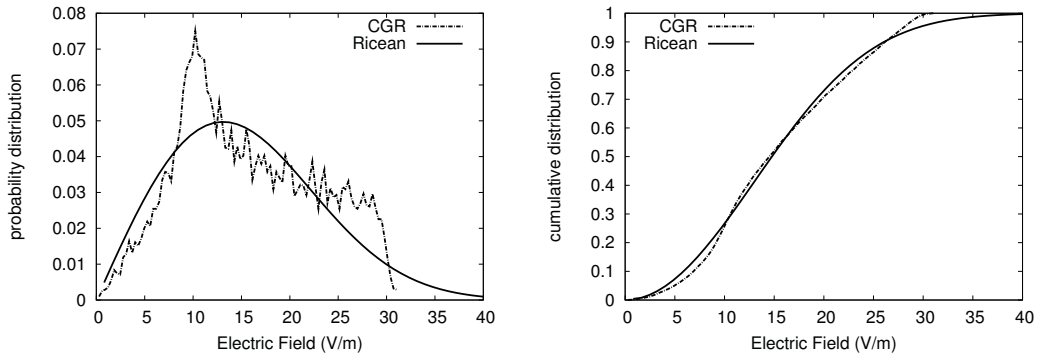

(a) pdf (b) cdf

Figure 4.6: Ricean approximation of the sum field of three transmitters which is simulated by computer-generated random numbers (CGR) when the direct field values are all equal to 10 V/m.

It is evident that the Ricean formula is a good approximation of the three-transmitter case; even better than in the two-transmitter case. With a similar analogy, a better performance is expected from the Ricean formula if another, the fourth, transmitter is added.

4.2.3 Four Ricean Events, $N = 4$

Four Ricean events with dominant components of 20, 10, 5 and 2 V/m are simulated with computer-generated random numbers. The multipath mean value for each transmitter is 0.5 V/m. So the K-factors are 1600, 400, 100 and 16. The pdf and cdf of the sum of fields of four events are compared with their Ricean approximation. In the Ricean approximation the direct field and the multipath mean value are determined as defined in (4.1) and (4.2).

The pdf of simulated sum of the four events is compared to its Ricean approximation in Fig. 4.7(a). It is seen that there is an agreement between the two curves. Their cdf is compared in Fig. 4.7(b) where the agreement is more prominent.

If the direct field values are all equal to 10 V/m, the Ricean estimation provides an even better approximation. The pdf and cdf of this Ricean estimation are compared

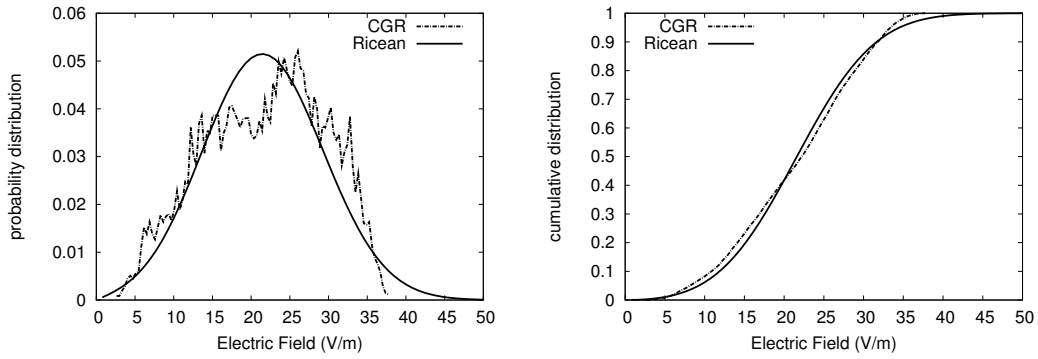

(a) pdf (b) cdf

Figure 4.7: Ricean approximation of the sum field of four transmitters which is simulated by computer-generated (CG) random numbers. The direct field values are 20, 10, 5 and 2 V/m.

to the pdf and cdf of the sum event in Fig. 4.8. It is evident that the cdf curves in this figure present a better agreement than those in Fig. 4.7 where the direct field values are different.

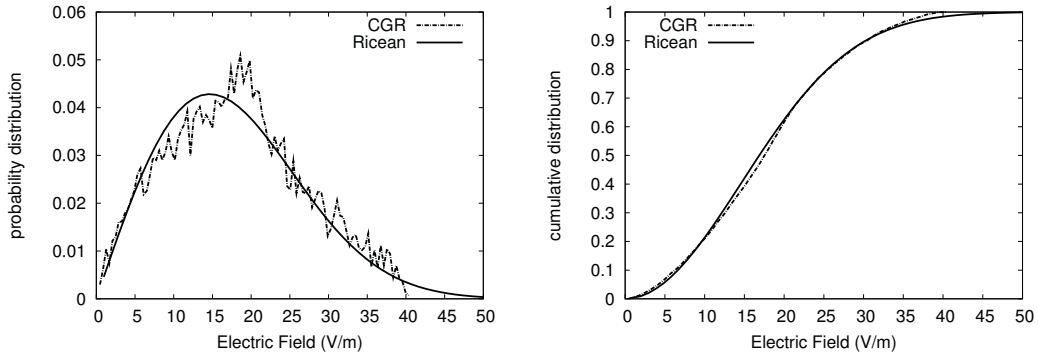

(a) pdf (b) cdf

Figure 4.8: Ricean approximation of the sum field of four transmitters which is simulated by computer-generated (CG) random numbers. The direct field values are all equal to 10 V/m.

The distribution of the sum events, in three- and four-event cases, can exhibit the worst agreement if two of the dominant components are very close to each other and the other/others are much smaller. This case is not analyzed here because it is in fact an approximate representation of the two-event case. In this worst-case scenario,

the smaller dominant component(s) can be considered as part of the multipath mean value and thus the two-event analysis can be applied.

It is concluded that the Ricean estimation (using (4.1) and (4.2)) of a sum event is a reliable tool. Also it is seen that adding more events, in fact, adds to the validity and accuracy of this method.

So far the simulations were done using computer-generated random numbers. In the following the analysis is furthered using the two-wave with diffuse power theory and some ray-tracing results. However these analyses are for the two-transmitter case only.

4.3 Two-Wave with Diffuse Power

Numerical evaluations of the function presented in (1.16) shows that it has two peaks if A_0 and A_1, as in (1.15), are well separated from each other and the diffuse power is small enough. In this case, the peaks are around $A_0 + A_1$ and $|A_0 - A_1|$. To demonstrate the TWDP theory clearly, the conditions for existence of the two peaks of (1.16) are aggrandized. One of the transmitters is located much closer to the observation area compared to the other transmitter. The multipath fields have to be much smaller than the direct fields. To meet the latter criterion, some impractical properties are assumed. The room is defined to be very large with walls which are barely reflective. In a large room, the image sources in the ray-tracing method are pushed far away thus have a smaller effect. If the reflecting surfaces are not much reflective (i.e. have a relative permittivity of near unity and a conductivity of near zero), the reflection coefficients will have small magnitudes, reducing the magnitude of the multipath field and the MMV. In a small room with highly reflective walls, the multipath field will have a strong effect on the total value of the field, downgrading the effect of A_0 and A_1 and their phases. This would prevent the demonstration of a

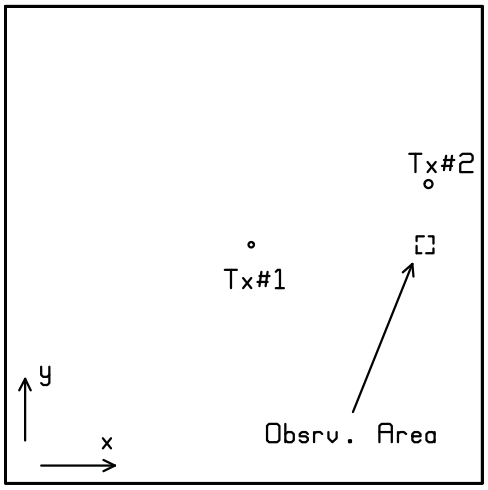

Figure 4.9: The floor plan of a large room, 20 m by 20 m with two transmitters shown at Tx #1 and Tx #2 and a small observation area. The observation area measures 40 cm by 40 cm and is at the same height as the transmitters.

TWDP function with well-separated peaks.

The room in which the simulation was performed measures 20 m by 20 m and is shown in Fig. 4.9. The ceiling is at the height of 12 m above the floor. The center of the horizontal observation area is at (17.6 m, 10 m, 6 m). The observation area is 40 cm by 40 cm and at the same height as the transmitters that is 6 m. The walls, floor and ceiling are all assumed to be slabs of 3 cm thickness and with the following electrical properties: $\epsilon_r = 1.2$ and $\sigma = 3$ mS/m. Each transmitter is a half-wave dipole oriented vertically and radiating 100 mW at 2.45 GHz. For simplicity the z coordinate of the positions are removed. The first transmitter is seven meters away in the x direction, and the second transmitter two meters away in the y direction, from the center of the local observation area.

Ray-tracing is used to obtain the electric field at many closely-spaced points over the local area for each transmitter. The two solutions are added together accounting for phase. The field intensities within the local area are used statistically to obtain the probability distribution. For the transmitter configuration shown in Fig. 4.9, the pdf and cdf of the total field due to the two transmitters are shown in Fig. 4.10 (see

the curves marked "RT").

At the center of the local area, the direct field and the multipath mean value of transmitter #1 are as follows, $E_{d1} = 0.304$ V/m and $E_{m1} = 2.43 \times 10^{-2}$ V/m. This means that the Ricean K-factor for transmitter #1 alone is 156. The direct field and the multipath mean value of transmitter #2 are $E_{d2} = 1.12$ V/m and $E_{m2} = 4.94 \times 10^{-2}$ V/m. This means that the Ricean K-factor for the transmitter #2 alone is 514.

To apply the TWDP theory, the direct field values of the two transmitters in the middle of the observation area are used as A_0 and A_1 in (1.16). The power-based sum of the multipath mean values, that is $\sqrt{{E_{m1}}^2 + E_{m2}^2}$, is used as E_{dp}. It is seen in Figs. 4.10(a) and 4.10(b) that the TWDP formula correctly predicts the pdf and the cdf of the total field of the two transmitters obtained using the ray-tracing method.

In Figs. 4.10(a) and 4.10(b), there is a third curve which is marked as "CG". This indicates that the distribution functions are obtained using computer-generated random numbers. Their purpose is to numerically demonstrate the theoretical validity of the not-well-known TWDP formula. Equation (1.15) is used 10,000 times to generate 10,000 outcomes. In each outcome k runs from 0 to 999. A_0 and A_1 are equal to E_{d1} and E_{d2} respectively. Then each A_k for $k \geq 2$ is equal to $\sqrt{{E_{dp}}^2/998}$. Figures 4.10(a) and 4.10(b) show that the TWDP predicts the computer-generated distribution very well.

It is shown in Fig. 4.10(a) that the probability density functions have two peaks. The left hand side peak is at around 0.83 which is close to $E_{d2} - E_{d1} = 0.816$. The right hand side peak is at around 1.39 which is close to $E_{d2} + E_{d1} = 1.42$

In the foregoing example, the local area was chosen in a way that the phases of the two direct fields could change in different ways if the location of the observer in the local area changed. This simulated the randomness of the phases thus the TWDP predicted the field distribution very well.

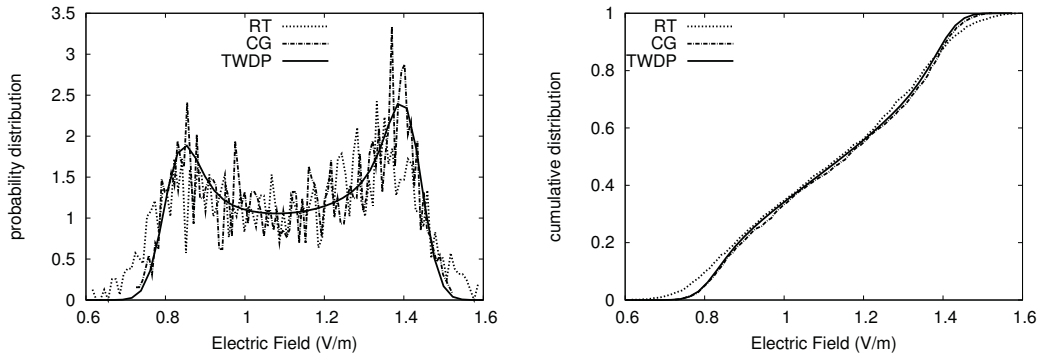

(a) pdf (b) cdf

Figure 4.10: Probability distribution of the field caused by two transmitters. The TWDP prediction, which is approximated by the computer-generated (CG) random numbers, matches the ray-tracing (RT) results. Transmitters are located at $(10.6, 10)$ and $(17.6, 12)$ resulting in $K_1 = 156$ and $K_2 = 514$.

In the following, the transmitters are located in a configuration where the phases of the direct field in the local area changes in the same way when the observer moves in the local area. In this case, it is shown that the TWDP theory fails in predicting the field distribution.

4.3.1 TWDP Fails

The transmitters and the center of the observation area lie on the same line as shown in Fig. 4.11. The observation area is made smaller in the x direction in order to reduce the effects of the variations in the magnitude of the direct field of the second transmitter as it is close to the area. To compensate for this, the area is made longer in the y direction, giving us the same surface area as in the previous example. Thus the area measures 20 cm by 80 cm.

In theory, the phases of the two direct fields ought to be independent. However, on the line passing through the transmitters, the distances from the center of the area to the transmitters are denoted by r_1 and r_2. The phase difference of the direct field will be $-\beta r_2 - (-\beta r_1)$ which is equal to a constant number $\beta \Delta x_0$ in which Δx_0 equals

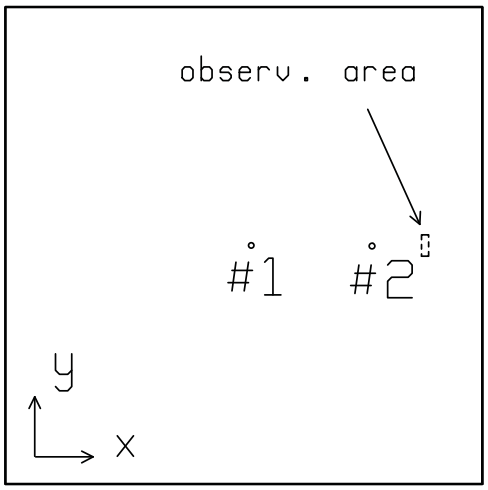

Figure 4.11: The floor plan of a large room with two transmitters shown at Tx #1 and Tx #2 and a small observation area. The first transmitter (Tx #1) is fixed at $x = 10$ m and the second transmitter (Tx #2) varies between $x = 15.39$ m and $x = 15.45$ m. The observation area measures 20 cm by 80 cm and is at the same height as the transmitters.

$r_1 - r_2$. If the first transmitter were located at $(10.3, 10)$, giving $E_{d1} = 0.304$ V/m, and the second transmitter at $(15.382, 10)$, giving $E_{d2} = 1.00$, the phase difference between the direct field components would be 179 degrees. The out-of-phase direct field components would make a resultant of 0.696 V/m. If the first transmitter stayed at $(10.3, 10)$ while the second transmitter moved to $(15.443, 10)$, the phase difference would become -0.42 degrees. The in-phase direct fields would make a resultant of 1.304 V/m.

The total field in the room includes the effect of the multipath field as well. In the large room, made of walls with small reflection as described before, the probability distribution of the total field is given as follows.

Large K-factor

In the same large room, as shown in Fig. 4.11 and with the same walls, the pdf and cdf of the field intensity, at the observation area and due to the two transmitters, are obtained by ray-tracing and compared to what the TWDP theory predicts by (1.16).

The first transmitter is fixed at $(10.3, 10)$, giving $E_{d1} = 0.304$ V/m at the center of the local area. The corresponding multipath mean value obtained by ray-tracing is $E_{m1} = 2.43 \times 10^{-2}$ V/m. This gives a Ricean K-factor of K_1=156. The second transmitter is first located at $(15.39, 10)$, giving $E_{d2} = 1.00$ V/m and $E_{m2} = 3.29 \times 10^{-2}$ V/m. This results in $K_2 = 923$. The distance between the antenna in the x direction gives a phase difference of 155 degrees between the direct field components in the center of the local area. The 155 degree phase difference is only 25 degrees different from 180 degrees hence the two components are supposed to be out of phase and the pdf is supposed to be concentrated around a value close to $1 - 0.304 = 0.696$ V/m.

It is seen in Fig. 4.12(a) that the pdf obtained from the statistics of the ray-tracing results over the local area is concentrated around 0.71 V/m (close to $1 - 0.304 = 0.696$), confirming the out-of-phase behavior of the direct field components. The TWDP formula and the computer-generated random numbers assume no correlation between the phases of the direct field components and thus have two peaks at 0.71 V/m and at 1.29 V/m which is close to $1 + 0.304 = 1.304$ V/m. The cdf curves are given in Fig. 4.13(a).

The distance between the transmitters is increased by moving the second transmitter a distance of 1 cm in the positive x direction towards the observation area. The magnitudes of the direct fields and the MMVs have almost the same values thus the Ricean K-factors remain to be the same. Hence the TWDP curve is not expected to change. The envelope of the pdf of the computer-generated random numbers is not expected to change either. However, due to the nature of the random numbers, the pdf curve will have a slightly different appearance for different repetitions of the same event. We see in Fig. 4.12(b) that the TWDP and the envelope of the computer-generated random numbers have not changed. However it is obvious that the pdf of the ray-tracing results over the local area is no longer concentrated at 0.71. It has

moved slightly towards the other peak of the TWDP curve. This is due to the fact that for the new location of the second antenna, the phase difference between the two direct fields become 126 degrees. The two components can no longer be considered out-of-phase. The cdf curves are shown in Fig. 4.13(b).

The second transmitter is moved five more times, each time in the same 1 cm step, and the comparisons of the probability distribution between the ray-tracing results, the computer-generated random numbers and the TWDP formula are shown in Figs. 4.12(c) through 4.12(g) and in Figs. 4.13(c) through 4.13(g).

The trend in all these pdf comparisons is that the probability distribution of the ray-tracing results is first concentrated at one of the two peaks of the TWDP pdf function. Then by moving the second transmitter, it moves towards the other peak. To make the peak of the envelope of the curve of the ray-tracing pdf move from one of the TWDP peaks to the other, the second transmitter has to move a distance of $\lambda/2$. If the second transmitter is moved further, the peak of the envelope of ray-tracing pdf will start moving back to the first peak of the TWDP. Thus the ray-tracing results show that the pdf of the electromagnetic field caused by the two transmitters moves periodically from one peak of the TWDP curve to the other and back as one of the antennas move. The period is λ.

The failure of the TWDP theory, in predicting the probability distribution of the two-antenna system in line with the center of the local observation area, is less conspicuous if the walls are more reflective and the K-factors smaller.

Medium K-factor

If in the same large room the relative permittivity of the wall material is increased to 5 and its conductivity to 1000 mS/m, the walls will be much more reflective. The K-factors are reduced from $K_1 = 156$ and $K_2 = 923$ to $K_1 = 2.91$ and $K_2 = 19.8$.

As before, the first transmitter is fixed at its location while the second transmitter

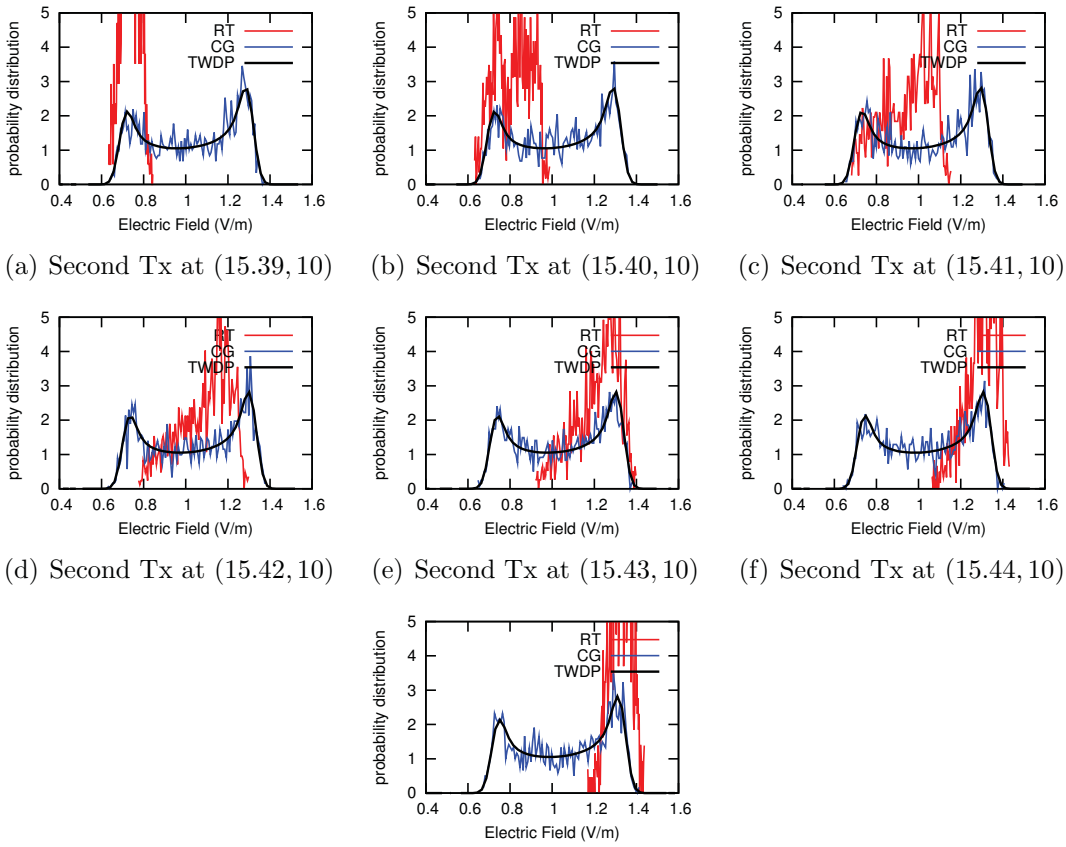

(a) Second Tx at $(15.39, 10)$ (b) Second Tx at $(15.40, 10)$ (c) Second Tx at $(15.41, 10)$

(d) Second Tx at $(15.42, 10)$ (e) Second Tx at $(15.43, 10)$ (f) Second Tx at $(15.44, 10)$

(g) Second Tx at $(15.45, 10)$

Figure 4.12: Probability distribution function of the field caused by two transmitters. The TWDP theory, which is approximated by the computer-generated (CG) random numbers, does not match the ray-tracing (RT) results. The first TX is fixed at $(10.3, 10)$ and $K_1 = 156$ and $K_2 = 923$.

moves in six steps of 1 cm for a total distance of $\lambda/2$. For the seven different positions of the second transmitter, the TWDP result at each case is compared to the statistics of the total field of the two transmitters obtained by ray-tracing. The computer-generated random numbers are used again to simulate the TWDP theory. The pdf and cdf comparisons are shown in Figs. 4.14(a) through 4.14(g) and Figs. 4.15(a) through 4.15(g).

It is seen that, contrary to the large K-factor case, the probability distribution function given by the TWDP formula does not have two peaks. This is simply due to

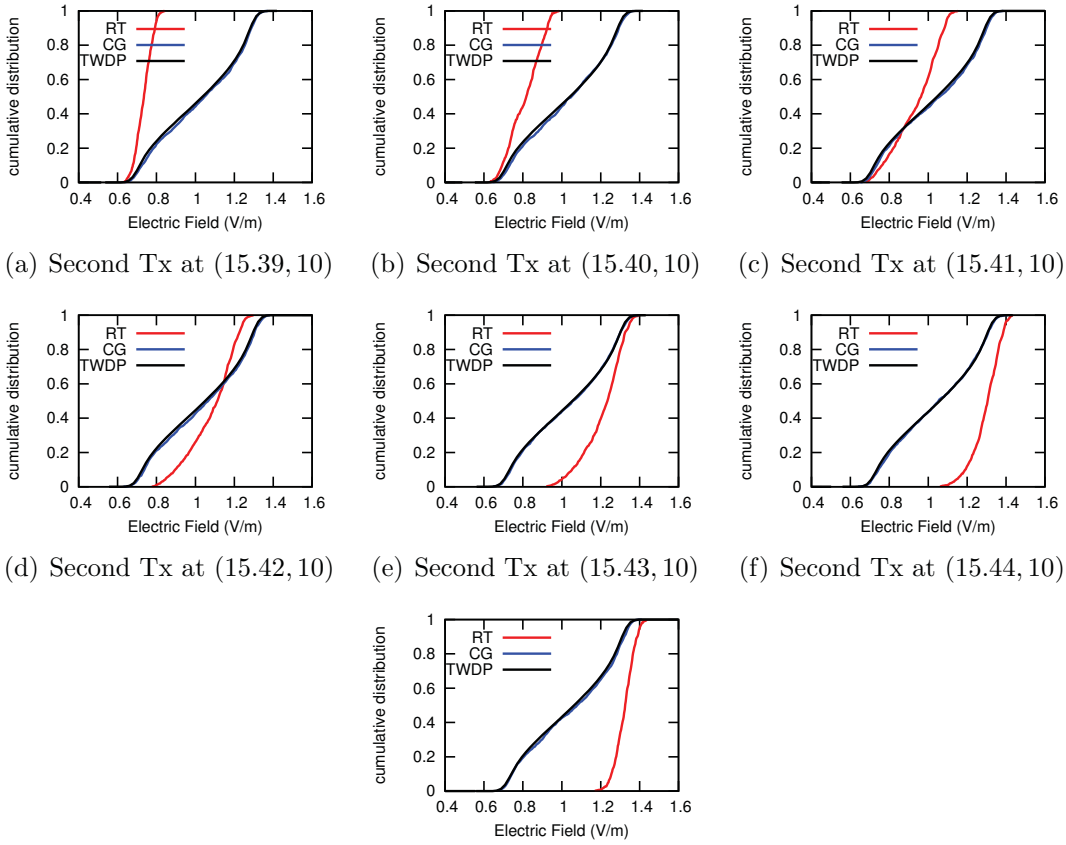

(a) Second Tx at $(15.39, 10)$ (b) Second Tx at $(15.40, 10)$ (c) Second Tx at $(15.41, 10)$

(d) Second Tx at $(15.42, 10)$ (e) Second Tx at $(15.43, 10)$ (f) Second Tx at $(15.44, 10)$

(g) Second Tx at $(15.45, 10)$

Figure 4.13: Cumulative distribution function of the field caused by two transmitters. The TWDP theory, which is approximated by the computer-generated (CG) random numbers, does not match the ray-tracing results. The first TX is fixed at $(10.3, 10)$ and $K_1 = 156$ and $K_2 = 923$.

the larger multipath fields and the larger diffuse power. Figs. 4.14 and 4.15 show that in fact the TWDP and the ray-tracing results does not demonstrate a conspicuous mismatch. However there is no agreement between them either. The ray-tracing pdf curves are concentrated at about 0.7 V/m (close to $1 - 0.304 = 0.696$ V/m) in Fig. 4.14(a). This figure corresponds to the case where the two direct field are almost out-of-phase. As the second transmitter moves a half-wavelength distance, it is seen in Fig. 4.14(g) that the ray-tracing pdf is concentrated at around 1.4 V/m which is close to $1 + 0.304$ V/m, demonstrating the in-phase behavior of the two direct fields.

The failure of the TWDP theory in predicting the ray-tracing results in a local area at the end-fire direction of the two-antenna system bears no novelty for the electromagnetics community. However it is shown in Figs. 4.12 and 4.14, for large and medium K-factors, that as the second transmitter moves, the peak of the ray-tracing pdf curve moves from one end of the graph to the other. If the movement of the transmitter continues, the peak comes back to the other end. This encourages one to obtain the pdf and cdf of the union of all the field intensity data related to different positions of the second transmitter.

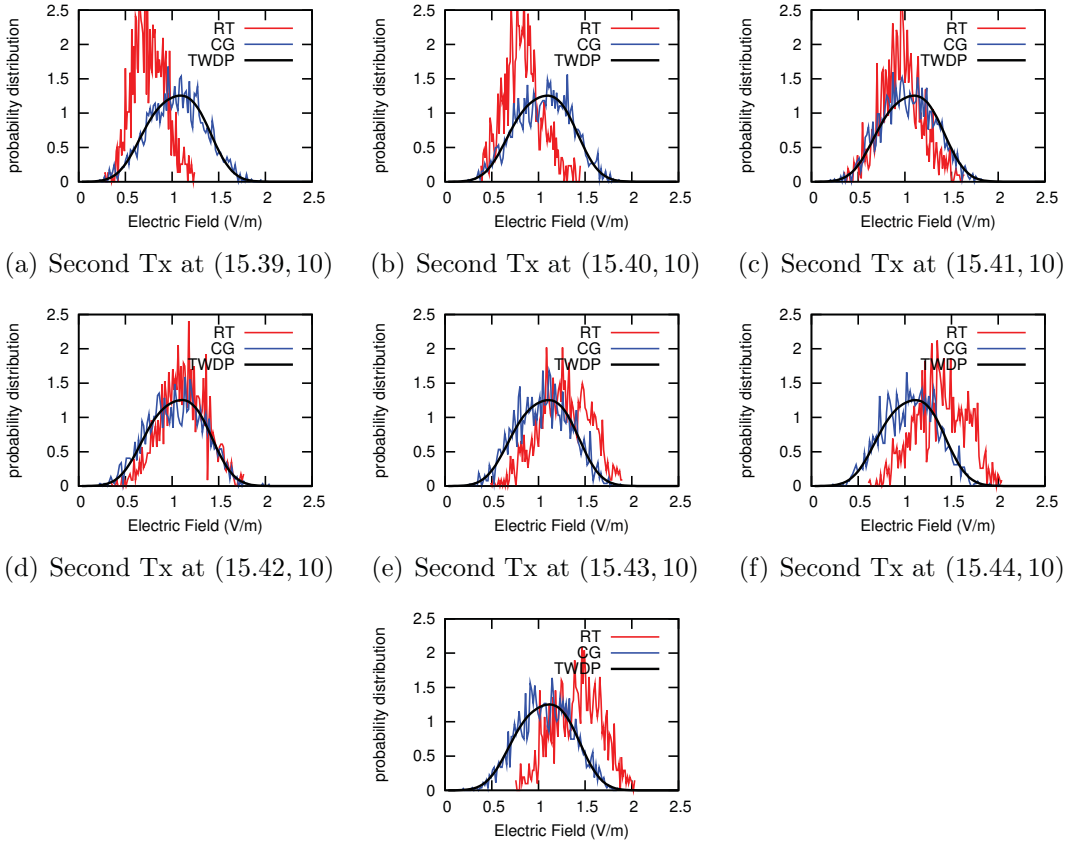

(a) Second Tx at $(15.39, 10)$ (b) Second Tx at $(15.40, 10)$ (c) Second Tx at $(15.41, 10)$

(d) Second Tx at $(15.42, 10)$ (e) Second Tx at $(15.43, 10)$ (f) Second Tx at $(15.44, 10)$

(g) Second Tx at $(15.45, 10)$

Figure 4.14: Probability distribution function of the field caused by two transmitters. The TWDP theory does not match the ray-tracing results. The first TX is fixed at $(10.3, 10)$ and $K_1 = 2.91$ and $K_2 = 19.89$.

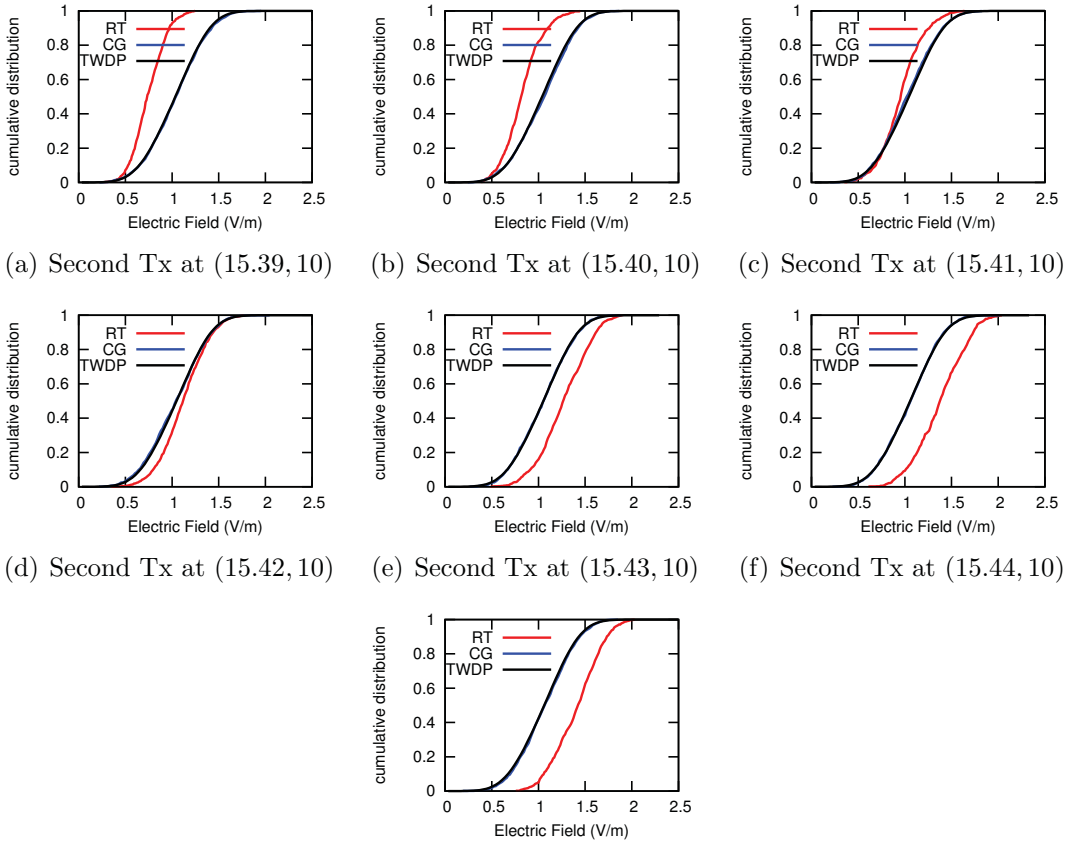

(a) Second Tx at $(15.39, 10)$ (b) Second Tx at $(15.40, 10)$ (c) Second Tx at $(15.41, 10)$

(d) Second Tx at $(15.42, 10)$ (e) Second Tx at $(15.43, 10)$ (f) Second Tx at $(15.44, 10)$

(g) Second Tx at $(15.45, 10)$

Figure 4.15: Cumulative distribution function of the field caused by two transmitters. The TWDP theory does not match the ray-tracing results. The first TX is fixed at $(10.3, 10)$ and $K_1 = 2.91$ and $K_2 = 19.89$.

4.3.2 TWDP Validity Restored For Moving Transmitters

The probability distribution of the union of all the field intensity data for different positions of the second transmitter is shown to be in agreement with the TWDP theory. Consider the two-transmitter system in line with the local area. Assume V_i is the set of the magnitudes of the field intensities over the local area due to the two transmitters, obtained by ray-tracing, when the second transmitter is at its i'th position, $i = 1, 2, \ldots, 7$. Thus B is defined as $\bigcup_{i=1}^{7} V_i$. The probability distribution of set B, for large and medium K- factors is compared to the TWDP prediction in the following.

Large K-factor

The data from the electric field strength over the local area caused by the two transmitters in the room with less reflective walls are collected from all the data sets for each position of the second transmitter. The distribution functions of this collection, set B, are obtained and shown in Figs. 4.16(a) and 4.16(b). They match the TWDP prediction. For the TWDP curve, the direct field value of the second transmitter at its middle location is used. This location is $(15.42, 10)$. However the direct field of the second transmitter in the center of the local area in fact does not much vary when the this transmitter moves between $(15.39, 10)$ and $(15.45, 10)$.

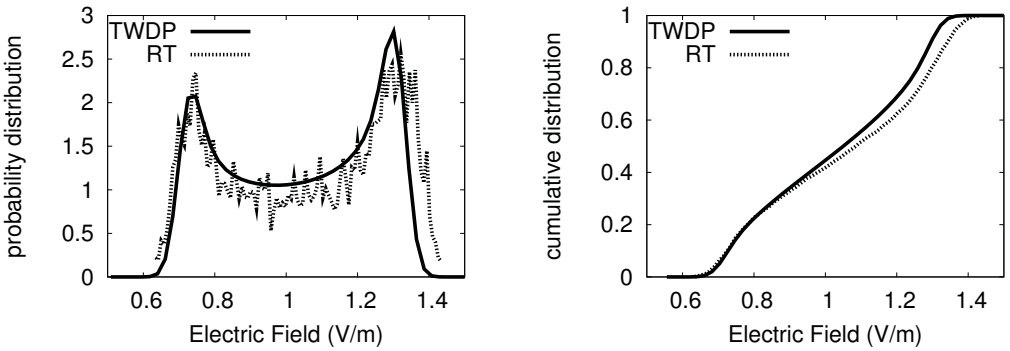

(a) pdf (b) cdf

Figure 4.16: Distribution functions. The TWDP against the statistics of all the field strength data combined from the sets of results each belonging to different locations of the second transmitter. $K_1 = 156$ and $K_2 = 923$.

Medium K-factor

The pdf and cdf of set B in the room with more reflective walls are compared to the TWDP in Figs. 4.17(a) and 4.17(b). The difference in the probability of exceeding certain immunity level, defined as $1 - \text{cdf}(\text{E}_\text{I})$, is less than 0.05 for most values of E_I. The maximum value of this difference between the TWDP and the ray-tracing results is 0.1. Hence the TWDP formula is in agreement with the pdf of the set B in the medium K-factor case as well.

Each transmitter, in a hospital ward is carried by a staff member. The location of a standing human-being is not fixed during their standing times. Movements of a few centimeters are normal. Hence the results presented here enable us to apply the TWDP theory in real-life scenarios where the location of the transmitters are not fixed.

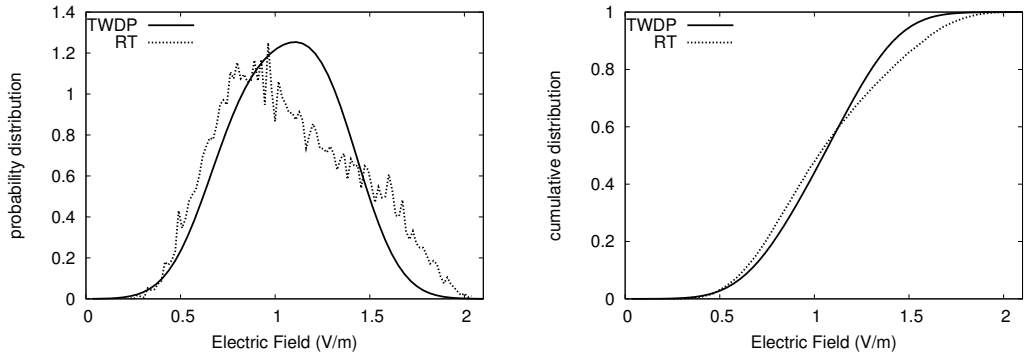

(a) pdf (b) cdf

Figure 4.17: Distribution functions. The TWDP against the statistics of all the field strength data combined from the sets of results each belonging to different locations of the second transmitter. $K_1 = 2.91$ and $K_2 = 19.89$.

So far the TWDP theory was compared to the ray-tracing results of two transmitters operating at the same frequency which implies the sources are coherent. In the following a small change in the frequencies is considered. Also in a different simulation, later in this chapter, the phases of the direct field vectors are replaced with truly random numbers.

4.3.3 Effect of Frequency Difference of the Two Transmitters on the Field Distribution

In an IEEE 802.11 communications scheme, channels are separated by a small fraction of the center frequency of each channel. Any difference in the frequency of CW signals indicate incoherence. In this section the frequency of the second transmitter is reduced to 2400 MHz while the first transmitter keeps operating at 2450 MHz. The walls and the room are the same as those in the large K-factor section.

The location of the first transmitter is not changed. The second transmitter is first located at $(15.39, 10)$. The pdf curves are shown in Fig. 4.18(a). As the transmitter moves 1 cm to the location $(15.40, 10)$ it is seen in Fig. 4.18(b) that the pdf of the ray-tracing results moves toward the right-hand side peak of the TWDP curve. The transmitter moves one more step forward and the pdf of the ray-tracing results, shown in Fig. 4.18(c), does not change much. After this position with five more 1 cm movements of the second transmitter, the peak of the envelope of the ray-tracing curves reaches left-hand side peak of the TWDP curve in Fig. 4.18(i). The corresponding cdf curves are presented in Fig. 4.19.

The second transmitter moves a half-wavelength distance from $(15.41, 10)$ to $(15.47, 10)$ in one-centimeter steps. At each step, the pdfs of the sum field within the local area are shown in Figs. 4.18(c) through 4.18(i). The sum field values are collected for all steps of the movement of the second transmitter. The pdf of this collection is shown in Fig. 4.20(a). It is seen that the TWDP validity is restored when the second transmitter is allowed to move even if its frequency is different from that of the first transmitter.

However in the following it is shown that if the phases of direct fields are replaced with random numbers, even for fixed transmitters, the TWDP correctly predicts the ray-tracing results.

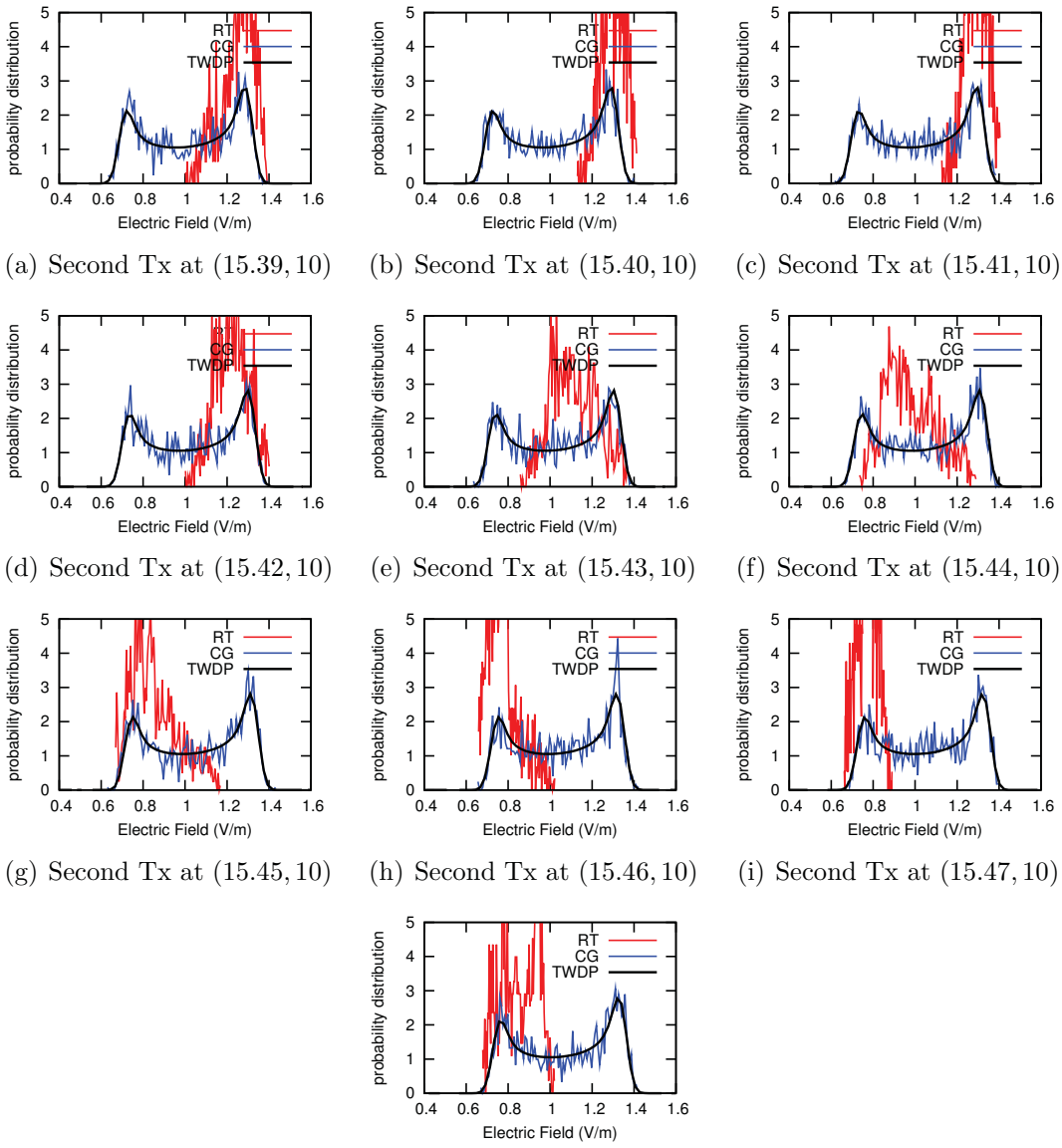

(a) Second Tx at $(15.39, 10)$ (b) Second Tx at $(15.40, 10)$ (c) Second Tx at $(15.41, 10)$

(d) Second Tx at $(15.42, 10)$ (e) Second Tx at $(15.43, 10)$ (f) Second Tx at $(15.44, 10)$

(g) Second Tx at $(15.45, 10)$ (h) Second Tx at $(15.46, 10)$ (i) Second Tx at $(15.47, 10)$

(j) Second Tx at $(15.48, 10)$

Figure 4.18: Probability distribution function of the field caused by two transmitters, one operating at 2.45GHz and one at 2.4 GHz. The TWDP theory, which is approximated by the computer-generated (CG) random numbers, does not match the ray-tracing (RT) results. The first TX is fixed at $(10.3, 10)$ and $K_1 = 156$ and $K_2 = 923$.

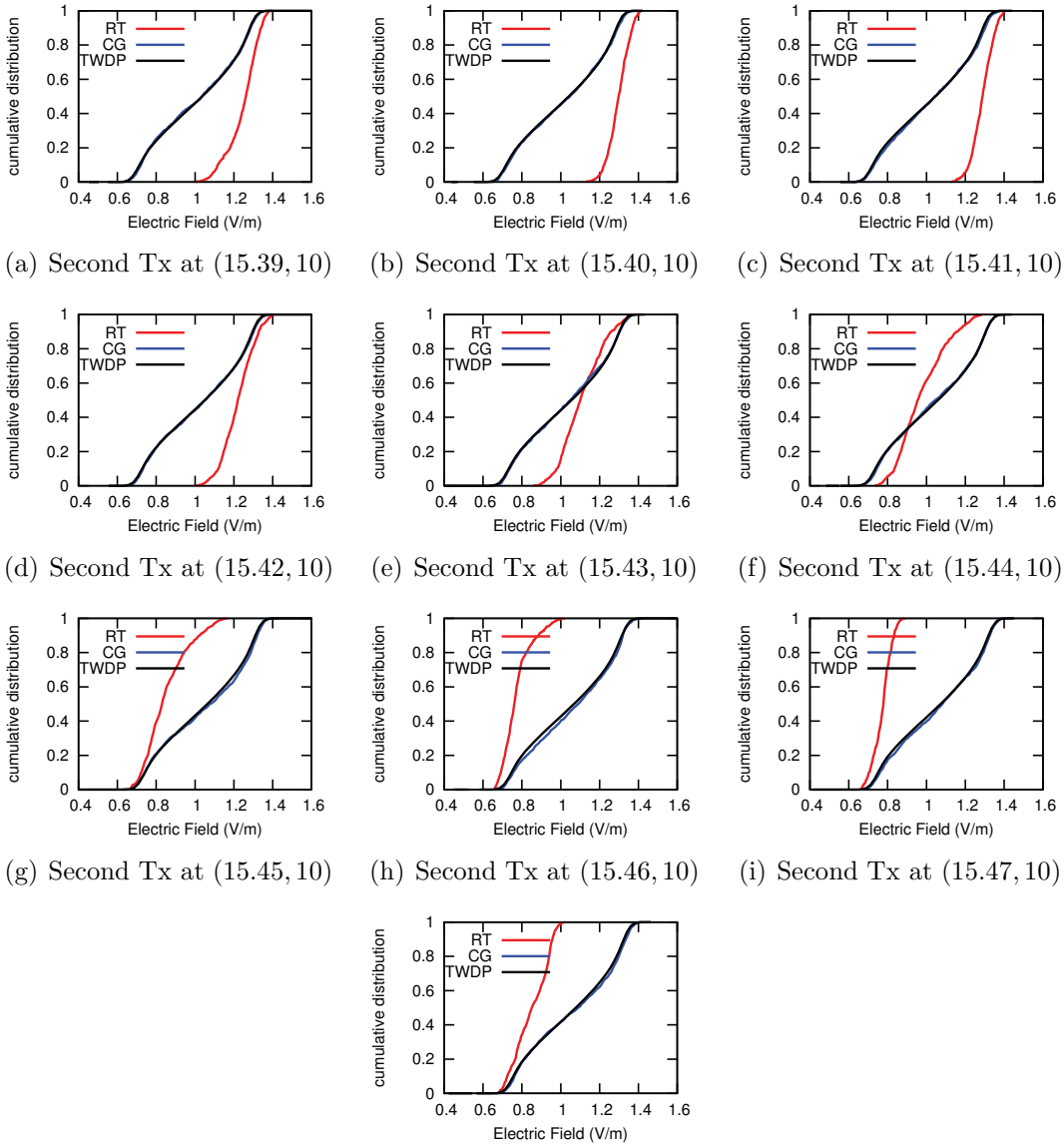

(a) Second Tx at $(15.39, 10)$ (b) Second Tx at $(15.40, 10)$ (c) Second Tx at $(15.41, 10)$

(d) Second Tx at $(15.42, 10)$ (e) Second Tx at $(15.43, 10)$ (f) Second Tx at $(15.44, 10)$

(g) Second Tx at $(15.45, 10)$ (h) Second Tx at $(15.46, 10)$ (i) Second Tx at $(15.47, 10)$

(j) Second Tx at $(15.48, 10)$

Figure 4.19: Cumulative distribution function of the field caused by two transmitters with different frequencies. The TWDP theory, which is approximated by the computer-generated (CG) random numbers, does not match the ray-tracing results. The first TX is fixed at $(10.3, 10)$ and $K_1 = 156$ and $K_2 = 923$.

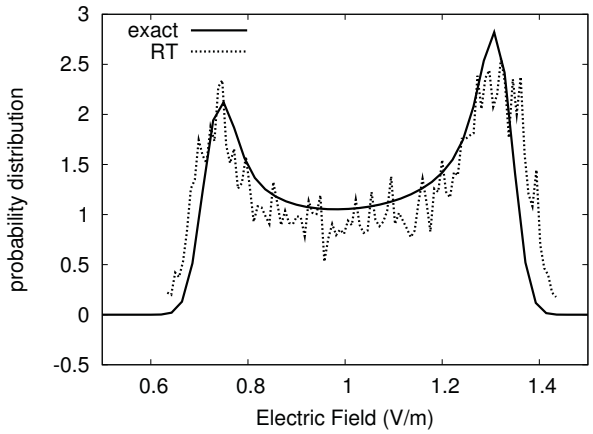

(a) pdf

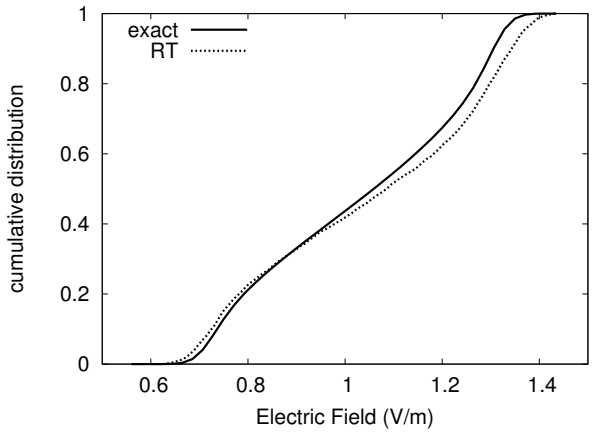

(b) pdf

Figure 4.20: Distribution functions for the field of two transmitters with different frequencies. The TWDP against the statistics of all the field strength data combined from the sets of results each belonging to different locations of the second transmitter. $K_1 = 156$ and $K_2 = 923$.

4.3.4 Direct Field Phase Randomness Enforced

The first transmitter is located at $(10.30, 10)$ and the second transmitter at $(15.39, 10)$. The room is the same large room with less reflective walls. In the ray-tracing algorithm, the direct field is denoted by $\mathbf{E_d}$. The x and y components of this vector are zero as the local area is on the same plane as the H-plane of the dipole antenna. The antenna is oriented vertically, that is in the z direction. So the direct field is denoted as $E_{dz}e^{-j\beta d}$ where d is the distance from the transmitter to the center of the observation area. For each transmitter, the direct field is replaced by $E_{dz}e^{j\phi_z}$ where ϕ_z is a random number distributed uniformly between 0 and 2π. This procedure is performed for the direct fields of both antennas. However the multipath fields and the diffuse power are determined as they were before, with no alteration of the phases. The field distribution at many points in the local area is determined and is shown in Fig. 4.21 with the curves marked "RT". The TWDP distribution and the pdf of the computer-generated random numbers are given in the same figure. For these two curves, the same direct field values and MMVs as given previously are used: $E_{d1} = 0.304$ V/m, $E_{m1} = 2.43 \times 10^{-2}$ V/m, $E_{d2} = 1.00$ and $E_{m2} = 3.29 \times 10^{-2}$ V/m.

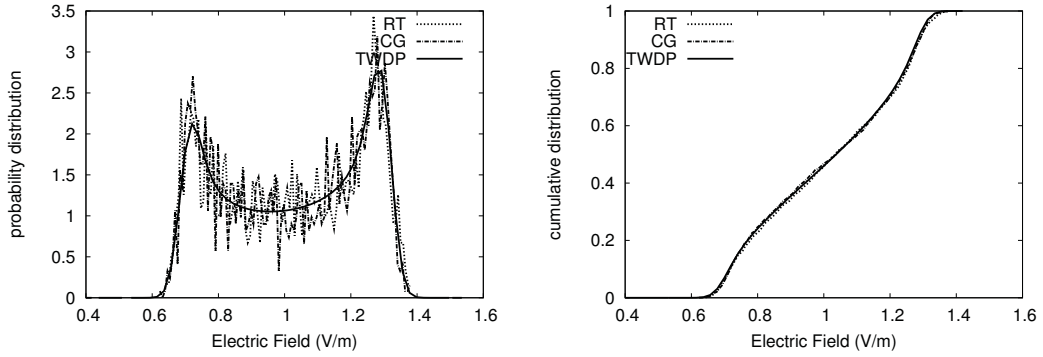

(a) pdf (b) cdf

Figure 4.21: Distribution functions. The two transmitters are fixed at $(10.30, 10)$ and $(15.39, 10)$. The direct fields of the ray-tracing results are given random phases. The TWDP against the statistics of the altered ray-tracing results. $K_1 = 156$ and $K_2 = 923$. This figure is comparable to Fig. 4.10(a) which is associated with the same location of the second transmitter as here.

It is seen in Fig. 4.21(a) that the pdfs of the TWDP formula and the computer-generated random numbers closely approximate the altered ray-tracing results. This figure is comparable to Fig. 4.10(a) which is associated with the same location of the second transmitter as here. In Fig. 4.10(a) the pdf of the ray-tracing results is completely different from the TWDP curve. The almost identical match between the cdf of the altered ray-tracing results and the TWDP pdf in Fig. 4.21(b) is due to the restored or the enforced randomness of the direct field phases. The almost identical match between the three cdf curves in Fig. 21(b) was not been seen in the previous results. This indicates that the randomness of the phases of the direct field vectors is essential in the validity of the TWDP formula.

4.4 Summary

In this chapter it was shown that the Ricean distribution can be used to approximate the pdf of the field strength due to two roaming transmitters. Adding more transmitters improves the accuracy of the approximation.

This chapter contained two main sections. In Section 4.2, using computer-generated random numbers, it was shown that a Ricean function can be used to approximate the sum of two and more Ricean events. Then in Section 4.3 it was shown that the TWDP formula can give the probability distribution of the sum field of two moving transmitters obtained by ray-tracing. The TWDP was also verified with computer-generated random numbers in order to strengthen the connection between the two main sections of this chapter. In the following, a summary of both sections is presented.

In Section 4.2, it was shown in in Figs. 4.1 through 4.4 that the probability distribution of the sum of two Ricean events can be approximated by the Ricean function whose dominant component is chosen as the greatest of the dominant components of the individual events. The total multipath mean value is the power-based sum of the

rest of the direct fields and all the multipath mean values as given in (4.2).

The sum of three and four Ricean events were analyzed in Figs. 4.5 and 4.6 and in Figs 4.7 and 4.8. The accuracy of the Ricean approximation of the sum events was improved by increasing the number of independent events.

In Section 4.3, the first electromagnetic verification of the TWDP theory was given. It was shown in Fig. 4.10 that for some configuration of the transmitter locations, the TWDP formula gives a valid estimation of the pdf of the field strength values, obtained using ray-tracing, over a local area. This is the first electromagnetic verification of this theory.

The TWDP theory can be unreliable if the two transmitters are fixed at the locations. It was shown in Figs. 4.12 and 4.13 that the TWDP prediction fails to estimate the field statistics given that the location of the two transmitters are fixed and in line with the center of the observation area. The two transmitters had high Ricean K-factors and small multipath mean values. The pdf predicted by the TWDP had two peaks, whereas the envelope of ray-tracing pdf had one. It was shown that if one of the transmitters is allowed to move on the same line, the peak of the ray-tracing results moves from one peak of the TWDP to the other and back. Moving between the two peaks is periodic with the movement of a transmitter; the period is λ.

The data sets of the two-transmitter field strengths, for all of the locations of the moving transmitter, was collected. These were all ray-tracing results. Analysis of the statistics of this collection, presented in Fig. 4.16 for a large Ricean K factor and in Fig. 4.17 for a medium K factor, showed that its pdf and cdf are well approximated by the TWDP formula. Thus the TWDP formula may be used if the transmitters are expected to roam in the room or have slight movements at their positions.

A small difference in the frequency of the transmitters was shown to have little effect on the pdf of the ray-tracing results. The 2% frequency difference did not

prevent the failure of the TWDP theory in the case of the fixed transmitters.

The phases of the direct fields, in ray-tracing, were replaced by random numbers and the TWDP was seen in Fig. 4.21 to be almost identical to the pdf obtained from the ray-tracing results, in the case of fixed transmitters.

In the following, the conclusions of the two mains sections of this chapter are used to deduce a more general conclusion. The TWDP approximates the ray-tracing results of two moving transmitters. The TWDP is well approximated by the computer-generated random numbers. The simulations done by the computer-generated random numbers, showed that the Ricean formula can estimate the sum field of two independent Ricean events despite the fact that the sum field is expected to be non-Ricean. These three statements imply that the probability distribution of the electric field of two moving transmitters can be approximated using a Ricean function. If the number of transmitters are increased, the accuracy of this approximation is increased.

The transmitters considered in the next chapter are allowed to roam in the room. The multipath mean value is approximated by the Sabine method demonstrated in Chapter 2. The pdf of the sum field of two transmitters is obtained by the Ricean function using the results presented in the current chapter.

Chapter 5

Presence-Weighted Risk of Exceeding Immunity

5.1 Introduction

The objective of this chapter is to determine the risk of exceeding immunity at the location of an electronic medical device in the presence of one and two roaming wireless transmitters. The location of the roaming transmitters is unknown and the staff members carrying them might be asked to maintain a minimum separation distance from the EMD. The staff may or may not fully comply with the MSD policy.[1]

To determine the REI, the modified ray-tracing-Rice method may appear to be a suitable technique as it was shown in Chapter 3 to be much faster than but as accurate as the RTR method. However the MRTR method, if used here, must be repeated for thousands of different transmitter locations, significantly increasing the computational cost. In was shown in Chapter 2 that the Sabine-Rice method provides an acceptable approximation of the RTR method. The SR approximation is much faster than the MRTR method and is used in this chapter to estimate the risk.

[1] A version of this chapter has been submitted to IEEE Transactions on Electromagnetic Compatibility [66].

The safety of an EMD is guaranteed if the electric field does not exceed its immunity level. As the transmitter approaches the EMD in free space, there is a separation distance at which the field strength of the transmitter equals the immunity level. This distance is defined in free space thus it is deterministic. The safety takes on a probabilistic nature when the location of the transmitter becomes a random variable as the transmitter wanders in an indoor environment such as the hospital ward. So in this chapter, two levels of probabilistic approach are considered: (i) probabilistic estimation of the field strength in indoor environments (ii) random location of the transmitter. This provides an overall description of the approach taken in this chapter to determine the REI which is in fact only one of the three steps in the occurrence of an EMI incident where a patient injury may occur.

Let P_1 denote the probability of exceeding the immunity level of the EMD, P_2 the malfunctioning probability of the EMD given its immunity is exceeded and P_3 the probability of causing a harm to a patient given the EMD has malfunctioned. Hence $P_1P_2P_3$ is the risk of patient injury related to EMI and must be kept below a safe level. Maybe an appropriate question to ask at this point is: what is the safe level of risk?

The product $P_1P_2P_3$ accounts for patient injury which may be a life threatening situation. It can be compared to the risk value of one in 10,000 that is introduced as a safe level in [67] in which 132 federal regulatory decisions are reviewed. Hence the *de facto* safe risk level for a population small compared to that of the United States is determined to be 10^{-4}.

This thesis deals neither with P_2 nor with P_3. It focuses on determining P_1. If P_1 is kept below the safe level then, regardless of P_2 and P_3, the policy makers at the hospitals can be sure of the safety of their electronic medical devices. Thus P_1 or the risk of exceeding immunity is a very conservative representation or approximation of $P_1P_2P_3$ and can be compared to the figure 1 in 10,000. This figure is used for both

immunity levels of 3 and 10 V/m despite the fact that the 3 V/m immunity level is initially defined for non-life support EMDs. Hence the assumption here is that the devices with 3 V/m immunity levels are in fact old life-support EMDs which were built according to lower standards.

In this chapter, the first level of the probabilistic approach to determining P_1 is to estimate the field distribution using the Sabine-Rice approximation. The second level accounts for the roaming nature of the transmitter(s). During the work day, a health-care staff member carrying a wireless transmitter moves around in the ward, shown in Fig. 5.1, and is more likely to be close to a patient bed than at a far location. In this chapter, the movement of the transmitter and its unknown thus random location are characterized by assigning a probability function that it is at a given location in the room, which will be called the *presence probability*. The presence probability function accounts for the minimum separation distance from the location of the EMD and thus it depends on the location of the EMD as well. Also the non-compliance possibility is accounted for by this function. To characterize the risk associated with a given pattern of transmitter location, the *presence-weighted risk of exceeding immunity* (PWREI) is presented.

When the transmitter location is not specified, the PWREI allows us to *quantitatively* compare the situations of (i) no restriction of the use of wireless technology in hospitals, (ii) enforcing an MSD between the transmitter and the EMD, and (iii) when the MSD policy is not fully complied with. In this chapter, these cases are investigated with one roaming transmitter and two roaming transmitters.

The PWREI accounts for both high- and low-risk situations where the transmitters are close to and far from the device. A worst-case analysis is given where the smallest separation between the transmitter and the EMD is found such that the risk of exceeding immunity at the location of the EMD is below the safe level. In the worst-case analyses, the location of the transmitter is not random and is in fact the quantity

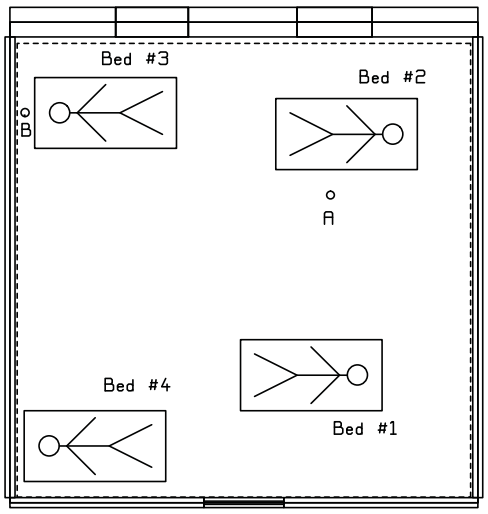

Figure 5.1: The floor plan of a four-bed ward. Beds are located in different positions and numbered as 1, 2, 3 and 4.

which is to be determined. The worst-case analysis may be useful, for example, in an operating room where the staff members stay close to the patient for a long period of time. The PWREI is useful when all possible scenarios are accounted for. The PWREI is more suitable for large-scale decision-making processes.

In the following, the first level of the probabilistic approach, that is estimating the probability distribution of the field in the room, is reviewed and the REI is defined for a steady transmitter. Then, the presence probability is introduced in Section 5.3 and the PWREI is presented in Section 5.4.

5.2 Steady Transmitter and Risk of Exceeding Immunity

Suppose that the transmitter is at (x', y') and the receiver is at (x, y), separated from the transmitter by distance r. If the immunity level is $\mathrm{E_I}$, then the risk of exceeding

immunity, similar to (2.2), is given by

$$P_c\left(E \geq \mathrm{E_I}, x, y, x', y'\right) = \int_{\mathrm{E_I}}^{\infty} p_c(E)\,\mathrm{d}E \tag{5.1}$$

where $p_c(E)$ is the Ricean equation given by (1.11). This probability is given for a local area where the EMD is located. A risk of one in 10,000 means that only one-ten thousandth of the area occupied by the medical device will have a field strength in excess of immunity. The multipath mean value is constant throughout the room in the Sabine model. The direct field as given by (1.5) is

$$\mathbf{E_d} = \sqrt{\frac{\eta D P_t}{4\pi}} \frac{e^{-j\beta r}}{r} \hat{\boldsymbol{\theta}}_{tx}$$

and depends on distance r between the transmitter and the EMD. Hence the risk of exceeding immunity is a function only of the separation of the transmitter to the EMD and can be shown simply by $P_c(E \geq \mathrm{E_I}, r)$.

For the case of two transmitters with direct field values E_{d1} and E_{d2} and multipath fields E_{m1} and E_{m2}, equations (4.1) and (4.2) are used. Use the larger direct field as E_d in (1.11), and estimate the net multipath mean value E_m as the square root of ${E_{ds}}^2 + {E_{m1}}^2 + {E_{m2}}^2$, where E_{ds} is the smaller of the direct fields.

The distance from the transmitter to the EMD, r, changes as the staff member moves around in the ward carrying a wireless transmitter. The risk of exceeding immunity changes with r. In the following, the movement pattern of the transmitter is modelled.

5.3 Presence Probability Function

A health-care staff member carrying a tablet computer enters the ward, approaches a patient, spends time examining the patient, and then quickly exits the room. The

likelihood that a transmitter is found near the bedside is higher than at other locations in the room. This behavior is modeled with a presence probability function. The value of the function at each location that assumed to be proportional to the time spent at that location.

The presence probability function in constructed as follows. Assume that α, β and γ are functions of the transmitter location, (x', y'). Function α demonstrates the relation between the presence probability and the distance to the closest bed. Its value is assumed to be zero over each bed, and elsewhere in the room it is defined by

$$\alpha = \begin{cases} 1 & \text{if } r_b < 0.7, \\ 1/(1 + 3(r_b - 0.7)) & \text{if } r_b \geq 0.7 \end{cases} \tag{5.2}$$

where r_b denotes the closest distance from (x', y') to a bed.

Function β is responsible for reflecting the fact that the staff members are not likely to spend time at a close distance to a wall and is equal to $1 - \exp(-5{r_w}^3)$ where r_w denotes the distance from the transmitter to the closest wall. Function γ represents the fact that staff members are less likely to go between a wall and the head of the bed and is equal to $1 - \exp(-{r_m}^3)$ where r_m denotes the distance from the transmitter to a point between the wall and the head of the bed. This definition for γ is only for the region between heads of beds #3 and #4 and the wall to the left as it is the only region at which the beds are close enough to a wall to hinder presence of a person. For all other regions and for the other two beds $\gamma = 1$.

The presence probability function, whose integral over the whole ward equals unity, is given by

$$p_{tx}(x', y') = \frac{\alpha(x', y')\beta(x', y')\gamma(x', y')}{\iint_S \alpha(x', y')\beta(x', y')\gamma(x', y')\,\mathrm{d}x'\,\mathrm{d}y'} \tag{5.3}$$

where S is the entire area of the ward at the height of h. For the 6.4 m by 6.5 m ward

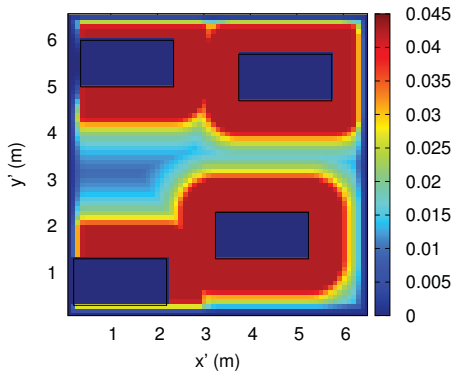

Figure 5.2: The map of the presence probability function, $p_{tx}(x', y')$.

shown in Fig. 5.1, the presence probability is determined and shown in Fig. 5.2.

5.3.1 Minimum Separation Distance

The presence probability is modified to account for a minimum separation distance policy. Consider that there is an EMD at (x, y) and that medical staff carrying transmitters are required not to approach the medical device closer than d_{MS} meters. Let C be the probability of compliance, $0 \leq C \leq 1$, where $C = 1$ indicates full compliance. Hence the presence probability becomes a function of both the transmitter location, (x', y'), and the EMD location, (x, y).

Assuming full compliance ($C = 1$), the presence probability is zero within a circle of radius d_{MS} and centered at (x, y). Medical staff approaching the medical device will now stop and stand at a distance of d_{MS}. A 25 cm is considered sufficient for a staff member to stand. Hence within an annulus of inner radius d_{MS} and outer radius $d_{MS} + 0.25$, the value of the presence probability function is increased in order to compensate for the zero probability within the MSD circle.

Considering some non-compliance, inside the MSD circle, the presence probability function is equated to $(1 - C)$ of its value when no MSD policy is in effect. If the medical device is located at (x, y) and an MSD policy is in effect, the presence

probability is defined as

$$p_{tx}^{(\mathrm{MSD})}(x,y,x',y') = \begin{cases} (1-C)p_{tx}(x',y') & \text{if } r \le d_{MS}, \\ a_0 p_{tx}(x',y') & \text{if } d_{MS} \le r \le d_{MS}+0.25, \\ p_{tx}(x',y') & \text{if } r > d_{MS}+0.25 \end{cases} \quad (5.4)$$

where a_0 is determined such that the likelihood that there is a wireless transmitter within the circle centered at (x, y) and of radius $d_{MS}+0.25$ remains the same as when no MSD policy was specified. Thus, integrating the presence probability function over the area of this circle results in the same value whether or not an MSD policy is applied. If $C = 0$ then $p_{tx}^{(\mathrm{MSD})}(x,y,x',y') = p_{tx}(x',y')$ which means that the MSD policy is not at all complied with.

The presence probability function, which gives the presence pattern of a roaming transmitter, is used together with the REI associated with a steady transmitter to determine the risk of exceeding immunity for a roaming transmitter.

5.4 Presence-Weighted Risk of Exceeding Immunity

The presence-weighted risk of exceeding immunity is given for one and two roaming transmitters.

5.4.1 One Mobile Transmitter

Suppose that there is only one transmitter in the ward. In order to give the presence-weighted risk of exceeding immunity, a theorem from probability is used. Let S be the entire sample space of all events and let $H_1, H_2, \ldots, H_n$ be events which (i) are mutually exclusive and (ii) their union is the sample space S. The *law of total*

probability [68] states that the probability of an event A is given by

$$P(A) = P(A|H_1)P(H_1) + P(A|H_2)P(H_2) + \ldots + P(A|H_n)P(H_n). \tag{5.5}$$

Assume event A is defined as the risk of exceeding immunity at (x, y). The probability of event A *given that* the transmitter is at (x', y') is here denoted by $P_c\left(E \geq \mathrm{E_I}, x, y, x', y'\right)$. Without losing its validity, let us extend (5.6) from summation in one dimension for H_k to summation in two dimensions for H_{ij}. Event H_{ij} is considered as finding the transmitter at a very small area around (x'_i, y'_j) and its probability is shown by $p_{tx}(x, y, x', y')\Delta x'\Delta y'$. Thus the risk of exceeding immunity at (x, y), $P(A)$, which accounts for the presence probability of the transmitter, becomes equal to $\sum_i \sum_j P_c\left(E \geq \mathrm{E_I}, x, y, x'_i, y'_j\right) p_{tx}(x, y, x', y')\Delta x'\Delta y'$. $P(A)$, or the presence-weighted risk of exceeding immunity, is specifically denoted by $P\left(E \geq \mathrm{E_I}, x, y\right)$ and in the limit where $\Delta x'$ and $\Delta y'$ approach zero, it is given by

$$P\left(E \geq \mathrm{E_I}, x, y\right) = \iint_S p_{tx}^{(\mathrm{MSD})}(x, y, x', y') P_c\left(E \geq \mathrm{E_I}, x, y, x', y'\right)\, \mathrm{d}x'\, \mathrm{d}y' \tag{5.6}$$

where the integration is over the area of the room.

For instance, for a medical device at (x, y) if there is 100% probability that the wireless transmitter will be at a point 1 m away from the EMD, the PWREI concept is not required and the risk should be simply determined by (5.1). If there is 30% probability that the transmitter will be at a point 1 m away and a 70% probability that it will be at another point 3 m away, then one must evaluate (5.1) for 1 m distance to determined p_1 and again for 3 m distance to obtain p_2, and add them using the presence probability as a weight, PWREI$= 0.3p_1 + 0.7p_2$. Equation (5.6) is a generalization of this concept.

5.4.2 Two Mobile Transmitters

If there are transmitters at (x'_1, y'_1) and (x'_2, y'_2), then the PWREI is given by

$$P(E > \mathrm{E_I}, x, y) = \iiiint_S p_{tx}^{(\mathrm{MSD})}(x, y, x'_1, y'_1) p_{tx}^{(\mathrm{MSD})}(x, y, x'_2, y'_2) \cdot P_c(E, x, y, x'_1, y'_1, x'_2, y'_2)\, \mathrm{d}x'_1\, \mathrm{d}y'_1\, \mathrm{d}x'_2\, \mathrm{d}y'_2 \quad (5.7)$$

where the risk of exceeding immunity with two transmitters, P_c, is given by (5.1) using a direct field, E_d and a net multipath mean value, E_m as explained following (5.1). If No MSD policy is applied, in (5.6) and (5.7), C should be equal to zero which is equivalent to using p_{tx} instead of $p_{tx}^{(\mathrm{MSD})}$.

In the following, the PWREI is determined for these cases: (i) no restriction on mobile transmitter location, and (ii) applying an MSD policy with full compliance, and (iii) an MSD with some non-compliance.

5.5 Application to a Hospital Ward

The PWREI model is applied to the hospital ward which is shown in Fig. 5.1 and measures 6.4 m by 6.5 m. The ceiling is at the height of 3 m. Each wireless transmitter is assumed to radiate 100 mW at 2.45 GHz (one of the frequencies of the IEEE 802.11 standards) with a half-wavelength dipole directivity of $D = 1.64$. The EMD and the transmitters are assumed to be at the same height of $h = 1.3$ m above the floor. There are four beds each located in a different position with respect to the closest wall in order to investigate the effects of bed configuration on the risk of exceeding immunity.

5.5.1 PWREI with No Policy Restricting Transmitter Location

In the no-restriction policy, the transmitters are assumed to be able to roam freely in the room and thus approach the medical devices closely.

One Transmitter

Fig. 5.3 shows the calculated PWREI for an EMD in the presence of one transmitter and for two immunity levels: 3 and 10 V/m. The axes indicate the location of the medical device, (x, y). This figure shows the PWREI at each location given the presence probability function in Fig. 5.2. At both immunity levels, the areas between the head of a bed and a wall have relatively smaller risk values given that the bed is located close enough to the wall. An EMD in a corner area, where the presence of a transmitter is restricted by two walls, is exposed to a lower risk in the low-immunity case. The locations with the highest risk are the regions near the patient bedside, probably the most common locations for medical devices.

When the immunity level is 3 V/m, as shown in Fig. 5.3(a), the maximum risk is 0.0713, much greater than the assumed safe risk level of 0.0001. For 10 V/m, as shown in Fig. 5.3(b), the maximum risk is 0.00642, almost an order of magnitude smaller, but still too large.

Two Transmitters

Figs. 5.4(a) and 5.4(b) show the PWREI maps in the presence of two transmitters. When $E_I = 3$ V/m, as shown in Fig. 5.4(a), the risk has a maximum of 0.160 which is more than twice as the maximum PWREI in the presence of only one transmitter. For $E_I = 10$ V/m, as shown in Fig. 5.4(b), the maximum PWREI is 0.0133 which is approximately as the maximum PWREI in the presence of one transmitter. Hence the presence of a second transmitter results in a PWREI with a maximum value

increased by a factor of almost two.

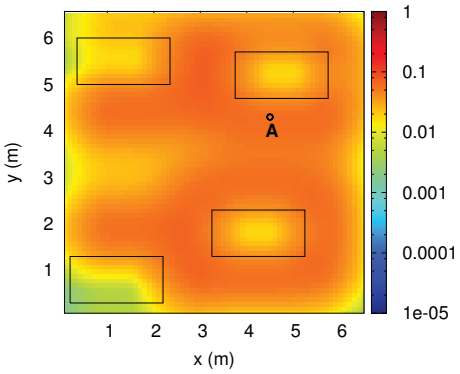

(a) E_I = 3 V/m. The maximum value of the PWREI is 0.0713.

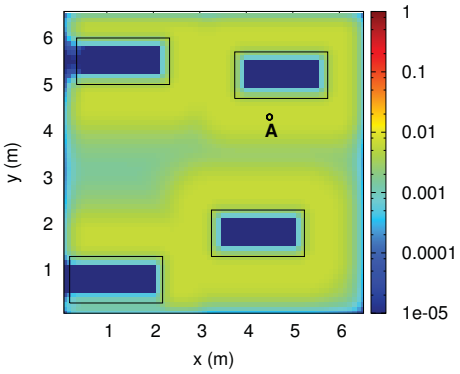

(b) E_I = 10 V/m. The maximum value of the PWREI is 0.00642.

Figure 5.3: The PWREI map in the presence of one transmitter. No EMI-control policy restricting the transmitter location is accounted for in this figure. The small black circle shows the position of point "A".

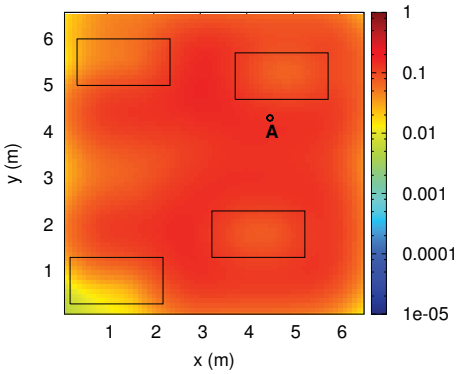

(a) E_I = 3 V/m. The maximum value of the PWREI is 0.160.

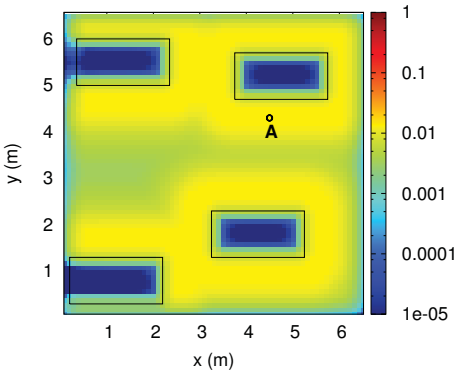

(b) E_I = 10 V/m. The maximum value of the PWREI is 0.0133.

Figure 5.4: The PWREI map in the presence of two transmitters. No EMI-control policy restricting the transmitter location is accounted for in this figure.

5.5.2 MSD Policy with Full Compliance

Here an MSD policy is assumed where medical staff carrying a wireless transmitter are required not to approach the medical device any closer than 70 cm. As a result, a nurse or a doctor carrying a tablet computer will stand at about an arm's length from a medical ventilator while reading the display screen of the device or setting the controls. The following compares the PWREI for full compliance ($C = 1$) and for some non-compliance ($0.9 \leq C < 1$).

One Transmitter

It is shown in Fig. 5.5(a), that at 3 V/m immunity, the maximum PWREI is reduced from 0.0713 with no MSD policy to 0.0274 assuming a 70 cm MSD. When $E_I = 10$ V/m, the maximum risk risk is calculated to be much less than 10^{-5} which is the accuracy of our Fortran implementation of the risk model, evaluating the Ricean function and (5.1). The risk map is presented in Fig. 5.5(b).

Two Transmitters

It is shown in Fig. 5.6(b) that at the higher immunity level, the maximum risk is much less than 0.0001. So the MSD policy, considering full compliance, can reduce the risk to less than 0.0001 for life-support EMDs having an immunity of 10 V/m. At the immunity level of 3 V/m, as shown in Fig. 5.6(a), the risk values at most locations remain above the safe level.

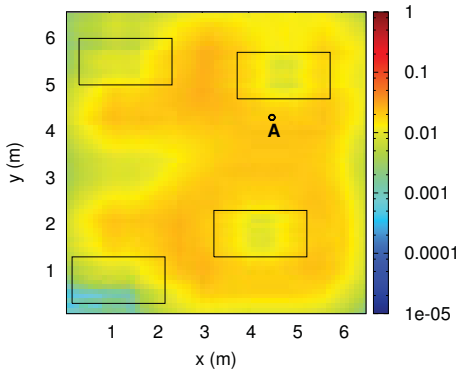

(a) $E_I = 3$ V/m. The maximum value of the PWREI is 0.0274.

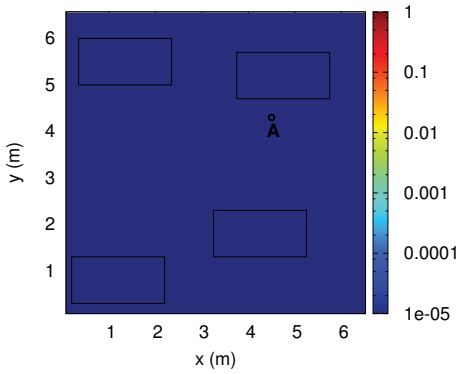

(b) $E_I = 10$ V/m. The maximum value of the PWREI is much less than 10^{-5}.

Figure 5.5: The PWREI map in the presence of one transmitter. An MSD of 70 cm is accounted for and fully complied with by the staff members. The small black circle shows the position of point "A".

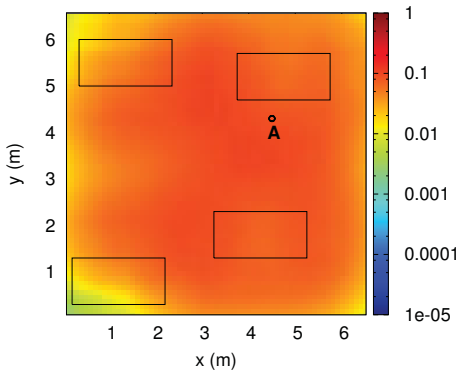

(a) $E_I = 3$ V/m. The maximum value of the PWREI is 0.104.

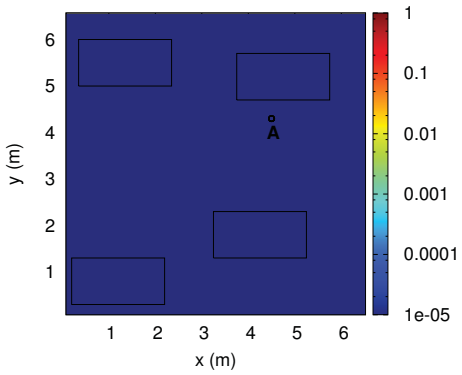

(b) $E_I = 10$ V/m. The maximum value of the PWREI is less than 10^{-5}.

Figure 5.6: The PWREI map in the presence of two transmitters. An MSD of 70 cm is accounted for and fully complied with by the staff members. The small black circle shows the position of point "A".

PWREI vs. MSD

How is the risk affected if the specified MSD value is changed? Is the risk significantly increased if a less-restrictive and smaller MSD is specified? Such questions are answered by plotting the PWREI versus MSD where the PWREI values belong to a single point. Assume that an EMD is located at point A, near a bedside at ($x = 4.5$ m , $y = 4.3$ m) which is shown in Fig. 5.1. The dashed curves in Figs. 5.7 and 5.8 show that the risk constantly decreases with the MSD, assuming full compliance with the policy. A 0-cm minimum separation distance means that no MSD policy is specified.

The *critical MSD* is defined as the MSD value for which the PWREI equals the safe risk figure of 0.0001. The *free space separation* is the distance from the transmitter in free space at which the field strength is equal to the immunity level. In the following the critical MSD is compared to the free space separation which assumes that the location of the transmitter is given.

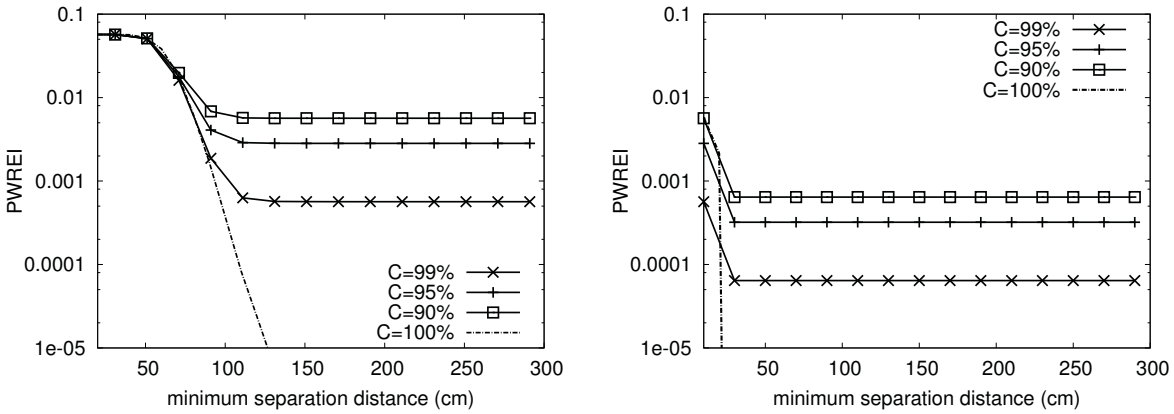

(a) $E_I = 3$ V/m (b) $E_I = 10$ V/m

Figure 5.7: The PWREI against MSD in the presence of one transmitter. The PWREI values are given for the point "A" as shown in Fig. 5.1. Each figure contains the PWREI plots for C=90%, 95%, 99% and 100%. The $C = 100\%$ means full compliance with the MSD policy.

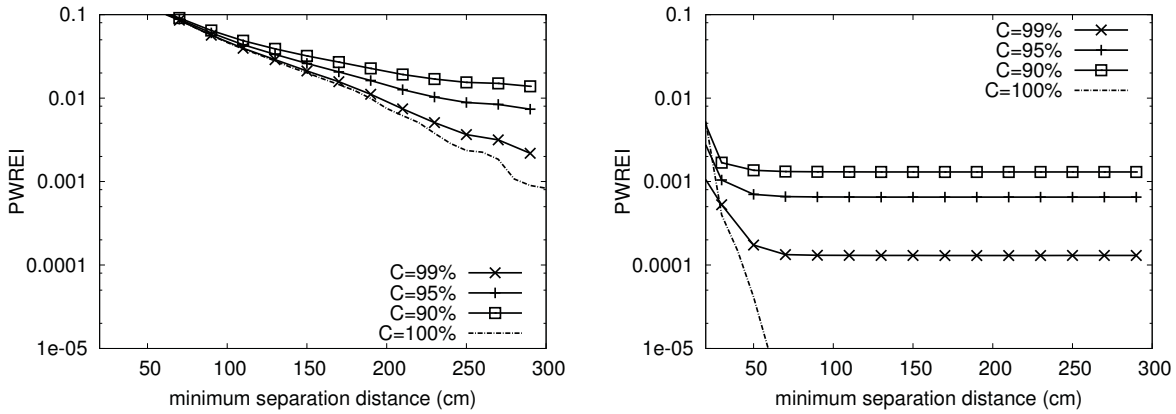

(a) $E_I = 3$ V/m (b) $E_I = 10$ V/m

Figure 5.8: The PWREI against MSD in the presence of two transmitters. The PWREI values are given for the point "A" as shown in Fig. 5.1. Each figure contains the PWREI plots for C=90%, 95%, 99% and 100%. The $C = 100\%$ means full compliance with the MSD policy.

One Transmitter In Fig. 5.7, the PWREI values at point A is plotted against the MSD using (5.6). For the 10 V/m immunity level, when the MSD is completely complied with, the PWREI quickly drops below 0.00001 after an MSD of around 22 cm. The free space separation at 10 V/m is 22 cm. For the 3 V/m immunity level, it takes an MSD of around 105 cm to bring the PWREI to lower than 0.0001. The free space separation at 3 V/m is 74 cm.

Two Transmitters The PWREI in the presence of two transmitters accounting for the MSD policy is obtained using (5.7). For 3 V/m immunity, even with full compliance, the PWREI remains above 0.01 for MSD values below 190 cm and above 0.001 for MSDs between 190 and 270 cm. MSD values larger than about a meter would require medical staff to set aside their wireless device before approaching a medical device to adjust the controls, so are not practical. With 10 V/m immunity and full compliance, as shown in Fig. 5.8, a minimum separation of only 40 cm is sufficient for a risk less than 0.0001.

Optimal Locations

There are some locations in the room which are relatively safer. It is seen in Figs. 5.3, 5.4, 5.5 and 5.6 that the corners of the room have relatively lower levels of risk of exceeding the 3 V/m immunity. A device with a lower immunity level is affected by a transmitter at farther distances. At areas near a corner, the two walls significantly limit the possibilities for presence of a transmitter. So the corners, which are close to a patient bed thus useful for locating an EMD, can be considered as *optimal locations* for lower immunity devices. However, higher immunity devices are only affected by transmitters which are at a close vicinity. So for a point, e.g. 30 centimeters from a corner and inside the room and when an MSD policy is not applied, the areas behind the two walls would not pose a considerable risk on the EMD if the walls did not exist. Hence the existence of the walls does not significantly reduce the risk for higher immunity devices. For the higher immunity, it is seen that the optimal location is the area behind the patient's head, if the bed is close enough to the wall.

In the foregoing results, a full compliance with the MSD policy – if applied – was assumed. The following section assesses the risk when medical staff do not fully comply with this policy.

5.5.3 Non-compliance Consideration

Medical staff may not fully comply with the minimum separation requirement, occasionally approaching medical devices closer than the MSD. Figures 5.7 and 5.8 show the PWREI as a function of the MSD for compliance levels of 90, 95 and 99%. With some non-compliance, the risk drops rapidly for small MSD values and then remains almost constant for larger MSDs. The minimum value for a given compliance level is the *risk floor*; further increase in the MSD does not reduce the risk below the risk floor. The smallest MSD needed to reach the risk floor is the *optimal MSD* for a given compliance level.

For a medical device at point A in Fig. 5.1, if the immunity is 3 V/m, then with one transmitter present in the room and a high compliance level of 99%, Fig. 5.7(a) shows that the risk floor is about 0.0006 for a minimum separation of 115 cm, above the desired risk of 0.0001. For 10 V/m immunity, Fig. 5.7(b) shows that with one transmitter and a compliance level of 99%, the risk floor is about 0.00006 for an MSD of 23 cm, below the desired level. But with less compliance the risk rises. With 95% compliance the risk floor is 0.0003, higher than desired. With two transmitters and 10 V/m immunity, even with 99% compliance the risk floor is 0.00013 for an MSD of 66 cm, and the desired risk level cannot be achieved. The PWREI-vs-MSD graph for the two-transmitter case is shown in Fig. 5.8.

5.5.4 Increasing Immunity

The risk floor, in the presence of two transmitters, can be reduced by increasing the immunity level. Figure 5.9 demonstrates the risk floor as a function of immunity level for compliance levels of 90, 95 and 99%. With a 99% compliance rate and a 20 V/m immunity level, the safe risk target of less than 0.0001 is achieved. If the compliance rate is only 95%, then a 30 V/m immunity level is required to achieve the desired risk level.

Point A is considered as a common bedside location for a medical device. An EMD between the head of the bed and the wall, point B near bed #3 as shown in Fig. 5.1, is exposed to much lower values of the risk. The curve labeled B, in Fig. 5.9, demonstrates that the risk floor for a 10 V/m immunity is below 0.0001 for a compliance rate of 90%. Hence the bed configuration near point B is inherently safe as the movement of the medical staff is restricted by the close distance between the bed and the wall.

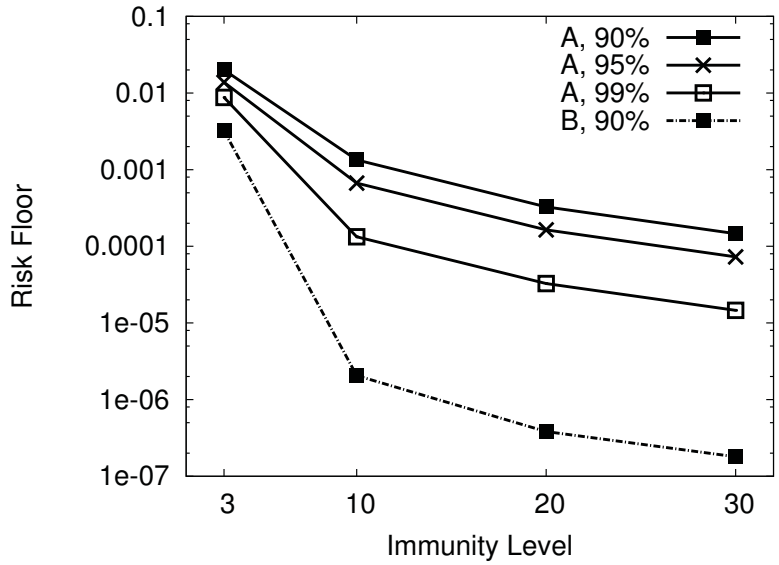

Figure 5.9: The risk floor against immunity level in the presence of two transmitters for C =90%, 95% and 99%. This risk floor is given for the locations of point A and point B.

5.5.5 Vertical Separation

In the foregoing, it was assumed that the medical device and the wireless transmitter are located at the same height above the floor. Thus the staff members were assumed to hold the tablet computers at chest level, and medical devices might be located at almost the same height for convenient use. Here a vertical separation of Δz m is specified which requires that the medical devices are located at Δz meters above the level at which tablet computers are used. The total distance between the transmitter and the EMD becomes $\sqrt{\Delta z^2 + r^2}$ where r is the distance in the horizontal plane. In the application of the MSD policy the distance Δz has no role. The MSD value is measured only in the horizontal plane. The risk floor as a function of the immunity level is presented in Fig. 5.10 for different values of Δz. The risk floor in this figure is calculated for point A where the rate of compliance is 90%. The curve marked as "0 cm" indicates that no vertical separation is accounted for. This curves is the same as the curve marked as "A, 90%" in Fig. 5.9.

It is seen in Fig. 5.10 that the risk floor for an immunity level of 3 V/m is not

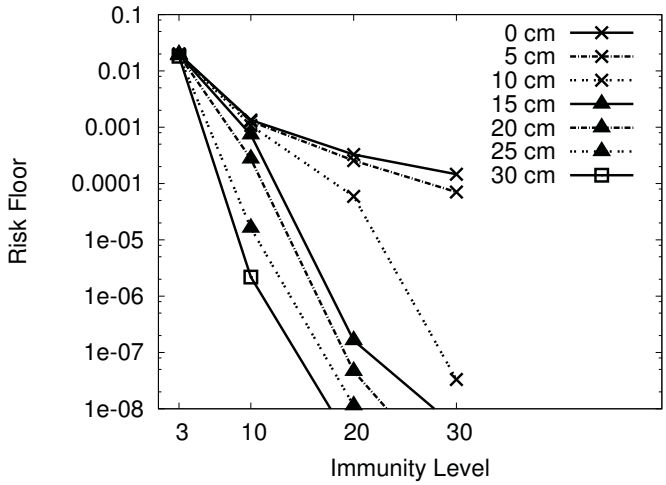

Figure 5.10: The risk floor at point A against immunity level in the presence of two transmitters for C =90%. Different values of vertical separation are analyzed.

affected even by a vertical separation as large as 30 cm. For an immunity of 10 V/m, a 10 cm vertical separation makes no tangible effect. A vertical separation of 25 cm is required to achieve a risk floor below the safe level at the 10 V/m immunity. When the immunity is 20 V/m, a 5 cm vertical separation makes very small difference. A 15 cm vertical separation, brings the risk floor well below the safe level. For an immunity of 30 V/m, a 10 cm vertical separation is enough to push the risk floor far below the safe level.

Figure 5.10 shows that a vertical separation of 5 cm is of no use even at very high immunity levels. The 30 cm vertical separation is more than enough for immunity levels of 10 V/m and above. Therefore the vertical separation can range from 10 cm to 25 cm. It is chosen based on the immunity level of the EMD in use. If EMDs with immunity levels as low as 10 V/m are used, a vertical separation of 25 cm is recommended.

In all vertical separation cases, considered above, a compliance rate of 90% is assumed. Figs 5.7 and 5.8 show that the risk values are very sensitive to the compliance rate. A compliance rate higher than 90% can be achieved if the staff members are educated to follow the MSD policy. In the following a sensitivity analysis is provided

for the relation between the risk floor and the compliance rate. The sensitivity analysis also investigates the effects of increasing or decreasing the multipath mean value. The effect of choosing a difference presence probability is also analyzed.

5.5.6 Sensitivity Analysis

Effects of Changing the Compliance Rate

The risk floor, for immunity levels of 10 V/m and above and at point A in the presence of two transmitters with no vertical separation is determined considering the following compliance rates: 90, 97, 95, 99 and 99.5%. The risk floor is not defined for a 100% compliance rate with which the PWREI can be reduced to any desired level by increasing the MSD. Point A is chosen for this analysis as it is one of the riskiest points in the room and any results obtained for this point can be deemed as a general solution covering the entire room. Presence of two transmitters is riskier and more likely in a busy hospital than the presence of a single transmitter. The 3 V/m immunity level is not considered since it is usually unsafe.

The risk floor is plotted against the compliance rate in Fig. 5.11. It is seen that with the 90% compliance rate, even EMDs with the 30 V/m immunity level are not safe. When $C = 99.5\%$, EMDs with immunity level as low as 10 V/m are safe. It is seen that the risk floor becomes more sensitive to the changes in the compliance rate as the compliance rate approaches 99.5%. If the compliance rate drops to 90% and below, even very high immunity devices are unsafe hence the MSD policy loses its efficiency. This indicates the necessity of educating the hospital staff on the subject of complying with the MSD policy as a one-percent reduction in the compliance rate could result in a significant increase in the risk floor.

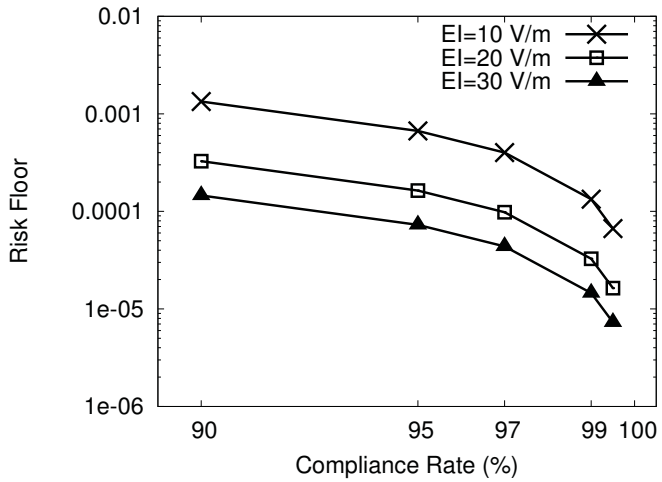

Figure 5.11: The risk floor at point A against the compliance rate in the presence of two transmitters for. Different immunity levels are considered. No vertical separation is assumed.

Effects of Having Different MMVs

The multipath mean value computed by the Sabine method of the room shown in Fig. 5.1 is 0.5621 V/m. If the walls were less reflective and the MMV was 0.2 V/m, the risk results is shown not to change considerably. The risk maps for the two immunity levels of 3 and 10 V/m are obtained in the presence of one and two transmitters for $E_m = 0.2$ V/m and are shown in Figs. 5.12 and 5.13. No MSD policy is applied. So these figures must be compared to Figs. 5.3 and 5.4.

If the MMV is raised to 1.3 V/m, the risk maps are given in Figs. 5.14 and 5.15. These figures must be compared to Figs. 5.3 and 5.4.

It is seen that lowering the MMV does not considerably affect the PWREI. Also increasing the MMV only affects the PWREI for the 3 V/m immunity. The 3 V/m immunity is considered unsafe and is not recommended/supposed to be used. In case of higher immunity, the PWREI is not much affected by increasing the MMV to 1.3 V/m.

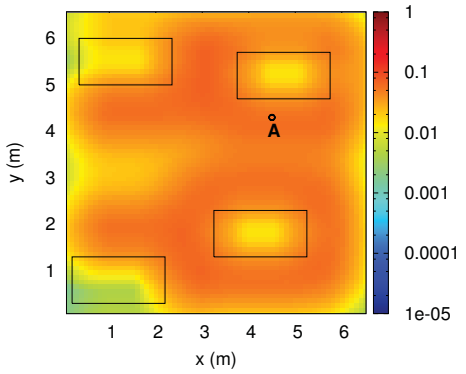

(a) E_I = 3 V/m. The maximum value of the PWREI is 0.06937.

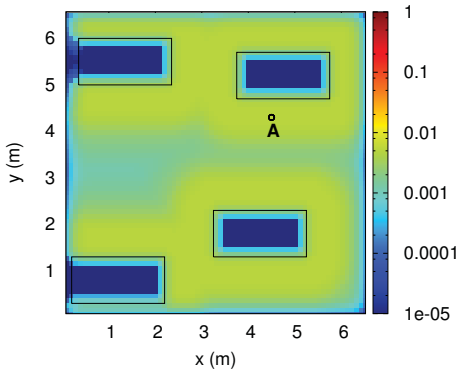

(b) E_I = 10 V/m. The maximum value of the PWREI is 0.005834.

Figure 5.12: The PWREI map in the presence of one transmitter. No EMI-control policy restricting the transmitter location is accounted for in this figure. The MMV is reduced to 0.2 V/m. The small black circle shows the position of point "A".

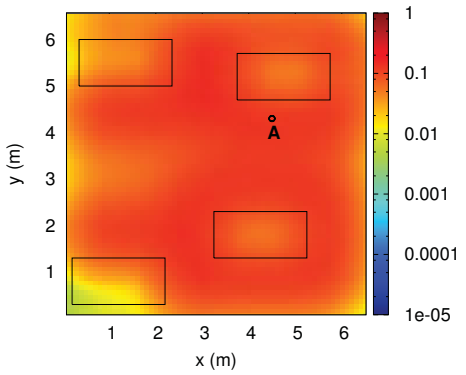

(a) E_I = 3 V/m. The maximum value of the PWREI is 0.14796.

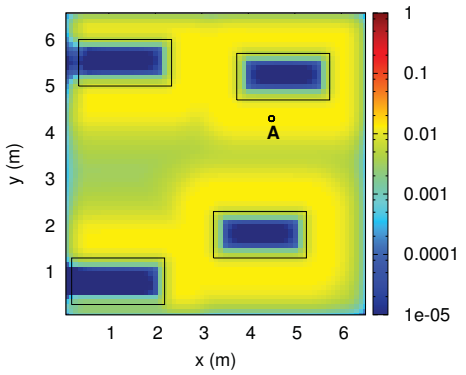

(b) E_I = 10 V/m. The maximum value of the PWREI is 0.013255.

Figure 5.13: The PWREI map in the presence of two transmitters. No EMI-control policy restricting the transmitter location is accounted for in this figure. Both MMVs are reduced to 0.2 V/m.

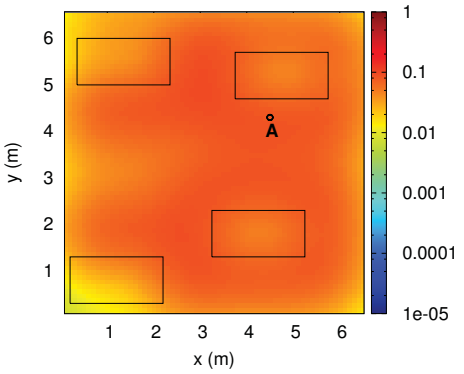

(a) $E_I = 3$ V/m. The maximum value of the PWREI is 0.09425.

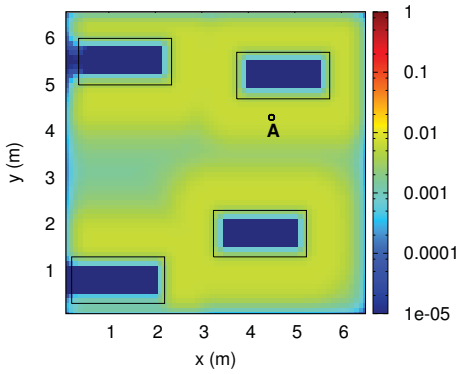

(b) $E_I = 10$ V/m. The maximum value of the PWREI is 0.006496.

Figure 5.14: The PWREI map in the presence of one transmitter. No EMI-control policy restricting the transmitter location is accounted for in this figure. The MMV is increased to 1.3 V/m. The small black circle shows the position of point "A".

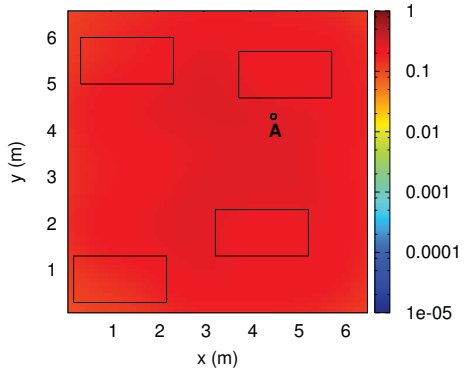

(a) $E_I = 3$ V/m. The maximum value of the PWREI is 0.2781.

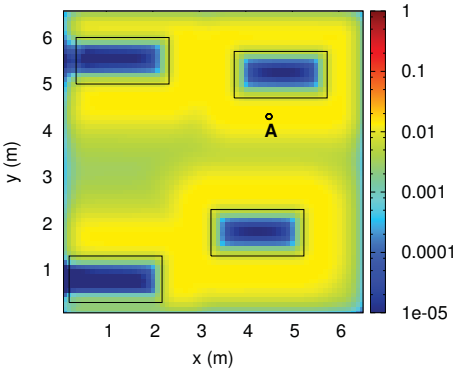

(b) $E_I = 10$ V/m. The maximum value of the PWREI is 0.01374.

Figure 5.15: The PWREI map in the presence of two transmitters. No EMI-control policy restricting the transmitter location is accounted for in this figure. Both MMVs are increased to 1.3 V/m.

Effects of Changing the Presence Probability Function

The presence probability is changed to a have a much simpler definition. Assume α is zero over the beds and elsewhere is redefined as

$$\alpha' = \begin{cases} 1 & \text{if } r_b < 1, \\ 0 & \text{if } r_b \geq 1 \end{cases} \tag{5.8}$$

and the presence probability is redefined as

$$p_{tx}\left(x', y'\right) = \frac{\alpha'(x', y')}{\iint_S \alpha'(x', y')\, \mathrm{d}x'\, \mathrm{d}y'}, \tag{5.9}$$

then the presence probability is evaluated again and is shown in Fig. 5.16 which looks rather different from Fig. 5.2.

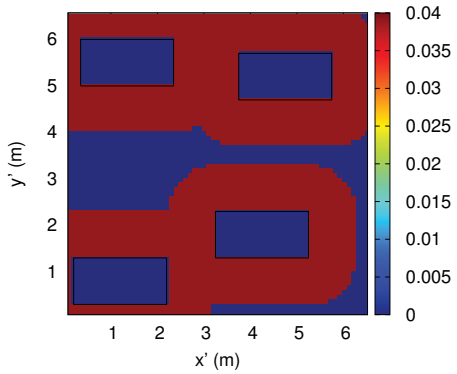

Figure 5.16: The new map of the presence probability function, $p_{tx}(x', y')$ as defined in (5.9).

With this new presence probability and with no MSD policy the risk maps are presented in Figs. 5.17 and 5.18. When these figures are compared to Figs. 5.3 and 5.4, no large changes are seen; especially at positions near a patient's bedside which is more suitable for locating a medical device. Hence the PWREI is seen to be not very sensitive to some changes in the presence probability.

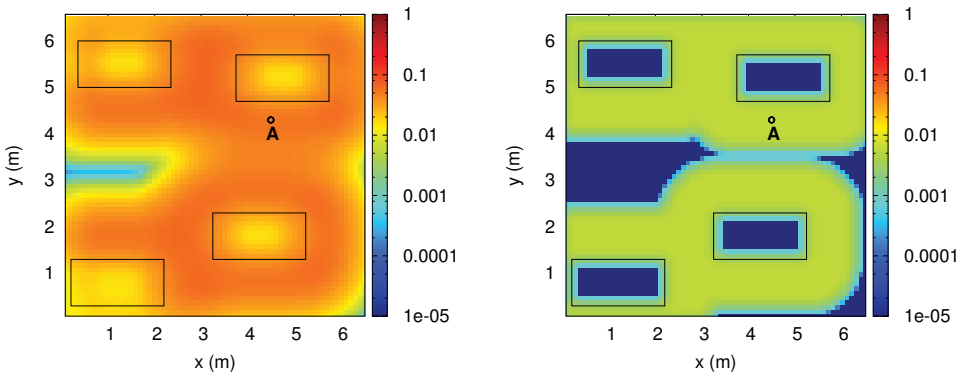

(a) $E_I = 3$ V/m. The maximum value of the PWREI is 0.0667.

(b) $E_I = 10$ V/m. The maximum value of the PWREI is 0.005894.

Figure 5.17: The PWREI map in the presence of one transmitter with the new presence probability shown in Fig. 5.16. No EMI-control policy restricting the transmitter location is accounted for in this figure.

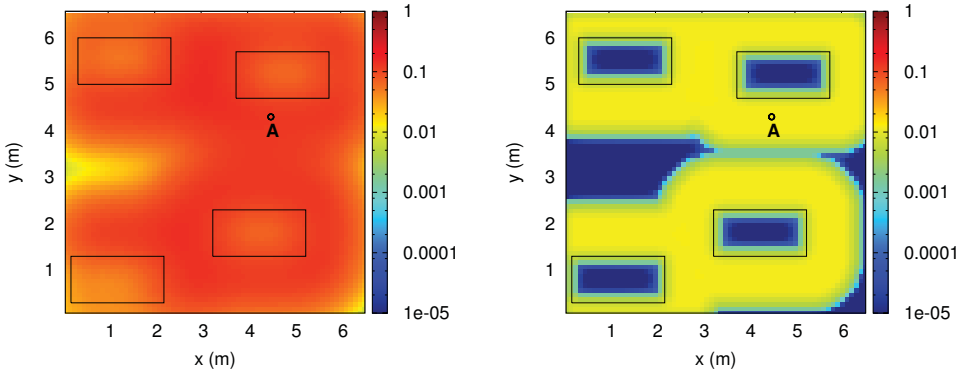

(a) $E_I = 3$ V/m. The maximum value of the PWREI is 0.1495.

(b) $E_I = 10$ V/m. The maximum value of the PWREI is 0.01221.

Figure 5.18: The PWREI map in the presence of two transmitters with the new presence probability shown in Fig. 5.16. No EMI-control policy restricting the transmitter location is accounted for in this figure.

Also the risk model presented in this chapter is not much sensitive to small changes in the frequency. For example if the frequency of operation is changed from 2.45 GHz to 2.4 or 2.5 GHz, the Sabine estimate of the multipath field remains to be almost the same. Hence the PWREI has a low sensitivity to small changes in frequency. However if the frequency is doubled, a different multipath field is expected which may affect the risk results.

In the following, a discussion on the computational time of the PWREI algorithm is presented.

5.6 Computational Time

To obtain the PWREI map in the presence of two transmitters and for the 10 V/m immunity level, using one core of a 2.93-GHz Intel Xeon CPU, 70 minutes was required. The cell size at 10 V/m immunity was 10 cm by 10 cm. When the immunity level is 20 or 30 V/m, the cell size must be reduced to 2 cm by 2 cm as the higher immunities are exceeded at closer distances and at closer distances the field varies more rapidly. With the 2 cm by 2 cm cell size, obtaining the PWREI map would require 760 days. Hence the PWREI calculations are only given for one EMD location at immunity levels 20 and 30 V/m and each calculation took slightly more than 10 minutes.

Also by increasing the number of transmitters, the number of permutations thus the computational time grows exponentially. For example, adding a third transmitter at high immunity levels, would require 741 days to complete the one-point calculation of the PWREI. Hence, as a future work, the computational efficiency of the PWREI algorithm must be increased.

The PWREI accounts for both close and far distances between the transmitter and the EMD. If only high-risk scenarios where the transmitters remain close the

EMD at most times then a worst-case analysis may be more suitable.

5.7 Worst-Case Risk Assessment

In this section it is assumed that the transmitters are at fixed distances from the EMD. For this fixed location, the risk of exceeding immunity is determined using the Sabine-Rice approximation. In a worst-case analysis, a distance is found such that the REI equals the safe level. This distance is then compared to the separation distance suggested by the International Electrotechnical Committee. These two distances are compared to the optimal MSD which assumes the transmitters are roaming.

For the worst-case analysis, the REI is used. The REI is dependent only on the distance between the EMD and the transmitter, r, and is given by

$$\mathrm{REI}(r) = P_c\left(E \geq \mathrm{E_I}, r\right) = \int_{\mathrm{E_I}}^{\infty} p_c(E)\,\mathrm{d}E. \tag{5.10}$$

where p_c is the Ricean distribution which uses the parameters E_d and E_m. E_m in our hospital ward was estimated by the Sabine method to be 0.5621 V/m. E_d is the direct field and is dependent on r.

In the worst case analysis, the transmitter is assumed to be at a fixed distance from the EMD. This distance, denoted by R_{REI}, is found such that $\mathrm{REI}(R_{REI})$ equals 10^{-4}, the safe risk level. This distance is compared to the optimal MSD at which the PWREI in the presence of one transmitter reaches the risk floor assuming a compliance rate of 99%. The optimal MSD is denoted here by R_{MSD} and is reported only if the risk floor is below the safe leve.

Separation distances R_{REI} and R_{MSD} are then compared to the separation distance suggested in IEC 60601-1-2 standard [9]. In this standard, for the frequency of 2.45 GHz, the separation distance is given as $23\sqrt{P_t}/\mathrm{E_I}$ for life-support devices and as $7\sqrt{P_t}/\mathrm{E_I}$ for the non-life-support devices. P_t is the transmitted power which is 100

Table 5.1: Comparison of Three Separation Distances Given by the REI, PWREI and IEC Standard

	R_{REI} (m)	R_{MSD} (m)	R_{IEC} (m)
1 Tx, 3 V/m	1.49	1.15	2.42
1 Tx, 10 V/m	0.27	0.23	0.73
2 Tx, 3 V/m	—	—	3.43
2 Tx, 10 V/m	0.86	0.65	1.03

mW.

In this section it is assumed that the EMDs are all life-support devices. In the IEC formula for the separation distance, the immunity level is a variable. So for life-support devices the immunity can be a number equal to or different from 10 V/m. Here two values are assumed, 3 and 10 V/m. The EMD with an immunity level of 3 V/m may be a very old life-support device. The IEC suggestion for the separation distance is denoted by R_{IEC} and is calculated by $23\sqrt{P_t}/\mathrm{E_I}$.

If there are two transmitters, they are assumed to be at the same distance from the EMD. In determining R_{REI}, the direct field stength of one of the transmitters is used as E_d and the total multipath mean value used in the Ricean equation in (5.10) is the square root of ${E_d}^2 + 2{E_m}^2$. The risk floor and the optimal MSD is already determined in this chapter. In determining R_{IEC}, the power of the two transmitters are added. Hence $P_t = 200$ mW. All three separation distances are obtained for the two immunity levels, 3 and 10 V/m, in the presence of one and two transmitters. The results are shown in Table 5.1.

5.7.1 One Transmitter

In the presence of one transmitter, the IEC standard gives a separation distance, I_{IEC}, of 2.42 m for a 3 V/m immunity level which is more conservative than $R_{REI} =$ 1.49 m. The PWREI method gives an optimal MSD, R_{MSD}, of 1.15 m which is less conservative than the other two. When the immunity level is 10 V/m, R_{MSD}

becomes 23 cm. The IEC suggests a 73 cm separation whereas the worst case analysis recommends a separation of R_{REI} =26.1 cm only.

5.7.2 Two Transmitters

In the presence of two transmitters, the REI and the PWREI never reach below the safe level within a reasonable separation distance (less than 3 m) for 3 V/m immunity level. Also the IEC standard suggests an impractically large separation of 3.43 m. For the 10 V/m immunity level, the IEC suggests a 103 cm separation and the worst case analysis suggests an 86 cm separation. The optimal MSD obtained by the PWREI method, R_{MSD}, is 65 cm.

In the presence of one or two transmitters, it is seen that the worst-case analysis suggests less conservative separation distances compared to the IEC standard.

In the presence of two transmitters, low immunity devices are unsafe and should not be used.

The risk values, i.e. the REI, and the worst-case separation distance, i.e. R_{REI}, are dependent on the multipath mean value, E_m. In the following a lower MMV is assumed.

5.7.3 Worst-Case Analysis in a Large Room

The worst-case analysis is repeated in a larger room where the multipath field is smaller and lower levels of the risk are expected. A new MMV is assumed and R_{REI} is recalculated. The hospital ward considered in this chapter measures 6.4 m by 6.5 m. The ceiling is at the height of 3 m. The floor plan is assumed to increase by a factor such that the multipath room absorption calculated by (1.7) is reduced by a factor of 4. Thus the MMV, E_m, is reduced by a factor of 2 and is 0.281 V/m. This is achievable by increasing the x and y dimensions of the room by a factor of about 2.3.

With the new MMV, the R_{REI} is recalculated. In the presence of one transmitter the new worst-case separation is 98.4 cm for the 3 V/m immunity level. This shows a 50.6 cm reduction compared to the case of the smaller room. R_{REI} is 24 cm for 10 V/m showing a 2 cm reduction compared to the previous case. In the presence of two transmitters, R_{REI} is 3.07 m for the 3 V/m immunity level. This shows a reduction of almost 2 m compared to the large room where E_{REI} was 4.99 m. Both separation values are impractical. For the 10 V/m immunity, R_{REI} is calculated to be 84 cm showing a 2 cm reduction from the case of the smaller room.

It is seen that increasing the dimensions of the room has little effect on the required separation distance for the high immunity devices. Whereas in the case of low immunity devices, the separation distance is considerably reduced.

The worst-case analysis presented here uses the Sabine-Rice approximation. A more exact analysis can be obtained using the modified ray-tracing-Rice method presented in Chapter 3. This suggestion is elaborated on in the following chapter.

This chapter has considered the presence of one and two transmitters in the room. It is possible that more than two transmitters be present in the room. One of the difficulties of accounting for higher number of transmitters in the PWREI model is the computational time which is discussed in the following.

5.8 Summary

In this chapter, a risk assessment study was conducted in the problem of mobile transmitters present in a four-bed hospital ward and electromagnetically interfering with the electronic medical devices. The Sabine-Rice method was used to obtain the risk of exceeding immunity given that the transmitter is at a specified location. The roaming nature of the transmitters was accounted for by the *presence probability function*. This function together with the Sabine-Rice estimate of the risk of exceeding

immunity was used to introduce and determine the *presence-weighted risk of exceeding immunity* which accounts for all possible locations of the transmitter. The PWREI provides a quantitative the measure of the risk and its variations as difference EMI control policies are applied. A minimum separation policy and a probability of non-compliance with the policy was considered. Also a vertical separation between the transmitters and the medical device was accounted for in this chapter.

The PWREI was applied to a 6.4 m by 6.5 m hospital ward with one and two roaming transmitters, each radiating 100 mW at 2.45 GHz. The Sabine-Rice approximation was used in order to approximate the pdf of the field of one or the sum field of two transmitters. The two values of the immunity level, 3 and 10 V/m, as suggested by the International Electrotechnical Committee (IEC) were used. The transmitters and the EMD are assumed to be at the same height unless a vertical separation policy is applied.

The engineer managing the risk of EMI in a hospital must develop a policy to ensure that the risk is below a safe level, chosen as 1 in 10,000. With no restriction on where portable transmitters can be used, Figs. 5.3 and 5.4 show that, with 10 V/m immunity, most locations in the room pose a risk of exceeding the immunity of a medical device that is above the desired safe level.

One risk-management strategy is to instruct staff to maintain a minimum separation distance between their tablet computer and medical devices. Applying a 70-cm MSD policy with a full compliance brought the presence-weighted risk of exceeding a 10 V/m immunity well below the assumed safe level in the presence of one and two transmitters as shown in Figs. 5.5(b) and 5.6(b).

Point A, as shown in Fig. 1.2, is close to a patient bedside, perhaps a typical location for a medical device and exposed to almost highest levels of risk. Fig. 5.7(b) showed that, in the presence of one transmitter, an MSD of 22 cm is sufficient to meet the safe level, assuming full compliance with the policy. In the presence of two

transmitters, it was seen in Fig. 5.8(b) that a 42 cm MSD is sufficient.

When the compliance rate is less than 100%, it was shown in Figs. 5.7 and 5.8 that increasing the MSD beyond a certain level is not useful. For very low values of the MSD, the PWREI decreases rapidly by increasing the MSD. The PWREI remains constant after a certain value of MSD which is called the *optimal minimum separation distance*. The PWREI at the optimal MSD is called the *risk floor*. Choosing MSD values larger than the optimal MSD is not recommended as larger values do not necessarily reduce the risk while they put more restriction on the movement of the staff members.

For an EMD with 10 V/m immunity and located in point A, in the presence of one roaming transmitter and assuming the compliance rate of 95% with the MSD policy, the risk floor, as shown in Fig. 5.7(b), is above the safe level . When the compliance rate is 99%, the safe risk target of 1 in 10,000 is achieved with an MSD of 23 cm. In the presence of two transmitters, as seen in Fig. 5.8(b), the risk floor is above the safe level even with a compliance rate of 99%.

In the presence of two transmitters, the safe level can be reached using three policies: (i) increasing the immunity level, (ii) locating the EMD at an optimal position, (iii) introducing a vertical separation between the wireless transmitters and the EMD. With a compliance rate of 99%, it is seen in Fig. 5.9 that the safe level is achieved by increasing the immunity level to 20 V/m. If the compliance rate is 95% or lower even an immunity of 30 V/m is not sufficient to reach the safe risk level.

It was also shown in Fig. 5.10 that a vertical separation between the transmitter and the EMD can significantly reduce the risk level. A 25 cm vertical separation was seen to be sufficient to bring the risk below the safe level for an EMD with 10 V/m immunity level and with 90% compliance rate and in the presence of two transmitters whereas the 5 cm vertical separation had negligible effect in reducing the risk floor even for a 30 V/m immunity level.

It is possible to significantly lower the risk by moving the EMD to a location where the risk values are inherently low. It was seen in Figs. 5.3, 5.4, 5.5 and 5.6 that there are some optimal locations in the room with inherently lower levels of the risk. For the 3 V/m immunity level, these locations are the corners close to a patient bed. For the 10 V/m immunity, the optimal location is the small area behind the patient's head if the bed is close enough to a wall. It is seen in Fig. 5.9 that if an EMD with a 10 V/m immunity is located in point B, the safe risk level is achieved when the compliance rate with the MSD policy is 90%.

It was shown in Figs. 5.5(a) and 5.6(a) that the EMDs with a 3 V/m immunity level are unsafe even with a 70 cm MSD policy with a full compliance. It is seen in Figs. 5.7(a) and 5.8(a) that for no practical value of MSD the risk can be brought below the safe level even assuming a compliance rate as high as 99%. It is shown in Fig. 5.10 that even a 30 cm vertical separation does not reduce the risk level for a 3 V/m immunity level. Therefore the use of medical devices with 3 V/m immunity level is not recommended.

Comparing the PWREI maps with no MSD policy in Figs. 5.17 and 5.18 to the maps in Figs. 5.3 and 5.4, it was seen that the PWREI is not much sensitive to some changes in the definition of the presence probability. This shows that the assumption of the presence probability, given by (5.3), can be considered as an acceptable hypothesis.

The risk maps in Figs. 5.3 and 5.4 were given for an MMV of 0.5621 V/m. The MMV was lowered to a hypothetical level of 0.2 V/m and no considerable changes were observed in Figs. 5.12 and 5.13. When the MMV was raised to 1.3 V/m, the risk maps in Figs. 5.14 and 5.15 show some change in the 3 V/m immunity with two transmitters. In case of high immunity devices no considerable changes were observed. It is then concluded that the results presented in this chapter are not much sensitive to the changes in E_m.

It was shown in Section 5.7 that the separation distance suggested by the IEC standard is too conservative even compared to the separation distance obtained using a worst-case analysis in the presence of one or two transmitters fixed at a distance close to an EMD. Both 3 and 10 V/m immunity levels were considered. The optimal MSD values given by the PWREI method for roaming transmitters were smaller than both the IEC suggestion and the result of the worst-case analysis. When the size of the room was increased to halve the multipath mean value, the required separation given by the worst-case analysis was seen to be barely affected in the case of high immunity devices. The effect was considerable in the case of low immunity devices.

The PWREI is suitable for large-scale decision making processes. This method quantifies the risk in the presence of one and two roaming transmitters in a hospital ward, accounting for times when they are close to an EMD, causing a high risk, and for times when they are far from the EMD, causing a low risk. The PWREI complements the worst-case analyses where the transmitters are fixed at close distances to the medical devices. The PWREI is useful in large-scale decision-making processes where both low- and high-risk scenarios occur. The MSD value, the minimum required compliance rate with the MSD policy, and the minimum required immunity level can be determined by the PWREI method for all wards of a hospital in a general policy-making process. Then a worst-case analysis can be used to provide more restrictive measures for high-risk places or situations such as an operating room where many staff members are constantly in a close vicinity of the patient bed where most of the electronic medical devices are located. In more general cases, the PWREI must be used.

Chapter 6

Conclusions

Thousands of patients die each year in US hospitals due to medical errors which may be prevented by providing the medical staff with instant access to patient records using wireless technology. The radiation from wireless transmitters may cause electromagnetic interference (EMI) with electronic medical devices (EMDs), causing them to malfunction with consequences as serious as harm to the patient. This thesis presented a quantitative risk assessment of the electromagnetic interference with EMDs in hospitals, considering one and two wireless transmitters and accounting for their mobility. Some EMI control policies were analyzed.

Absolute prevention of electromagnetic interference by guaranteeing that the electric field intensity is below the *immunity level* of the EMD is impractical chiefly due to the roaming nature of the transmitters and the rapid fluctuations of the field known as *fast fading* which occurs in indoor and some other environments. In a probabilistic approach, the *risk of exceeding immunity* (REI) is determined and control policies are developed to maintain the REI below a safe level chosen to be 10^{-4}. To determine the REI, the electromagnetic field distribution in the hospital ward is required.

This thesis developed fast methods for estimating the probability distribution of the field of one and the sum field of two roaming transmitters. In Chapters 2 and 3,

the Sabine-Rice approximation and the modified ray-tracing-Rice method were shown to provide reliable estimates of the risk of exceeding immunity due to one transmitter. The computational time of the MRTR method is much higher than that of the Sabine-Rice approximation. Hence the Sabine-Rice approximation is used to estimate the risk of exceeding immunity. It was shown in Chapter 4 that, the Ricean function can be used to estimate the probability distribution of the sum field of two roaming transmitters.

The *presence probability function* was defined in Chapter 5 to account for the roaming nature of the transmitters. The transmitter location, (x', y'), was simulated as a pair of random numbers bound to the coordinates of the room. The risk of exceeding immunity together with the presence probability function of the transmitters were then used to introduce the *presence-weighted risk of exceeding immunity*. The PWREI is quantitative gauge for conducting an EMI risk assessment in a 6.4 by 6.5 m hospital ward with one and two roaming transmitters, each transmitting 100 mW at 2.45 GHz. The PWREI can account for a minimum separation policy and a possibility of non-compliance. The PWREI is suitable for large-scale decision making and complements worst-case analyses which account only for high risk-scenarios.

The main contributions of this thesis are as follows.

- It was shown in Chapter 2 that the presence of some furniture does not considerably affect the probability distribution of the electromagnetic field strength within a local area.

- In Chapter 2, the pdf of the field strength within a local area was given by the ray-tracing-Rice and Sabine-Rice methods which eliminate the need for a large mesh with small cell size. It was shown that the lost accuracy of the Ricean distribution in regions very near the transmitter is restored by decreasing the size of the local area.

- The Ricean and Nakagami distributions were compared in Chapter 2. It was shown that determining the Nakagami parameters requires more computation with no improvement in accuracy if the uniformity of the phase distribution of the Ricean event is preserved. If the phase distribution of the field values associated with the reflected rays arriving at an observation point is uniform between 0 and 2π, which is usually true, the use of the Nakagami distribution for field estimation is not recommended.

- In Chapter 3, the modified ray-tracing-Rice method was presented in which reflections of orders higher than three do not have to be determined at more than one single point throughout the room. The MRTR method was shown to be up to many orders of magnitude faster than but as accurate as the RTR method.

- Using ray-tracing, it was shown in Chapter 4 that the two-wave with diffuse power theory is unreliable in the case of fixed transmitters and reliable in the case of roaming transmitters.

- It was shown in Chapter 4 that the Ricean distribution can give the pdf of the sum field of two roaming transmitters.

- The PWREI was presented in Chapter 5 and gives the risk of exceeding immunity accounting for the roaming nature of the transmitters, the MSD policy and a possibility of non-compliance.

- Applying the PWREI to a 6.4 m by 6.5 m hospital ward, the following were concluded.

  - The medical devices with a 3 V/m immunity level are unsafe and should not be used.

  - With full compliance with the MSD policy, any low level of the PWREI can be reached by increasing the MSD value.
  - With some non-compliance, there is an optimal MSD at which the PWREI reaches the risk floor and does not decrease for greater MSDs, suggesting that larger MSDs are not necessarily safer.
  - There are optimal locations in the room where the risk level is inherently lower. If possible, medical devices should be located at these positions.
  - Vertical separation between the EMD and the wireless transmitter is shown to be very effective in reducing the risk.
  - With a compliance rate as low as 90%, with no vertical separation and in the presence of two transmitters, even an EMD with a 30 V/m immunity, located at a non-optimal position, is unsafe. With a compliance rate of 99.5%, an EMD with a 10 V/m immunity is safe.
  - The PWREI had a very low sensitivity to the changes in the MMV.
  - The PWREI had a very low sensitivity to the changes in the presence probability.

- Separation distances suggested by the IEC standard were shown to be too conservative compared to the results of a worst-case analysis.

Based on the findings of this thesis, the following EMI control policies are recommended: (i) choosing the optimal value of the minimum separation distance, (ii) choosing a medical device with an appropriate immunity level according to the conditions of use, (iii) choosing an optimal location for the medical device if possible, and (iv) applying a vertical separation between the wireless transmitters and the medical devices. Since it was shown that the PWREI is not much sensitive to the changes in the multipath mean value and the presence probability, the results presented in this

thesis can be considered valid for a wide range of possibilities of the MMV and the presence probability.

However, this thesis showed that the compliance of the staff members with the MSD policy is of tremendous importance in controlling the EMI. To maintain a high compliance rate, the staff should be educated on the MSD policy and be frequently reminded of its importance.

Future Work

The following are some research opportunities in the field of EMI risk assessment in a hospital ward.

Worst-Case Analysis with Transmitters Roaming Around Patient Bed

At a high risk emergency situation, where several transmitters are present near the patient bed and the medical device, the REI can be obtained using the MRTR method. The MRTR method is faster than the RTR method. The MRTR method can be rerun multiple times to account for different locations of one or more transmitters. Hence if the transmitter is roaming between a limited number of points close to the patient, the MRTR method can account for the mobility of the transmitter. This analysis will depend on the locations of both the EMD and transmitter and is much more accurate than the SR approximation. The worst-case analysis given in the previous chapter used the Sabine-Rice method and depends only on the distance between the transmitter and the EMD.

Computational Time

As mentioned in Section 5.6, the computational time of the risk assessment grows exponentially with the number of present transmitters. Hence, in order to account

for the presence of more than two transmitters, it is essential to develop algorithms to decrease the computational time.

One possible option is to benefit from the fact that the very-high-immunity EMDs are only affected by the transmitters which are within a very close vicinity. It is possible to generate the mesh differently for each location of the transmitter. Near each transmitter, the grid points can be very close to each other. At far distances, the grid points can be far from each other, saving large amounts of computation.

Another approach is to re-design the PWREI algorithm so that the job of determining the risk can be divided into parallel computational blocks each being run on one core of a multi-core processor.

Risk of Harm to Patient

The risk model presented in thesis, calculates the probability of exceeding immunity, P_1. In order to determine the risk of harm to patient, two more probabilities are required: (i) the probability that the EMD malfunctions given that its immunity level is exceeded, P_2, and (ii) the probability of any harm to patient given that the EMD malfunctions, P_3. If studies are conducted to determine P_2 and P_3, the product $P_1P_2P_3$ will give the risk of harm to patient.

Modulation Schemes and the Risk of Exceeding Immunity

This thesis considered CW signals in determining the risk of exceeding immunity whereas a tablet in the hands of a hospital staff member does not transmit continuously with full power. When two or more transmitters are transmitting, they might be transmitting with full power at a small fraction of a bigger time period and at different time slots. These considerations will significantly reduce the risk of exceeding immunity. Hence it is suggested that a statistical study of the IEEE 802.11 protocols considering multiple transmitters be conducted in the time domain. The phase of the

transmitted signal must be studied as well in order to make sure of the validity of the TWDP for the fixed transmitters.

Field Strength Monitor

In the hospital environments where the compliance rate with the MSD policy is expected to be low, a field strength monitor can be installed on the sensitive medical devices. The field strength monitor notifies the staff members if the field strength at the location of the medical device is near or higher than its immunity level. The staff members carrying wireless transmitters will then have to vacate the close vicinity of the medical device.

Bibliography

[1] A. Goldsmith, *Wireless communications*. Cambridge University Press, 2005.

[2] L. T. Kohn, J. M. Corrigan, M. S. Donaldson *et al.*, *To err is human: building a safer health system*. National Academies Press, 2000, vol. 627.

[3] P. Wells, "Can technology reduce health care costs?" *Engineering Management Journal*, vol. 12, no. 4, pp. 194 –200, Aug. 2002.

[4] E. J. van Lieshout, S. N. van der Veer, R. Hensbroek, J. C. Korevaar, M. B. Vroom, M. J. Schultz *et al.*, "Interference by new-generation mobile phones on critical care medical equipment," *Crit Care*, vol. 11, no. 5, p. R98, 2007.

[5] H. Furahata, "Electromagnetic interferences of electric medical equipment from hand-held radiocommunication equipment," in *Electromagnetic Compatibility, 1999 International Symposium on*, 1999, pp. 468–471.

[6] G. Calcagnini, E. Mattei, F. Censi, M. Triventi, R. Lo Sterzo, E. Marchetta, and P. Bartolini, "Electromagnetic compatibility of wlan adapters with life-supporting medical devices," *Health physics*, vol. 100, no. 5, p. 497, 2011.

[7] H.-Y. Chen and C.-Y. Chou, "Evaluation of emi risk due to the interaction between cellular phones and medical devices," *Microwave and Optical Technology Letters*, vol. 52, no. 6, pp. 1449–1454, 2010. [Online]. Available: http://dx.doi.org/10.1002/mop.25221

[8] S. E. Lapinsky and A. C. Easty, "Electromagnetic interference in critical care," *Journal of Critical Care*, vol. 21, no. 3, pp. 267 – 270, 2006. [Online]. Available: http://www.sciencedirect.com/science/article/pii/S0883944106000499

[9] I. E. Commission, "General requirements for basic safety and essential performance collateral standard: Electromagnetic compatibility requirements and tests," *INTERNATIONAL STANDARD, Medical electrical equipment*, 2007.

[10] F. Censi, G. Calcagnini, E. Mattei, M. Triventi, and P. Bartolini, "Rfid in healthcare environment: electromagnetic compatibility regulatory issues," in *Engineering in Medicine and Biology Society (EMBC), 2010 Annual International Conference of the IEEE*. IEEE, 2010, pp. 352–355.

[11] M. Fernandez-Chimeno and F. Silva, "Mobile phones electromagnetic interference in medical environments: A review," in *Electromagnetic Compatibility (EMC), 2010 IEEE International Symposium on*, 2010, pp. 311–316.

[12] R. van der Togt, E. J. van Lieshout, R. Hensbroek, E. Beinat, J. Binnekade, and P. Bakker, "Electromagnetic interference from radio frequency identification inducing potentially hazardous incidents in critical care medical equipment," *JAMA: the journal of the American Medical Association*, vol. 299, no. 24, pp. 2884–2890, 2008.

[13] S. Iskra, B. Thomas, R. McKenzie, and J. Rowley, "Potential gprs 900/180-mhz and wcdma 1900-mhz interference to medical devices," *Biomedical Engineering, IEEE Transactions on*, vol. 54, no. 10, pp. 1858 –1866, Oct. 2007.

[14] D. Giri and F. Tesche, "Classification of intentional electromagnetic environments (ieme)," *Electromagnetic Compatibility, IEEE Transactions on*, vol. 46, no. 3, pp. 322 – 328, Aug. 2004.

[15] C.-K. Tang, K.-H. Chan, L.-C. Fung, and S.-W. Leung, "Electromagnetic interference immunity testing of medical equipment to second- and third-generation mobile phones," *Electromagnetic Compatibility, IEEE Transactions on*, vol. 51, no. 3, pp. 659 –664, Aug. 2009.

[16] M. Fernandez-Chimeno, M. Quilez, and F. Silva, "Understanding electrosurgical unit perturbations in order to address hospital operating room electromagnetic compatibility," *Biomedical Engineering, IEEE Transactions on*, vol. 53, no. 6, pp. 1206–1209, 2006.

[17] C. Luca and A. Salceanu, "Study upon electromagnetic interferences inside an intensive care unit," in *Electrical and Power Engineering (EPE), 2012 International Conference and Exposition on*, 2012, pp. 535–540.

[18] P. Phunchongharn, D. Niyato, E. Hossain, and S. Camorlinga, "An emi-aware prioritized wireless access scheme for e-health applications in hospital environments," *Information Technology in Biomedicine, IEEE Transactions on*, vol. 14, no. 5, pp. 1247 –1258, sept. 2010.

[19] K. Armstrong, "Opportunities in the risk management of emc," in *Electromagnetic Compatibility (EMC), 2011 IEEE International Symposium on.* IEEE, 2011, pp. 988–993.

[20] P. Phunchongharn, E. Hossain, and S. Camorlinga, "Electromagnetic interference-aware transmission scheduling and power control for dynamic wireless access in hospital environments," *Information Technology in Biomedicine, IEEE Transactions on*, vol. 15, no. 6, pp. 890–899, 2011.

[21] B. Segal, D. Davis, C. Trueman, and T. Pavlasek, "Risk of patient injury due to electromagnetic-interference malfunctions: estimation and minimization," in

Electromagnetic Compatibility, 2001. EMC. 2001 IEEE International Symposium on, vol. 2, 2001, pp. 1308 –1312 vol.2.

[22] K.-S. Tan and I. Hinberg, "Radiofrequency susceptibility tests on medical equipment," in *Engineering in Medicine and Biology Society, 1994. Engineering Advances: New Opportunities for Biomedical Engineers. Proceedings of the 16th Annual International Conference of the IEEE*, 1994, pp. 998 –999 vol.2.

[23] J. L. Tri, R. P. Severson, A. R. Firl, D. L. Hayes, and J. P. Abenstein, "Cellular telephone interference with medical equipment," in *Mayo Clinic Proceedings*, vol. 80, no. 10. Elsevier, 2005, pp. 1286–1290.

[24] J. G. Van Bladel, *Electromagnetic fields*. Wiley, 2007.

[25] D. M. Sullivan, *Electromagnetic simulation using the FDTD method*. Wiley-IEEE Press, 2000.

[26] A. Austin, M. Neve, G. Rowe, and R. Pirkl, "Modeling the effects of nearby buildings on inter-floor radio-wave propagation," *Antennas and Propagation, IEEE Transactions on*, vol. 57, no. 7, pp. 2155–2161, 2009.

[27] W. Stutzman and G. Thiele, *Antenna Theory and Design*. Wiley, 2012.

[28] C. A. Balanis, *Advanced engineering electromagnetics*. Wiley New York, 1989.

[29] J. B. Keller, "A ray-tracing approach for indoor/outdoor propagation through window structures," *Journal of the Optical Society of America*, vol. 52, no. 2, pp. 116–130, 1962.

[30] R. Kouyoumjian, P. Pathak, and W. Burnside, "A uniform gtd for the diffraction by edges, vertices and convex surfaces," *Theoretical Methods for Determining the Interaction of Electromagnetic Waves with Structures, Ed. JK Skwirzynski*, 1981.

[31] P. Y. Ufimtsev, "Method of edge waves in the physical theory of diffraction," DTIC Document, Tech. Rep., 1971.

[32] C. W. Trueman, R. Paknys, J. Zhao, D. Davis, and B. Segal, "Ray tracing algorithm for indoor propagation," in *The 16th Annual Review of Progress in Applied Computational Electromagnetics Society*, 2000, pp. 493–500.

[33] C.-F. Yang, B.-C. Wu, and C.-J. Ko, "A ray-tracing method for modeling indoor wave propagation and penetration," *Antennas and Propagation, IEEE Transactions on*, vol. 46, no. 6, pp. 907 –919, jun 1998.

[34] Z. Zhang, R. Sorensen, Z. Yun, M. Iskander, and J. Harvey, "A ray-tracing approach for indoor/outdoor propagation through window structures," *Antennas and Propagation, IEEE Transactions on*, vol. 50, no. 5, pp. 742–748, 2002.

[35] H. Ling, R.-C. Chou, and S.-W. Lee, "Shooting and bouncing rays: calculating the rcs of an arbitrarily shaped cavity," *Antennas and Propagation, IEEE Transactions on*, vol. 37, no. 2, pp. 194–205, 1989.

[36] C. W. Trueman, D. Davis, B. Segal, and W. Muneer, "Validation of fast site-specific mean-value models for indoor propagation," *Applied Computational ElectromagneticS Society Journal*, vol. 24, no. 3, p. 306–317, 2009.

[37] O. Landron, M. Feuerstein, and T. Rappaport, "A comparison of theoretical and empirical reflection coefficients for typical exterior wall surfaces in a mobile radio environment," *Antennas and Propagation, IEEE Transactions on*, vol. 44, no. 3, pp. 341–351, 1996.

[38] ——, "In situ microwave reflection coefficient measurements for smooth and rough exterior wall surfaces," in *Vehicular Technology Conference, 1993., 43rd IEEE*, 1993, pp. 77–80.

[39] S. Kim, B. Bougerolles, and H. Bertoni, "Transmission and reflection properties of interior walls," in *Universal Personal Communications, 1994. Record., 1994 Third Annual International Conference on*, 1994, pp. 124–128.

[40] C. D. Taylor, S. J. Gutierrez, S. L. Langdon, K. L. Murphy, and W. A. Walton III, "Measurement of rf propagation into concrete structures over the frequency range 100 mhz to 3 ghz," in *Wireless Personal Communications*. Springer, 1997, pp. 131–144.

[41] P. Rattanadecho, "The simulation of microwave heating of wood using a rectangular wave guide: Influence of frequency and sample size," *Chemical Engineering Science*, vol. 61, no. 14, pp. 4798 – 4811, 2006. [Online]. Available: http://www.sciencedirect.com/science/article/pii/S0009250906001552

[42] A. Muqaibel, A. Safaai-Jazi, A. Bayram, A. M. Attiya, and S. Riad, "Ultrawideband through-the-wall propagation," *Microwaves, Antennas and Propagation, IEE Proceedings*, pp. 581–588, Dec 2005.

[43] Forest Products Laboratory (U.S.) and U. S. Department of Agriculture, *The Encyclopedia of Wood*. Skyhorse Pub., 2007. [Online]. Available: http://books.google.ca/books?id=mUGSaiTsBAIC

[44] H. Sabine, "Room acoustics," *Audio, Transactions of the IRE Professional Group on*, no. 4, pp. 4–12, 1953.

[45] J. B. Andersen, J. Nielsen, G. Pedersen, G. Bauch, and M. Herdin, "Room electromagnetics," *Antennas and Propagation Magazine, IEEE*, vol. 49, no. 2, pp. 27–33, 2007.

[46] H. Hashemi, "The indoor radio propagation channel," *Proceedings of the IEEE*, vol. 81, no. 7, pp. 943 –968, jul 1993.

[47] Y. Lustmann and D. Porrat, "Indoor channel spectral statistics, k-factor and reverberation distance," *Antennas and Propagation, IEEE Transactions on*, vol. 58, no. 11, pp. 3685–3692, 2010.

[48] M. Hasna and M.-S. Alouini, "Optimal power allocation for relayed transmissions over rayleigh-fading channels," *Wireless Communications, IEEE Transactions on*, vol. 3, no. 6, pp. 1999–2004, 2004.

[49] M. Matthaiou, D. Laurenson, and J. Thompson, "A mimo channel model based on the nakagami-faded spatial eigenmodes," *Antennas and Propagation, IEEE Transactions on*, vol. 56, no. 5, pp. 1494–1497, 2008.

[50] L. Greenstein, D. Michelson, and V. Erceg, "Moment-method estimation of the ricean k-factor," *Communications Letters, IEEE*, vol. 3, no. 6, pp. 175–176, 1999.

[51] J. Sijbers, A. den Dekker, P. Scheunders, and D. Van Dyck, "Maximum-likelihood estimation of rician distribution parameters," *Medical Imaging, IEEE Transactions on*, vol. 17, no. 3, pp. 357–361, 1998.

[52] S. Jiang and D. Kececioglu, "Maximum likelihood estimates, from censored data, for mixed-weibull distributions," *Reliability, IEEE Transactions on*, vol. 41, no. 2, pp. 248–255, 1992.

[53] L. Rayleigh, "Xii. on the resultant of a large number of vibrations of the same pitch and of arbitrary phase," *The London, Edinburgh, and Dublin Philosophical Magazine and Journal of Science*, vol. 10, no. 60, pp. 73–78, 1880.

[54] S. O. Rice, "Mathematical analysis of random noise," *Bell Systems Tech. J., Volume 23, p. 282-332*, vol. 23, pp. 282–332, 1944.

[55] A. Abdi, H. Hashemi, and S. Nader-Esfahani, "On the pdf of the sum of random vectors," *Communications, IEEE Transactions on*, vol. 48, no. 1, pp. 7–12, 2000.

[56] G. Durgin, T. Rappaport, and D. A. De Wolf, "New analytical models and probability density functions for fading in wireless communications," *Communications, IEEE Transactions on*, vol. 50, no. 6, pp. 1005–1015, 2002.

[57] Z. Yu, C. C. Chai, and T.-T. Tjhung, "Envelope probability density functions for fading model in wireless communications," *Vehicular Technology, IEEE Transactions on*, vol. 56, no. 4, pp. 1907–1912, 2007.

[58] S. Oh, K. Li, and W. Lee, "Performance of bpsk pre-detection mrc systems over two-wave with diffuse power fading channels," *Wireless Communications, IEEE Transactions on*, vol. 6, no. 8, pp. 2772–2775, 2007.

[59] H. Suraweera, W. Lee, and S. Oh, "Performance analysis of qam in a two-wave with diffuse power fading environment," *Communications Letters, IEEE*, vol. 12, no. 2, pp. 109–111, 2008.

[60] Y. Lu and X. Wang, "On the performance of opportunistic amplify-and-forward relaying in two-wave with diffuse power fading channels," in *Wireless Communications and Networking Conference (WCNC), 2012 IEEE*, 2012, pp. 54–58.

[61] Y. Lu, N. Yang, H. Dai, and X. Wang, "Opportunistic decode-and-forward relaying with beamforming in two-wave with diffuse power fading," *Vehicular Technology, IEEE Transactions on*, vol. 61, no. 7, pp. 3050–3060, 2012.

[62] A. Henderson, C. Durkin, and G. Durgin, "Finding the right small-scale fading distribution for a measured indoor 2.4 ghz channel," in *Antennas and Propagation Society International Symposium, 2008. AP-S 2008. IEEE*, 2008, pp. 1–4.

[63] D. Townsend, "Risk analysis and emi risk abatement strategies for hospitals: scientific and legal approaches," in *Electromagnetic Compatibility, 2001. EMC. 2001 IEEE International Symposium on*, vol. 2, 2001, pp. 1304–1307 vol.2.

[64] M. Ardavan, C. Trueman, and K. Schmitt, "Ricean and rayleigh distribution functions for estimating field distributions in indoor propagation," in *Applied Computational Electromagnetics Society Conference*, march 2011.

[65] ——, "A sabine-rice approximation for the risk of exceeding immunity," in *Antennas and Propagation (APSURSI), 2011 IEEE International Symposium on*, july 2011, pp. 2363 –2366.

[66] M. Ardavan, C. W. Trueman, and K. A. Schmitt, "Emi risk assessment in a hospital ward with one and two roaming wireless transmitters," *To be submitted to Electromagnetic Compatibility, IEEE Transactions on*.

[67] C. C. Travis, S. A. Richter, E. A. Crouch, R. Wilson, and E. D. Klema, "Cancer risk management a review of 132 federal regulatory decisions," *Environmental Science & Technology*, vol. 21, no. 5, pp. 415–420, 1987.

[68] J. A. Gubner, *Probability and random processes for electrical and computer engineers*. Cambridge University Press, 2006.

[69] D. Witters, S. Seidman, and H. Bassen, "Emc and wireless healthcare," in *Electromagnetic Compatibility (APEMC), 2010 Asia-Pacific Symposium on*. IEEE, 2010, pp. 5–8.

[70] V. Cehlot and E. B. Sloane, "Ensuring patient safety in wireless medical device networks," *Computer*, vol. 39, no. 4, pp. 54–60, 2006.

[71] N. LaSorte, S. Rajab, and H. Refai, "Developing a reproducible non-line-of-sight experimental setup for testing wireless medical device coexistence utilizing zigbee," *Biomedical Engineering, IEEE Transactions on*, vol. 59, no. 11, pp. 3221–3229, Nov 2012.

[72] N. J. LaSorte, H. H. Refai, D. M. Witters Jr, S. J. Seidman, and J. L. Silberberg, "Wireless medical device coexistence," *Journal of Medical Electronics Design*, 2011.

[73] M. Ardavan, C. W. Trueman, and K. A. Schmitt, "Optimal location of medical devices in hospitals," in *INFORMS Healthcare*, vol. 2, June 2011.